Near-Miscible CO_2 Application to Improve Oil Recovery

By

Ly Huong Bui

Submitted to the graduate degree program in Chemical and Petroleum Engineering and the Graduate Faculty of the University of Kansas in partial fulfillment of the requirement for the degree of Master of Science

Committee: _____

G. Paul Willhite

_____

Jyun Syung Tsau

_____

Aaron M. Scurto

Date defended: _____

Thesis Committee for Ly Huong Bui certifies

that this is the approved version of the following thesis

Near-Miscible CO_2 Application to Improve Oil Recovery

Committee: _____

G. Paul Willhite

_____

Jyun Syung Tsau

_____

Aaron M. Scurto

Date approved: _____

ABSTRACT

Carbon dioxide (CO_2) injection for enhanced oil recovery is a proven technology. CO_2 injection is normally operated at a pressure above the minimum miscibility pressure (MMP), which is determined by crude oil composition and reservoir conditions. This is the lowest pressure at which the injected CO_2 becomes dynamically miscible with the crude oil remaining in the reservoir. However, many reservoirs are located at depths or under geologic conditions such that they must operate at pressures below the MMP. When CO_2 is injected at below the MMP, displacement efficiency decreases as a result of the loss of miscibility. CO_2 injection is usually not considered as an enhanced oil recovery process in these reservoirs. Near miscible displacement generally refers to the process that occurs at pressures slightly below the MMP, but the actual pressure range has never been clearly defined.

The objectives of this study were to investigate the feasibility of near-miscible CO_2 application and improve our understanding of the mechanisms of near-miscible CO_2 flooding by conducting appropriate experimental work and reservoir simulation. The pressure range of interest was from 0.8 MMP to MMP in our study. The Arbuckle formation of Kansas was used as an example to demonstrate our approach to evaluate CO_2 flooding at near-miscible conditions. The suite of laboratory experiments used to evaluate the feasibility of operating at pressures below MMP for Arbuckle reservoirs included phase behavior studies, core flow tests and phase behavior model construction using CMG software package.

Phase behavior studies were carried out to characterize the near miscible conditions. Slim tube displacements and swelling/extraction tests were performed to identify the near miscible range and the mass transfer mechanisms which were responsible for the oil recovery within this range. A phase behavior model was constructed and well-tuned to simulate oil properties, CO_2/crude oil interactions and slim tube results. Core flow tests were conducted to evaluate the oil recovery efficiency in the near miscible range.

Initial laboratory works indicated that miscibility was not achievable, however at least 65% to 80% of the waterflood residual oil for dolomite cores and lesser from 45% to 60 % for sandstone core in the near-miscible region was observed. The principal oil recovery mechanism in the near-miscible range appeared to be extraction/vaporization of hydrocarbon components from crude oil into the CO_2 rich vapor phase, coupled with enhanced mobility control due to the reduction of oil viscosity. This suggested that application of carbon dioxide in the field would require injection and recycling of large volumes of carbon dioxide. Further study is needed to determine if such a process is economically feasible. However the prospect of recovering up to 1 billion barrels of oil from Arbuckle reservoirs offers significant economic potential.

TABLE OF CONTENTS

LIST OF FIGURES

LIST OF TABLES

NOMENCLATURE

S_{wr}	Connate water saturation
S_{orw}	Residual oil saturation after waterflooding
S_{orm}	Residual oil saturation after CO2 flooding
S_{wf}	Water saturation after CO2 flooding
k_{rg}	Gas relative permeability
k_{ro}	Oil relative permeability
S_g	Gas saturation
μ	Viscosity
T_c	Critical temperature
T	Temperature
P_c	Critical pressure
P	Pressure
R	Molar gas constant
M	Molecular weight
Ωa	Equation of state parameter
Ωb	Equation of state parameter
ω	Accentric factor
d_{ij}	Binary interaction coefficient
α	Rotational coupling coefficient
x_{CO2}	Mole fraction of CO_2 in the liquid phase

MW	Molecular Weight
PVT	Pressure Volume Temperature
PV	Pore volume
HCPV	Hydrocarbon pore volume

ACKNOWLEDGMENTS

First and foremost, I would like to express my sincere gratitude to my advisors, Dr. G. Paul Willhite and Dr. Jyun-Syung Tsau for their guidance, support and encouragement throughout my graduate study at University of Kansas. I appreciate their patience to guide me through and make graduate study an invaluable experience to me.

I would like to extend my appreciation to Dr. Aaron M. Scurto for serving on my thesis committee and giving me insightful comments.

I would like to give my special thanks to Mr. Scott Ramskill and Dr. Karen Peltier for their assistance on setting up and maintaining laboratory equipment as well as providing me necessary laboratory supplies to get my work done.

I would like to thank the faculty and staff members of the University of Kansas Center for Research's Tertiary Oil Recovery Project (TORP), especially Dr. Jenn-Tai Liang and Ms. Mayumi Crider. I would also like to thank other fellow students of the Chemical and Petroleum Department for their friendship.

I would like to acknowledge Research Partnership to Secure Energy for America (RPSEA) and the University of Kansas Center for Research's Tertiary Oil Recovery Project (TORP) for financial support. I would like to acknowledge Kansas Geological Survey and Carmen Schmitt, Inc. for providing representative core samples and crude oil samples. I would like

to acknowledge Computer Modeling Group (CMG) for their permission of using the software.

Finally I want to express the deepest appreciation to my mother and my sister for their love and support.

1 Introduction and Literature Review

Crude oil production can include up to three phases: primary, secondary, and tertiary (or enhanced) oil recovery. Primary oil recovery, which relies on natural reservoir pressure to drive the oil to the surface, typically produces 5 to 20 % of the original oil in place (OOIP). Secondary recovery techniques prolong the field's productive life generally by injecting water or gas to displace oil to production wells, increasing the oil recovery from 20 to 40% OOIP. Several tertiary, or enhanced oil recovery (EOR) techniques, which have been attempted with the goal of ultimately recovering/producing 30 to 60 % OOIP and found to be commercially successful to varying degrees, could be categorized mainly as thermal recovery, gas injection and chemical injection.

Gas injection involves injecting natural gas, nitrogen or carbon dioxide (CO_2) into the reservoir. The gases can either expand and push oil through the reservoir, or dissolve in the oil, decreasing its viscosity and facilitating oil flow to the wellbore. While other EOR methods decline over the years, gas injection increased from 18% in 1984 to about 48% in 2008, proving to be the most popular method in the U.S. The percentage of gas injection share in total EOR production in the U.S is depicted in Figure 1.1.

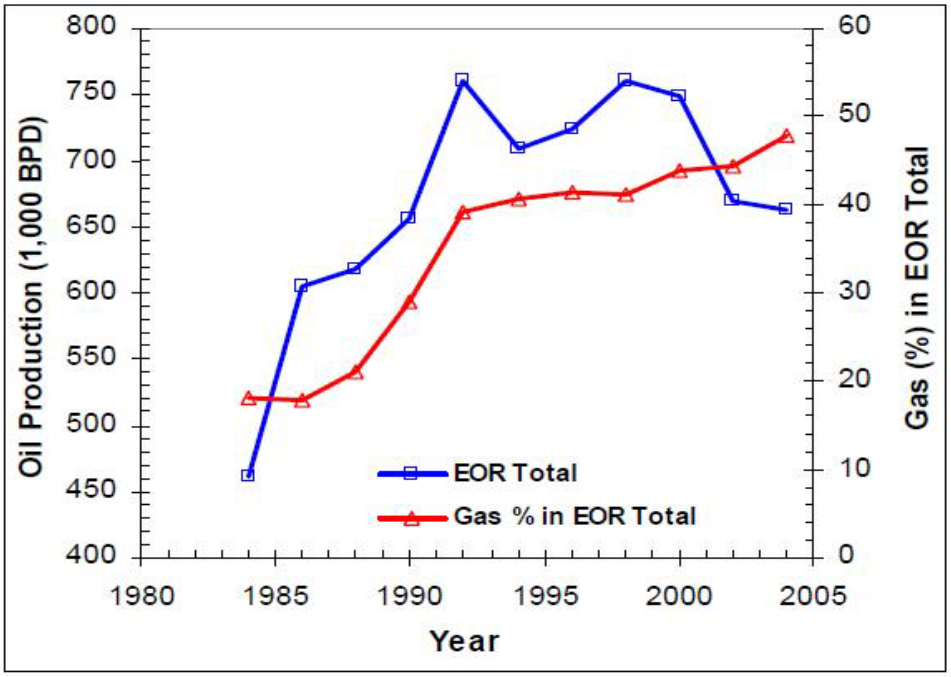

Figure 1-1 Gas injection EOR in U.S [1]

CO_2 injection for secondary and tertiary oil recovery is the primary gas injection method. Miscible CO_2 displacement offers the greatest oil recovery potential, but it can only be achieved at a pressure greater than a certain minimum referred to as the minimum miscibility pressure. In a study of EOR developments and their future potential in the U.S, Stosur et al. [1] concluded that miscible CO_2 gas injection was slowly becoming popular and would continue to grow faster than any other EOR methods. He pointed out that miscible CO_2 gas injection increased from 38% in 1984 to about 65% in 2004.

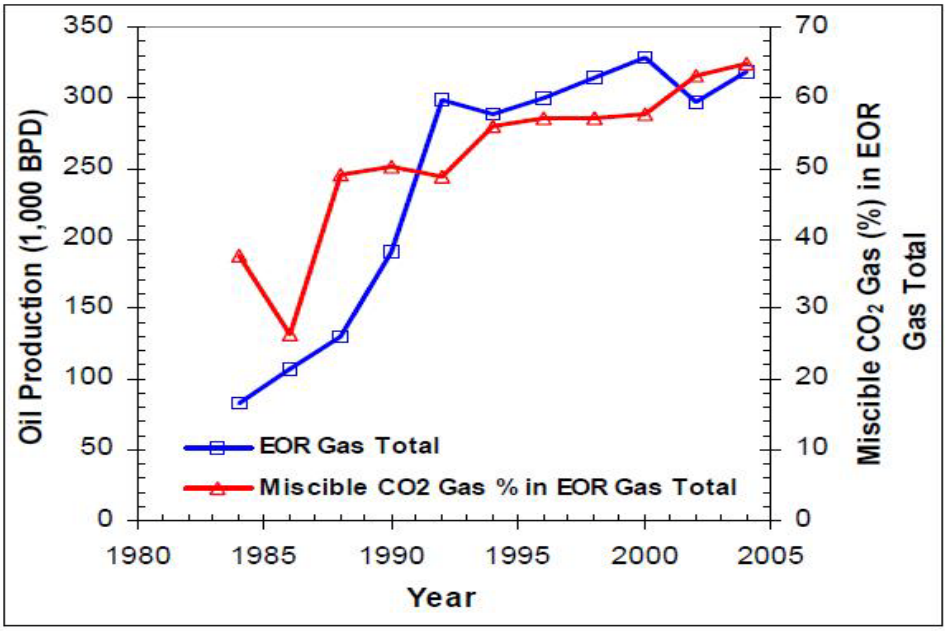

Figure 1-2 Miscible CO_2 gas injection EOR in US [1]

CO_2 EOR not only provides a value-added opportunity to recover substantial remaining trapped oil but also offers environmental benefits if industrial CO_2 is used and stored in reservoirs. With existing but non-utilized industrial CO_2 sources, such as natural gas byproducts, hydrogen plants, ethanol, cement, petroleum coke gasifiers, fossil fuel power plants, the growing concern about greenhouse gases and climate change has significantly increased interest in CO_2 sequestration and storage.

1.1 The Basics of CO_2 EOR

1.1.1 CO_2 Properties

CO_2 has numerous characteristics that make it a favorable oil-displacing-agent. One of the most important characteristics is the pressure at which CO_2 becomes miscible with crude oil is substantially lower than other gases, although there may be exceptions at high temperature. When miscibility is attained, residual oil saturation is reduced nearly to zero, which means high oil recoveries and favorable project economics.

High solubility of CO_2 in crude oil is another important characteristic. CO_2 dissolution in oil causes the oil to swell and expand out of dead end pores. In addition, viscosity of crude oil decreases as it becomes saturated with CO_2 at increasing pressures, which helps facilitating flow to the wellbore. The ability of dense-phase CO_2 to extract hydrocarbon components from oil, coupled with the ability of CO_2 to dissolve into oil helps establishing dynamic miscibility.

At high pressures, CO_2 density has a density close to that of a liquid and is greater than that of either nitrogen (N_2) or methane (CH_4), which makes CO_2 less prone to gravity segregation compared with N_2 or CH_4.

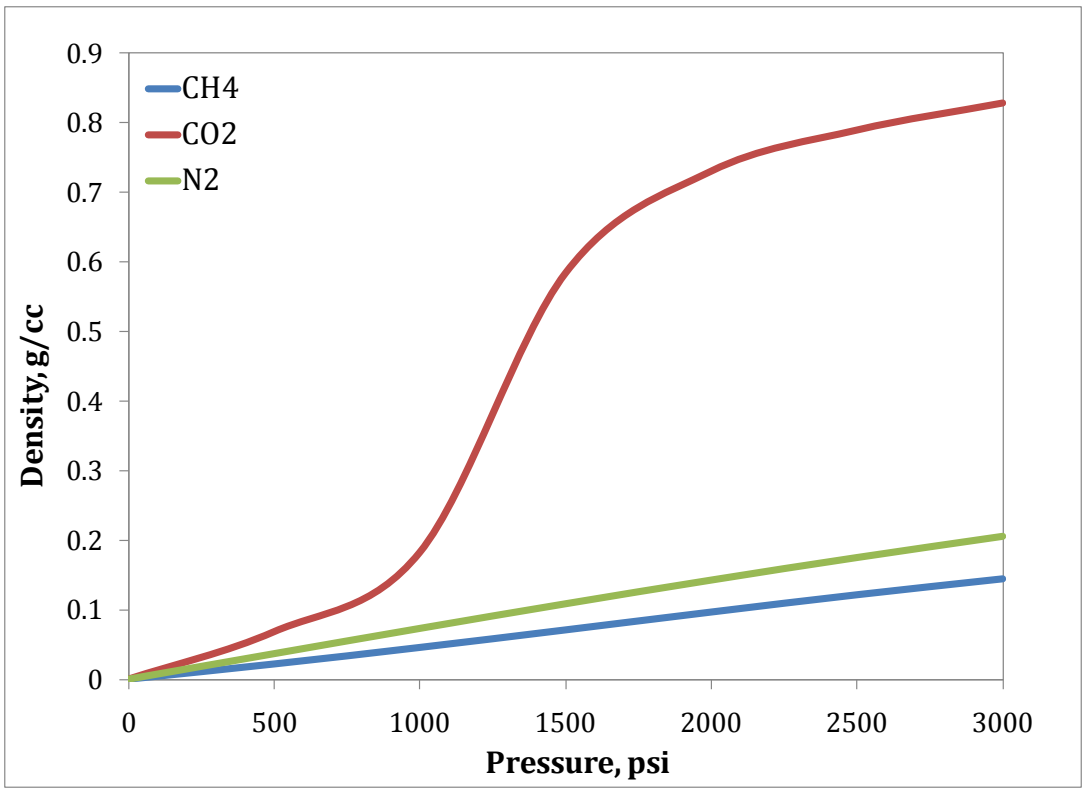

Figure 1-3 Comparison of CO_2, CH_4, N_2 density at 110°F (REFPROP)

In addition, at high pressures, viscosity of CO_2 is also greater than that of N_2 or CH_4, resulting in better mobility control and better sweep efficiency compared with other gases.

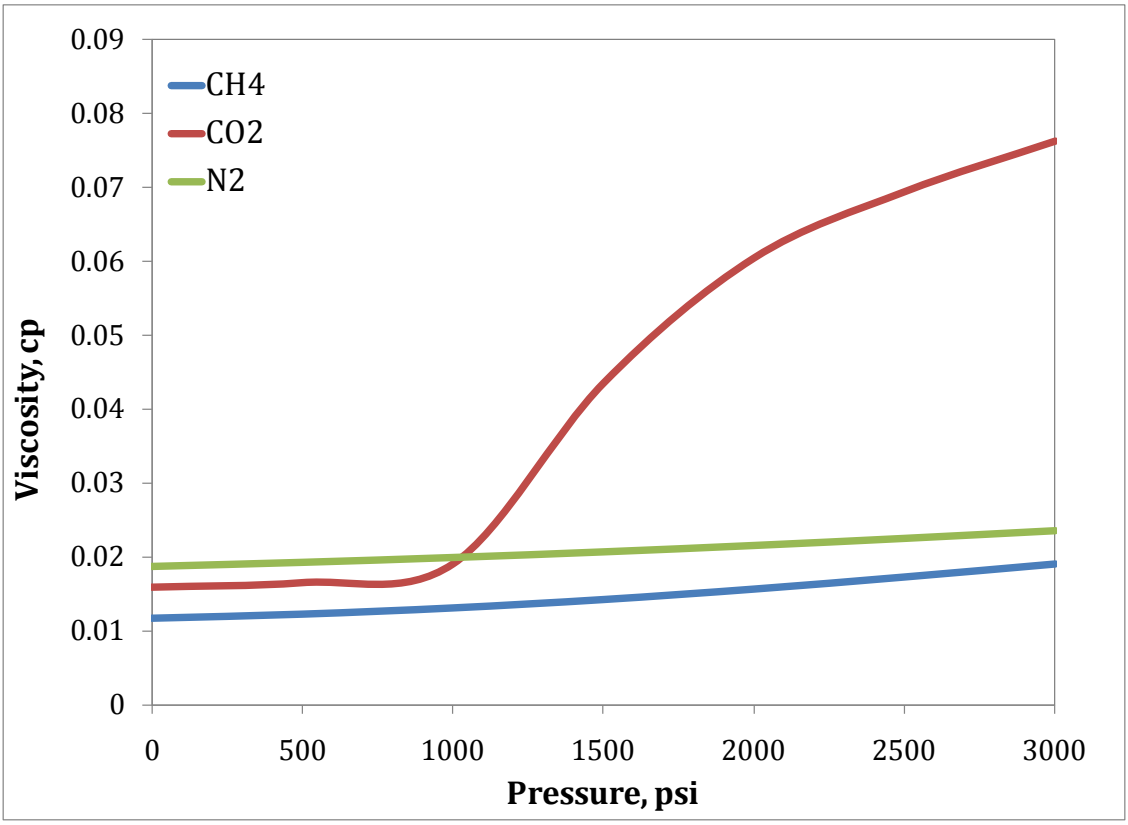

Figure 1-4 Comparison of CO_2, CH_4, N_2 viscosity at 110°F (REFPROP)

1.1.2 Immiscibility & Miscibility

Holm [2] describes miscibility as: "the ability of two or more substances to form a single homogeneous phase when mixed in all proportions. For petroleum reservoirs, miscibility is defined as that physical condition between two or more fluids that will permit them to mix in all proportions without existence of an interface. If two fluid phases form after some amount of one fluid is added to others, the fluids are considered immiscible". Examples of miscibility and immiscibility are shown in Figure 1.5 and Figure 1.6 respectively.

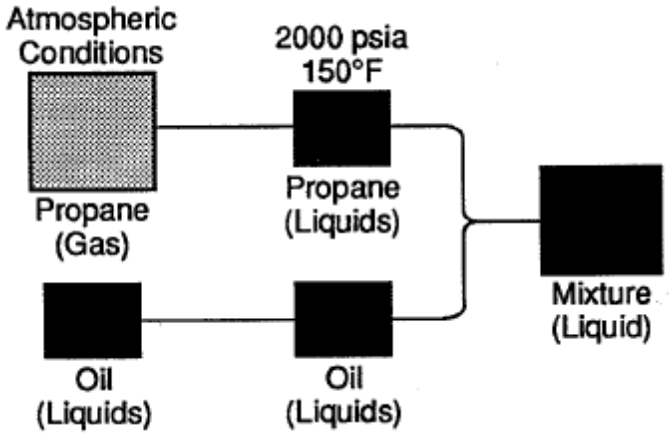

Figure 1-5 Miscibility of propane (or LPG) liquid and oil liquid at reservoir temperature and pressure conditions [3]

Oil exists as a liquid and propane exists as a gas at atmospheric conditions. If the temperature and pressure are increased to the indicated reservoir conditions, however, the propane exists as a liquid, as does the crude oil. These two liquids will mix completely and are thus miscible.

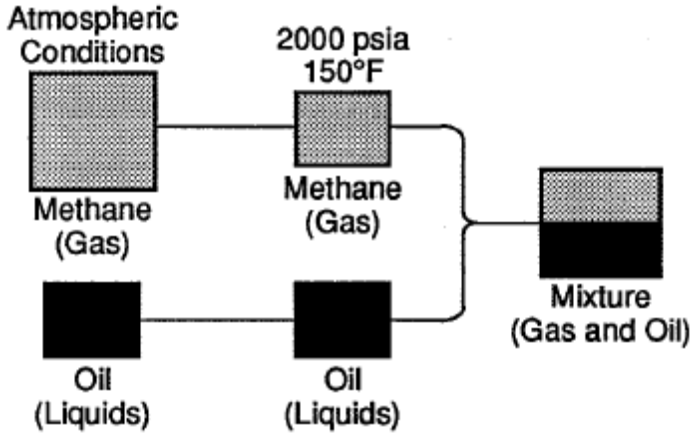

Figure 1-6 Immiscible two-phase mixture of methane gas and oil liquid at typical reservoir conditions [3]

Methane and crude oil are partially soluble in one another. At conditions typically encountered in a reservoir, however, they do not mix in all proportions and two phases exist.

1.1.3 Minimum Miscibility Pressure

Miscible recovery of reservoir oil can be achieved by CO_2 displacement at a pressure greater than a certain minimum. This minimum pressure is hereafter called as the CO_2 minimum miscibility pressure (MMP). CO_2 MMP is an important parameter for screening and selecting reservoirs for CO_2 EOR. For the highest recovery, a candidate reservoir must be capable of withstanding an average reservoir pressure greater than the CO_2 MMP.

MMP depends on crude oil composition and reservoir conditions, and is typically determined using slim tube tests. There are no fixed criteria for determining miscibility within slim tube and individual researchers have defined their own criteria to identify slim tube miscibility. Holm and Josendal [4] defined MMP as the pressure at which 80% of oil in place was recovered at CO_2 breakthrough and more than 94% when gas-oil ratio (GOR) reaches 40,000 scf/bbl, whereas Metcalfe and Yellig [5] defined MMP as a pressure at which recovery at 1.2 pore volume gas injected was near the maximum recovery. Others used the pressure corresponding to the break-over point in the plot of percentage of oil recovery at 1.2 HCPV of CO_2 injected versus pressure as the MMP. In this study, the pressure at which 90% of original oil in place was recovered at 1.2 HCPV of CO_2 injected was considered MMP.

1.1.4 Mechanisms of Oil Displacement by CO_2

Mechanisms of CO_2 displacing crude oil from porous media rely on the phase behavior of CO_2 /crude oil system, which is strongly dependent on reservoir temperature, pressure and crude oil composition. Displacement mechanisms fall into one of five regions illustrated in Figure 1.7. It is important to note that the lines that divide region from region are generalizations that will vary from oil to oil.

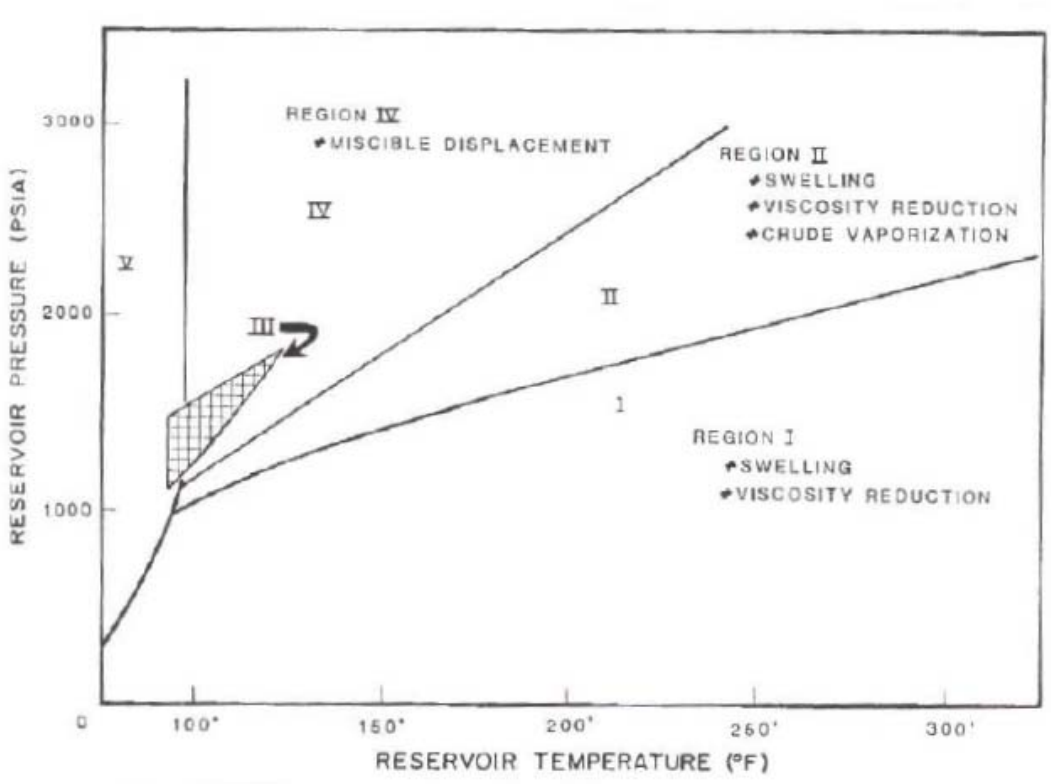

Figure 1-7 Effect of temperature and pressure on CO_2 injection displacement mechanisms [6]

In Region I (low pressure applications), CO_2 swells the oil, reduces the viscosity of crude oil and contributes to internal solution gas drive. Swelling of oil is important since the oil left in the reservoir after flooding is inversely proportional to the swelling factor. Swollen oil droplets will force water out of pore spaces, creating drainage rather than imbibitions

process for water wet system. Drainage oil relative permeability curves are higher than the imbibitions counterparts, creating a more favorable oil flow environment at any given saturation conditions. The importance of viscosity reduction was mentioned earlier. Another mechanism of oil displacement by CO_2 in Region I is solution gas drive effect. CO_2 goes into the solution with an increase in reservoir pressure, after termination of the injection phase of a gas flood, gas will come out of solution and continue to drive oil to the wellbore.

At reservoir pressures higher than those in Region I but lower than Region IV, supplemental production mechanisms come into play in Region II. In addition to increasing reservoir pressure, oil swelling, viscosity reduction, hydrocarbons may be vaporized into the gas phase.

Region III (intermediate pressure, low temperature applications) is very similar to Region II, except that CO_2, rather than vaporize crude oil, extract the crude's lighter hydrocarbons forming CO_2-rich liquid mixtures. In addition to the potential for reduced total mobility in the three-phase region, Orr et al (1983) report that CO_2-rich liquid phases extract more and much heavier hydrocarbons than their rich vapor counterparts.

Region IV is the most important region where CO_2 vaporizes or extracts a significant amount of hydrocarbon components from crude oil so rapidly that multiple-contact miscibility occurs in a very brief time period and over a very short reservoir distance.

1.1.5 Mechanisms for CO_2 Miscibility with Oil

In general, miscibility between two fluids can be achieved through two mechanisms: first contact miscibility and multiple contact miscibility.

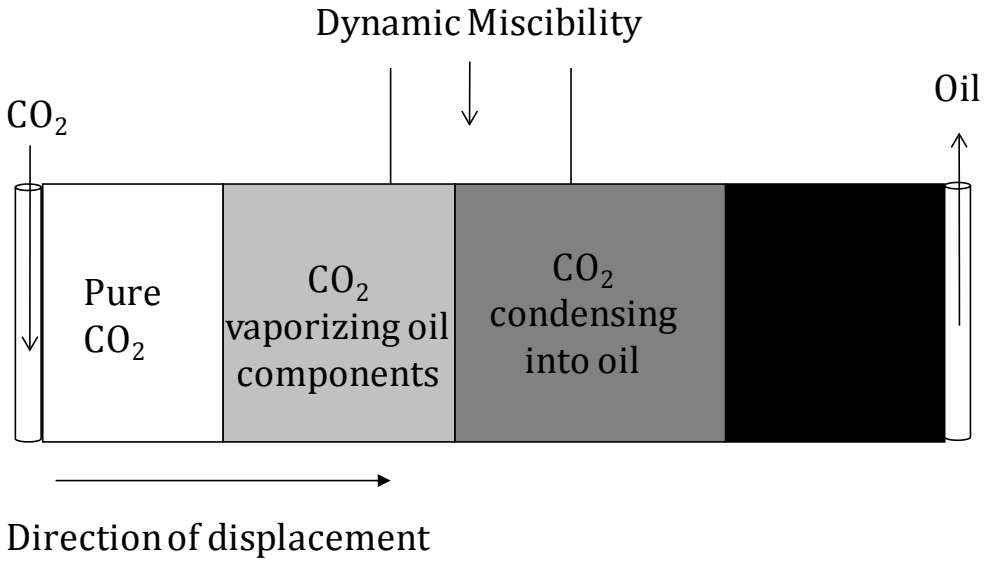

Figure 1-8 One dimensional schematic showing how CO_2 becomes miscible with crude oil

CO_2 is not first contact miscible with most crude oils within the reasonable range of reservoir pressures. It requires many contacts in which components of the oil and CO_2 transfer back and forth until the oil-enriched CO_2 cannot be distinguished from the CO_2-enriched oil in terms of fluid properties. These processes are called vaporizing/condensing processes and are described in detail in Green & Willhite [3].

Ternary diagram is used to describe the phase behavior of three-component systems at constant system temperature and pressure and is useful in describing the development of miscibility in a multiple contact process. The apexes of the diagram represent 100%

concentration of methane, nitrogen or CO_2; intermediate hydrocarbons (C2-C6) and heavy hydrocarbons (C7+) respectively. Temperature and pressure are constant and equal to the displacement conditions in the reservoir. VO is the saturated vapor curve. LO is the saturated liquid curve. Point O is the critical or plait point. Point A represents the composition of injected gas A. Point C represents the composition of crude oil. The area inside the envelope is the two-phase region and outside the envelope is the single phase region.

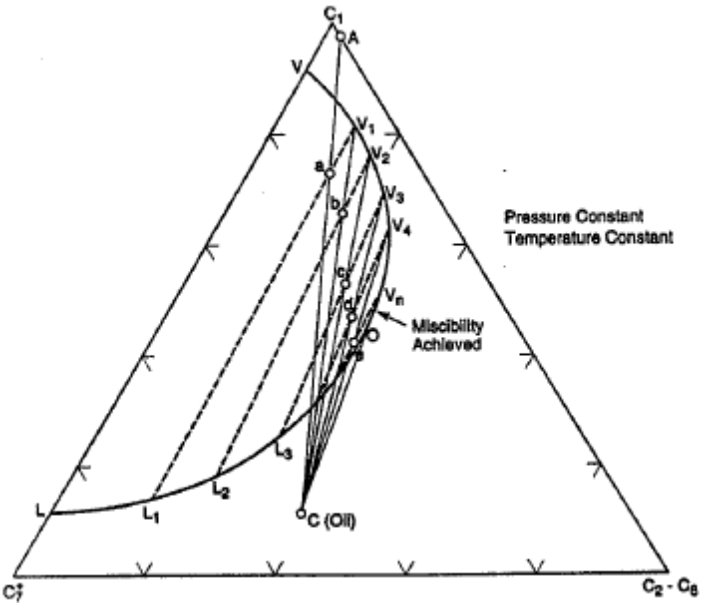

Figure 1-9 Concept of multiple-contact miscibility by vaporization [3]

Concept of multiple-contact miscibility by vaporizing is illustrated in Figure 1.9. The injected gas is a relatively lean gas, for example, it contains mostly methane and other low molecular weight hydrocarbons or sometimes inert gases such as nitrogen. In this approach, the composition of the injected gas is modified as it moves through the reservoir so that it becomes miscible with the original reservoir oil, that is, the injected fluid is enriched in composition through multiple contacts with the oil, during which intermediate

components in the oil are vaporized into the injected gas. The process operates conceptually as follows:

- Gas A mixes with Oil C. The resulting composition of the mixture is along AC, say Point a.
- Mixture a is in the two-phase region, therefore, separates into a vapor V1 and a liquid L1
- Vapor V1 moves ahead of Liquid L1 and contacts Oil C. The resulting composition of the mixture is along Line V1C, say at Point b.
- Mixture b separates into Vapor V2 and Liquid L2
- The process continues with vapor-phase composition changing along the saturated vapor curve, V3, V4 etc
- Finally, at point e, the vapor becomes miscible with Oil C because the mixing line lies in the single-phase region.

If miscibility is lost due to reservoir mixing, miscibility is re-developed the same way as described above. Also, in order for multiple contact miscibility vaporization process to be successful, the reservoir fluid composition must lie to the right of the critical tie line. If both fluids lie to the left, vaporization will occur but not in sufficient quantities to develop miscibility. If the injection fluids and original oil both lie to the right of the critical tie line, the fluids are miscible on first contact.

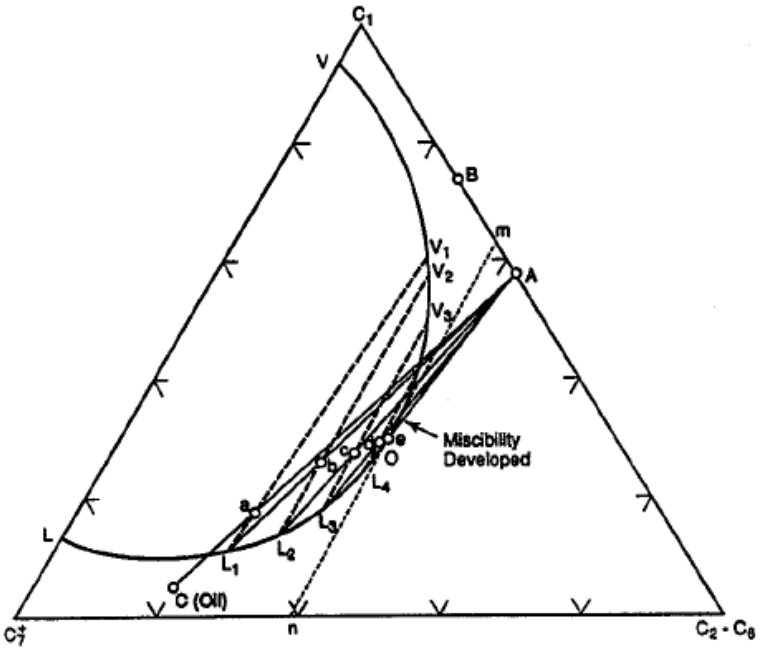

Figure 1-10 Concept of multiple contact miscibility by condensation [3]

Concept of multiple-contact miscibility by condensation is illustrated in Figure 1.10. The injected fluid generally contains larger amounts of intermediate molecular weight hydrocarbons. In this approach, reservoir oil near the injection well is enriched in composition by contact with the injected fluid since hydrocarbon components are condensed from the injected fluid into the oil. Under proper conditions, the oil will be sufficiently modified in composition to become miscible with additional injected fluid. Conceptually, the process is very similar to vaporizing process, except vapor phase V1, V2 moves ahead, leaving immobile liquid phase L1, L2 etc to mix with additional injected Gas A.

For multiple contact miscibility by condensation to occur, the injected fluid must be to the right of the critical tie line. If it is not, condensation of CO_2 into crude oil will still occur, however, miscibility will not be developed.

1.2 Motivations behind this study

The Arbuckle formation has played an important role in total Kansas oil production. These Arbuckle reservoirs have produced 2.19 billion barrel of oil by a bottom-water drive mechanism via an underlying aquifer, representing 36% of total Kansas oil production to date. Today, more than 90% of wells produce less than 5 barrel of oil per day.

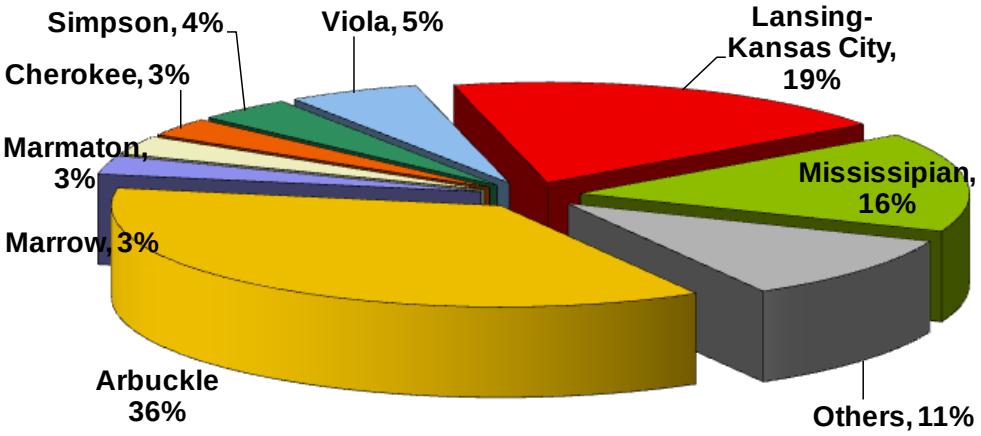

Figure 1-11 Oil production from Arbuckle formation in total Kansas oil production

Previous assessments of CO_2 miscible flooding in these Arbuckle reservoirs indicate that miscibility is not achievable at the current reservoir operating pressures. Therefore, the possibility of operating at pressures below the MMP means that these reservoirs, which might be otherwise abandoned with substantial remaining oil left in place, could be considered for CO_2 injection.

In addition, a lower-pressure process is attractive from both economic and operational standpoints, including purchasing smaller gas volumes and decreased gas compression costs.

In general, pressures below MMP are not high enough to vaporize sufficient oil into the CO_2 phase or to allow sufficient CO_2 to dissolve into the oil so that the two phases to become miscible. Loss of miscibility results in loss of oil recovery efficiency. Slim tube results usually show a dramatic loss of recovery at pressures below MMP. To date, however, conflicting experimental results have led to considerable disagreement in the literature regarding the feasibility of operating at pressures below MMP.

Shyeh-Yung et al. [7] studied the effect of operating pressure by conducting tertiary CO_2 displacements on two systems,

- System 1-Berea sandstone (strongly water wet)/CO_2/decane at 160^{o}F
- System 2-San Andres outcrop carbonate (mixed wet)/CO_2/ degassed west Texas separator oil 100^{o}F

Laboratory results presented in Figure 1.12 and Figure 1.13 showed that tertiary CO_2 flood oil recovery decreased linearly as pressure decreased. No dramatic loss of recovery was observed below the MMP as suggested by slim tube test results.

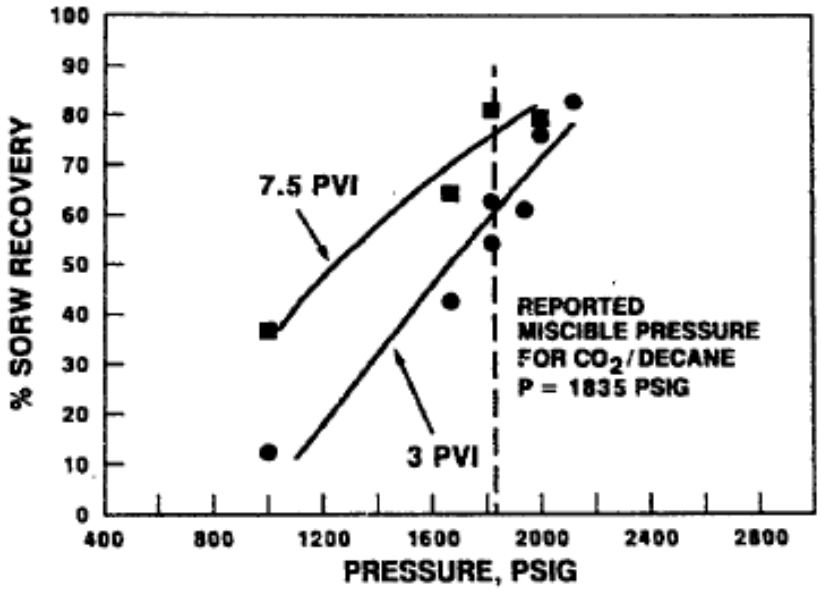

Figure 1-12 Effect of pressure and Pore Volume Injected on tertiary flood oil recoveries in System 1: CO_2/Decane/Berea [7]

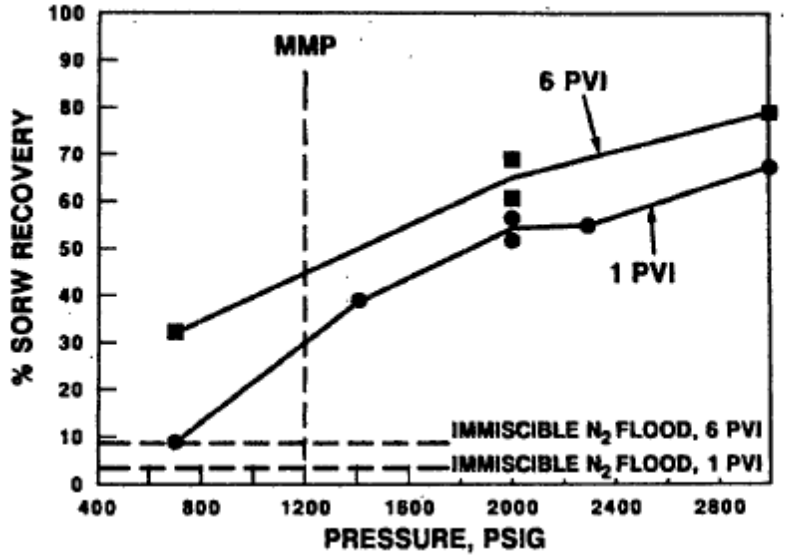

Figure 1-13 Effect of pressure and Pore Volume Injected on tertiary oil recoveries in System 2: CO_2/West Texas crude/Mixed-wet carbonate core at 100^{0}F [7]

The author attributed the high oil recoveries at pressures below MMP to the possible improvement of mobility ratio between CO_2 and oil, the low IFT displacement and mass transfer.

Schechter et al. [8] conducted coreflood tests and simulations to examine the possibility of optimizing the performance of Wellman Unit by reducing CO_2 injection pressure, thereby reducing the volume of CO_2. They found that dropping the pressure from above the MMP to near the MMP or below the MMP did not reduce the efficiency in laboratory coreflooding.

Similarly, a laboratory study on near-miscible CO_2 injection in Steelman Reservoir by Dong et al. [9] showed that the microscopic displacement efficiency improved with operating pressure in the near-miscible region, but no dramatic change in oil recovery was observed with a change in operating pressure.

In a recent overview of industrial experience with CO_2 injection, Hadlow [10] cited field data with good recovery at pressures below the CO_2 flood MMP in the North Cross and Dollarhide reservoirs while they were being pressured up.

In another effort by Grigg et al. [11]; however, a rapid decrease in oil recovery was noted as pressure fell below the MPMP for the CO_2 floods conducted at near the CO_2 critical temperature, as slim tube data showed. He also concluded that the concept of hydrocarbon gas injection is a more feasible concept, and this maybe the case for CO_2 injection at temperatures well above its critical temperature since the hydrocarbon floods did not

show a drastic change in oil recovery near the MMP, unlike the CO_2 floods. The residual oil saturations to gasflood as percent of oil after the waterflood are plotted vs. the ratio of the flood pressure to the slim tube MMP in Figure 1.14 to Figure 1.17.

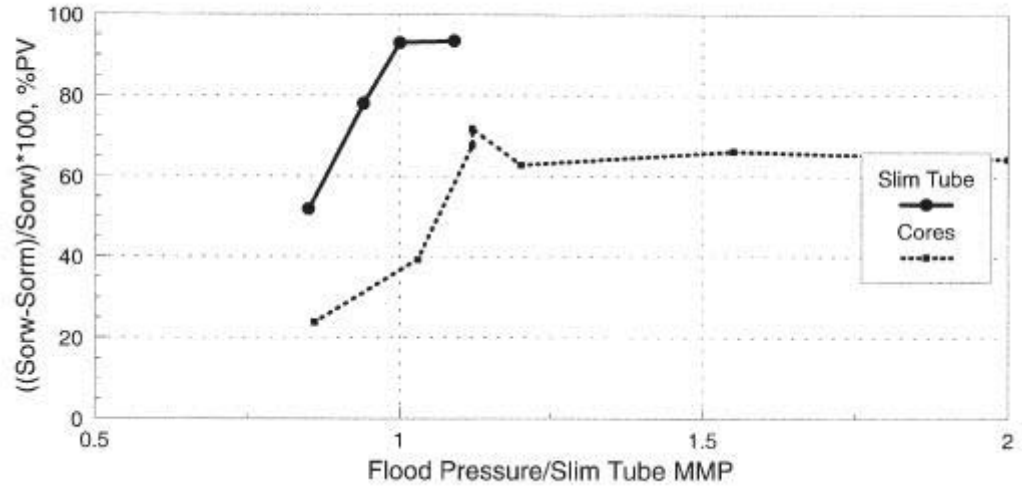

Figure 1-14 Comparison of Reservoir S CO_2 corefloods with Texas Cream limestone core and slim-tube tests [11]

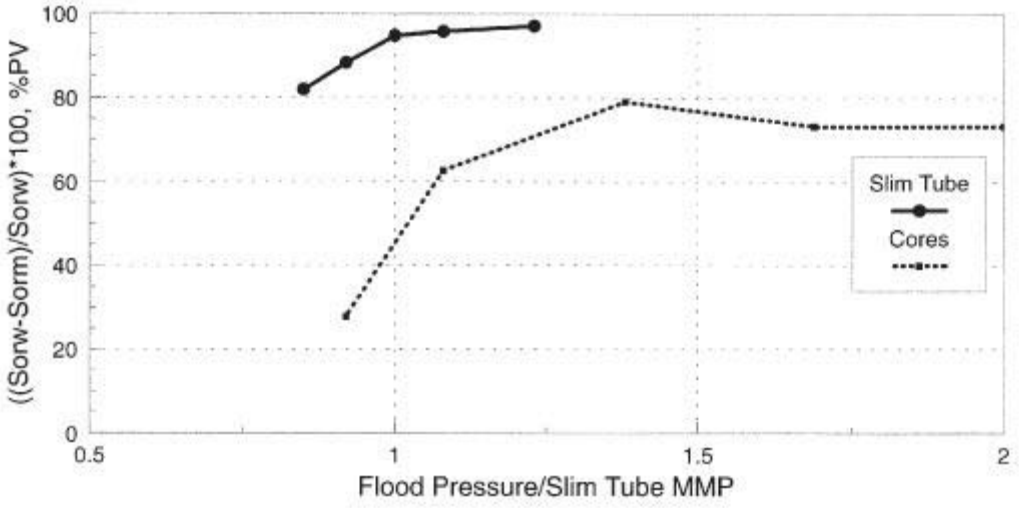

Figure 1-15 Comparison of Reservoir H CO_2 corefloods with Texas Cream limestone core and slim-tube tests [11]

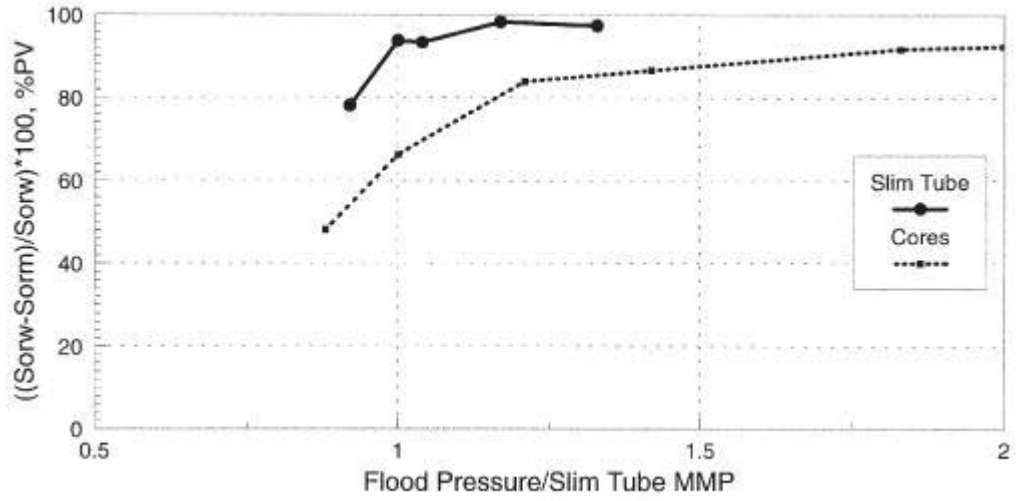

Figure 1-16 Comparison of Reservoir M CO_2 corefloods with Texas Cream limestone core and slim-tube tests [11]

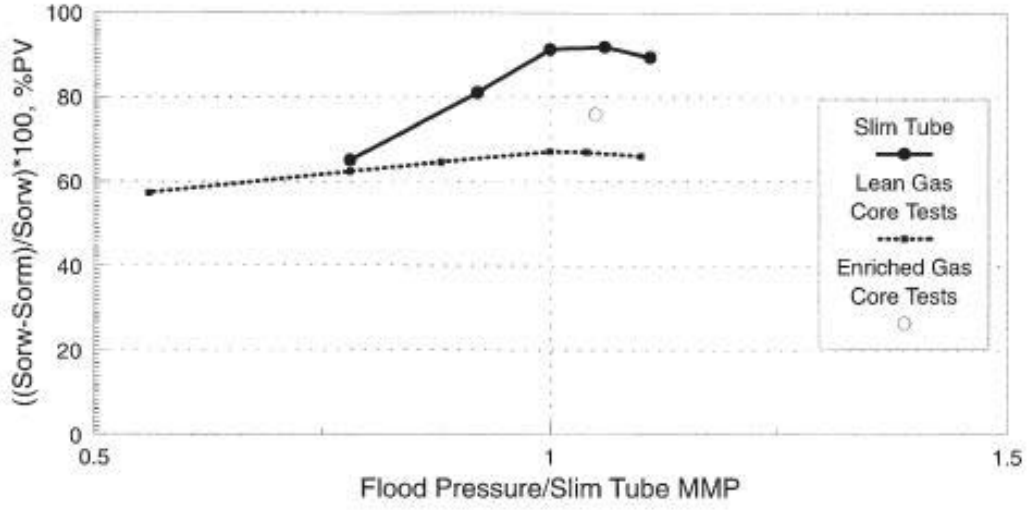

Figure 1-17 Comparison of hydrocarbon lean gas slim tube tests and Reservoir A corefloods [11]

Finally, the most important motivation behind the study is the environmental benefit of capturing and sequestering CO_2 emissions by utilizing an industrial source of CO_2. As significant volumes of injected CO_2 used in the displacement stay in the reservoir formation

and the produced CO_2 from the productions wells is recycled and re-injected into the reservoir, CO_2 emission into the atmosphere and its impact to the environment is very limit.

1.3 Objectives of the study

The objectives of this study are to (1) investigate the feasibility of near-miscible CO_2 application (2) improve our understanding of the mechanisms of near-miscible CO_2 flooding by conducting appropriate experimental work and reservoir simulation. The Arbuckle formation of Kansas is used as an example to demonstrate our approach to evaluate CO_2 flooding at near-miscible conditions. The suite of laboratory experiments used to evaluate the feasibility of operating at pressures below MMP for Arbuckle reservoirs includes phase behavior studies, core flow tests and phase behavior model construction using CMG software package.

The term near miscible is understood as the transition from immiscible to miscible. Near miscible refers to displacements at pressures slightly below MMP, where the recovery efficiency is improved over immiscible displacements. Since it is not clearly defined in the literature, the pressure range of interest in this study is from 0.8 MMP to MMP.

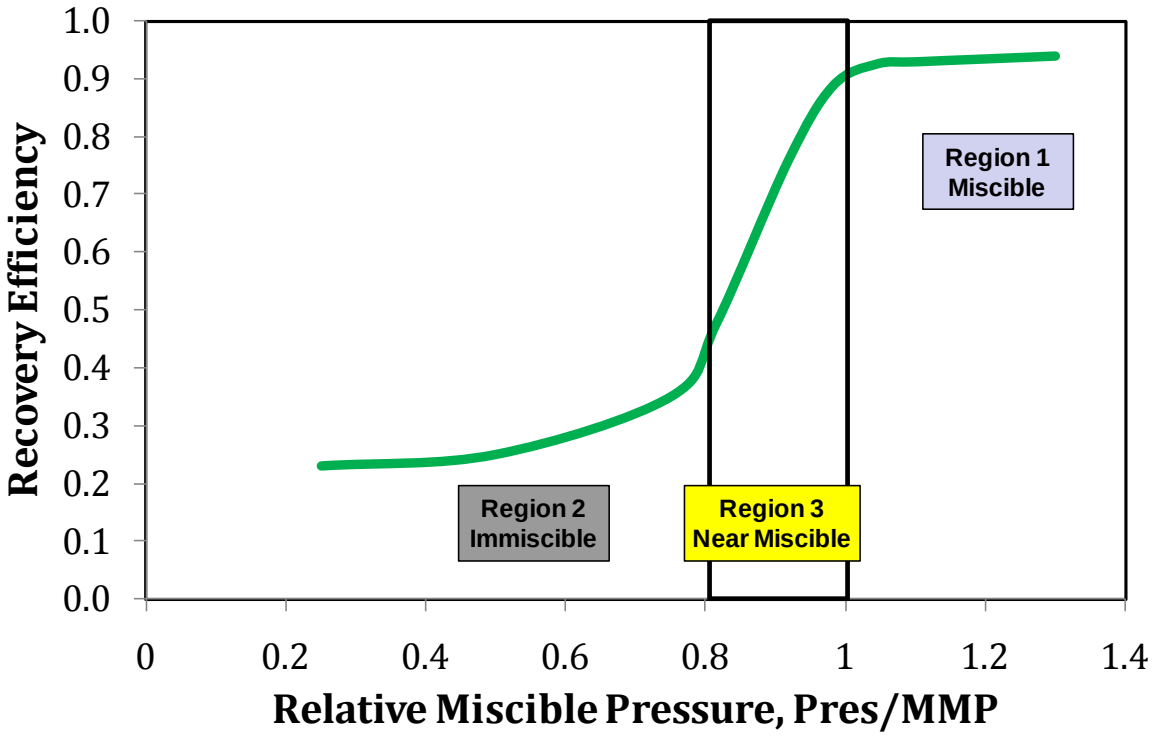

Figure 1-18 Generalized recovery response to pressure

2 Phase Behavior Studies

Phase behaviors studies are conducted for several purposes: (1) to characterize the oil/CO_2 system (2) to understand the mechanism of oil displacement by CO_2 (3) to provide experimental PVT data to fine-tune the phase behavior model.

Phase behavior studies included slim tube displacements, swelling/extraction tests and viscosity/density measurements. Slim-tube displacements were conducted to determine the minimum miscibility pressure for this system and to define the near miscible range. Swelling/extraction tests were performed to examine the mechanisms of oil recovery in the near miscible region. Viscosity of oil saturated with CO_2 was measured at various pressures. A phase behavior model based on the Peng-Robinson Equation of State (EOS) was constructed and well-tuned to characterize the fluid properties and the phase behavior interaction between CO_2 and the oil. Slim tube model was constructed using 1-D compositional simulation with tuned equation of state. Detail descriptions of phase behavior studies are presented and discussed in this chapter.

2.1 Fluid Properties

All experiments were performed with centrifuged and filtered Ogallah stock tank oil. The crude oil was centrifuged at the rate of 20 rpm for at least an hour to separate water, oil and solid particles. Two layers of glass microfibre filters with the size of 1.6 micron and 1

micron were used respectively to filter the crude oil. The location of the unit is shown in Figure 2.1. The crude oil was obtained from Ogallah Unit, Trego County, Kansas. The unit is currently operated by Carmen Schmitt, Inc. The unit produces from Arbuckle formation (3950-4060 ft). Reservoir temperature ranges from 92^{o}F to 130^{o}F with an average pressure of 111 ^{o}F. Active water drives have maintained reservoir pressure at approximately 1150 psi.

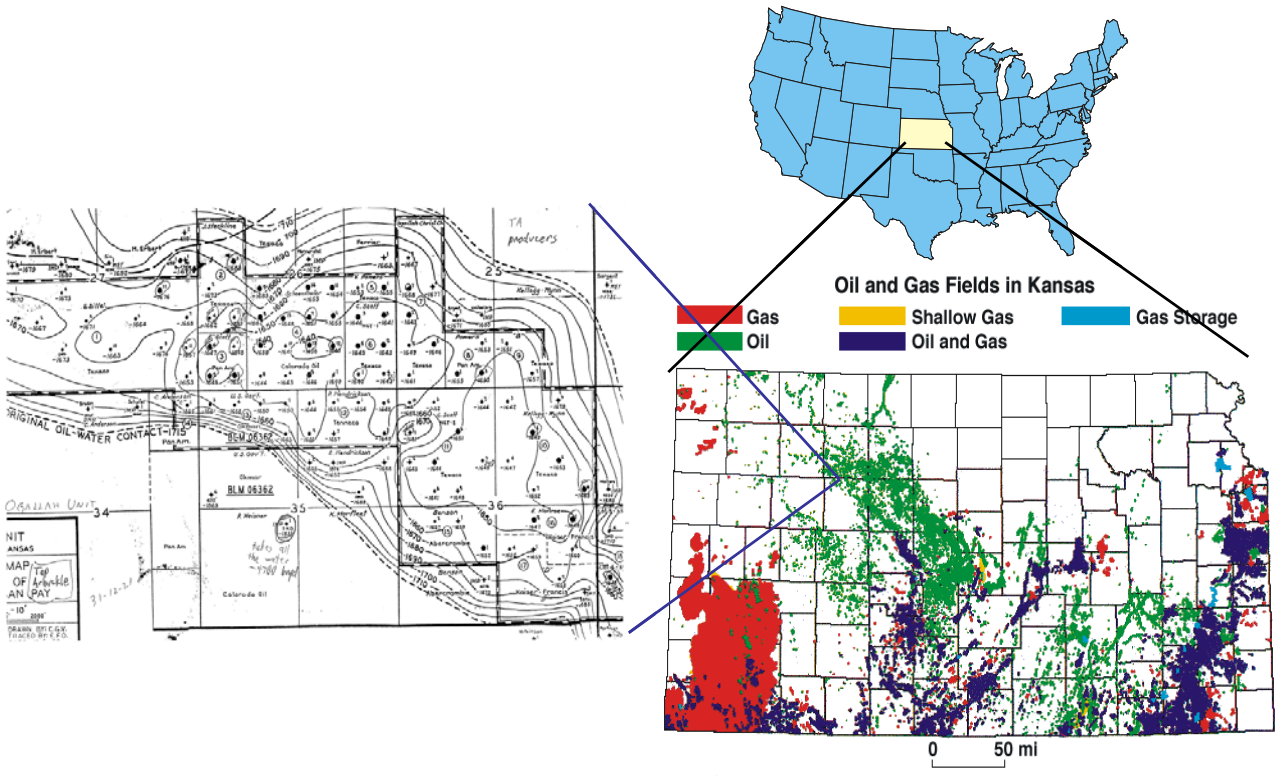

Figure 2-1 Ogallah Unit, Trego County, Kansas

A compositional analysis of the crude oil using Gas Chromatography (GC) technique was performed by Core Labs and shown in Figure 2.2. % Asphaltenes (heptane insolubles) was determined approximately 0.93 % based on ASTM D 893-85.

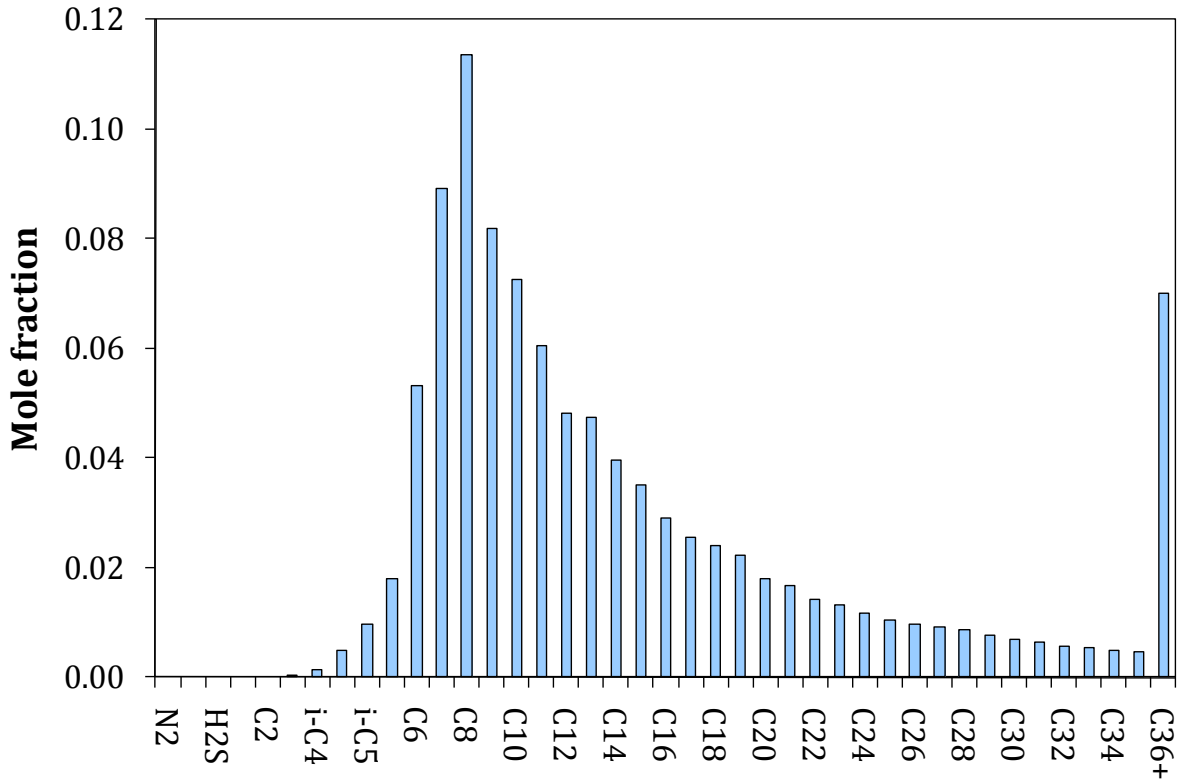

Figure 2-2 GC compositional analysis result of Ogallah crude oil

Core Labs also provided physical properties of the oil and the lumped heavy component C36+, as presented in Table 2.1.

Molecular Weigh, g/mol	228.71
API	33.34
Density @ 14.7 psi & 60°F, g/cc	0.8584
Viscosity @ 14.7 psi & 60°F, cp	13.4
C36+ molecular weight, g/mol	873.24
C36+ density @ 14.7 psi & 60°F, g/cc	0.9978

Table 2.1 Physical properties of Ogallah crude oil and the lumped heavy component C36+

Commercial CO_2 of 99.99 % purity was used

2.2 Slim Tube Displacements

The basis of slim tube tests is that the small-diameter tube filled with an unconsolidated porous medium serves as an idealized medium for CO_2 and crude oil to contact and develop dynamic miscibility. Non-idealities such as viscous fingering and gravity effect are ignored because of the large length to diameter ratio in slim tube configuration. Oil recovery is therefore attributed to the thermodynamic phase behavior of the system. The recovery performance at different pressures can be used to determine the MMP. Slim tube tests have not only been used to determine reservoir candidates for miscible processes but also widely used for fine tuning the reservoir simulator.

In this study, a number of slim tube displacements were conducted for a range of pressures, holding the temperature constant at the reservoir temperature (110^oF-125^oF) to determine the MMP of this system. An oil recovery factor of at least 90% at 1.2 HCPV of CO_2 injected is used to define the MMP of the system.

2.2.1 Experimental Setup and Specifications

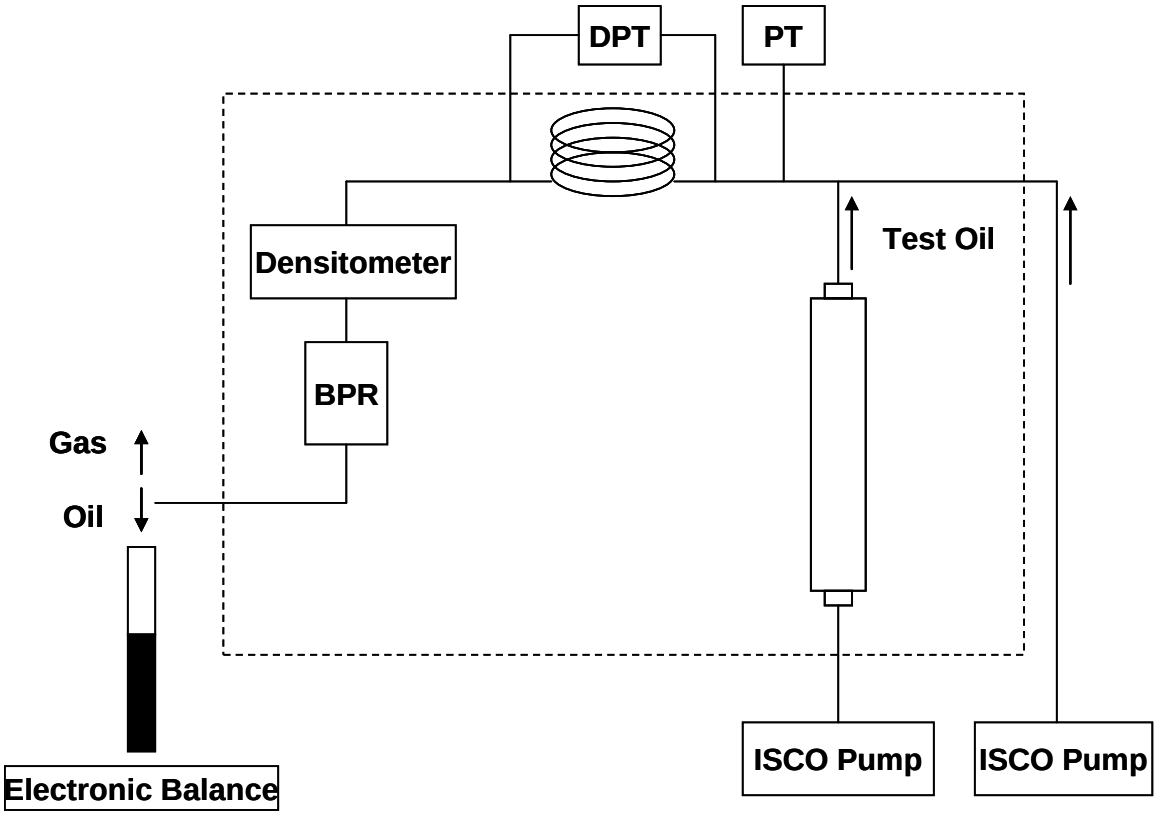

Figure 2-3 Schematic of slim tube setup

Schematic of the slim tube setup is shown in Figure 2.3. Temperature of the system is controlled and maintained in a Linberg/Blue M oven with Eurotherm temperature controller. Pressure of the system is controlled and maintained by a back pressure regulator at the outlet. Back pressure regulator models BPR-50 is a dome-load type, which controls the upstream back pressure to whatever pressure is applied to the dome. It is designed to operate using compressed gas in the dome and water, oil, gas in the body. A

high pressure bottle of inert gas, such as nitrogen, is required to pressurize the unit. The back pressure regulator has a working pressure of 5000 psi at 200^{o}F.

Three Valydine pressure transducers are installed to measure pressures at different locations, such as pressure drop across the slim tube, upstream pressures (CO_2/oil pressure), and downstream pressure (back-pressure regulator pressure). The transducers have the capability of measuring pressures up to 2500 psi with the accuracy of 0.25% of their full scale (0-2500 psi).

The injection system consists of two Isco, Inc. 260DM syringe pumps (for CO_2/crude oil transfer and injection at a desired rate) and a transfer cylinder (for crude oil storage). The capacity of the transfer cylinder is 485 cc. The cylinder can withstand a maximum pressure of 3000 psi.

The slim tube consists of a coiled 38.29 ft-long stainless steel tube with an ID of 0.24 in. packed with glass beads. Slim tube properties were evaluated by Rahmatabadi [12] and listed in Table 2.2.

Length, ft	38.29
O.D, in	0.31
I.D, in	0.24
Porosity	0.37
Bulk volume, cc	347.8
Pore volume, cc	127.76
Permeability, mD	4900
Packing beads	No. 2024

Table 2.2 Slim tube properties

Density of the effluent is measured continuously by an inline densitometer. The densitometer consists of two units. The DPRn 422 density transducer measures the characteristic frequency of vibration. The Anton Paar mPDS 2003V3 Evaluation unit translates the characteristic frequency of vibration into a density value. The measuring range is 0-3g/cc within the temperature range of -13^{o}F – 257^{o}F and the pressure range of 0-2900 psi.

Effluent is continuously flashed to atmospheric conditions. The separator gas is connected to a flow meter. The separator liquid is collected in a graduated cylinder. The graduated cylinder is placed on an electronic balance which is connected to the data acquisition system.

2.2.2 Experimental Procedures

At least 2 PV of methylene chloride followed by 2 PV of mineral oil were injected to clean the slim tube prior to the experiment. The slim tube was then saturated with at least 2 PV of crude oil at the desired temperature. While the slim tube was being saturated with crude oil, the system was pressurized gradually to the desired operating pressure using the back pressure regulator. Upstream pressure changed accordingly to the pressure of the back pressure regulator as it was set. To prevent pressure from one side of the diaphragm of the back pressure regulator from becoming significantly higher than the pressure on the other side and damage the diaphragm, it was necessary to pressurize the system slowly, for

example, 0-100 psig, switch off the gas supply valve and wait for the upstream pressure to catch up with the downstream pressure. Once the desired pressure was reached, the system was allowed to equilibrate under pressure. Pressure of the CO_2 pump was set slightly above the pressure of the back pressure regulator. Temperature of the pump was set at temperature of the system. CO_2 flow rate was set at a constant of 0.05cc/min. This corresponds to a Darcy velocity of 8 ft/day.

A log file was created to record the following parameters: temperature of the system, pressure of the system (back-pressure regulator pressure/downstream pressure), upstream pressures (CO_2/oil pressure), pressure drop across the slim tube, weight of the separator liquid, and separator gas flow rate. The initial and final volumes of CO_2 in the pump were recorded manually.

The experiment was terminated when at least 1.2 HCPV of CO_2 at the temperature and pressure of the pump were injected. The system was depressurized by venting the dome load gas slowly. Residual oil in the slim tube was removed by following the same cleaning procedure as mentioned earlier.

The entire experiment was then repeated several times at different pressures holding other variables constant.

2.2.3 Results and Discussions

Slim tube displacements were conducted at 110°F and 125°F representing the range of temperatures reported from the field. The effluent was observed when it was flashed to the atmosphere during the displacement. A gradual change of color of the flowing fluid from the oil to clear gas was observed for pressures above MMP. Two-phase flow was observed for pressures below MMP. Gas breakthrough was seen earlier from displacements at pressures below MMP compared with displacements at pressures above MMP.

The recovery results of slim tube displacements at 110°F and 125°F are presented in Figure 2.4 and Figure 2.5.

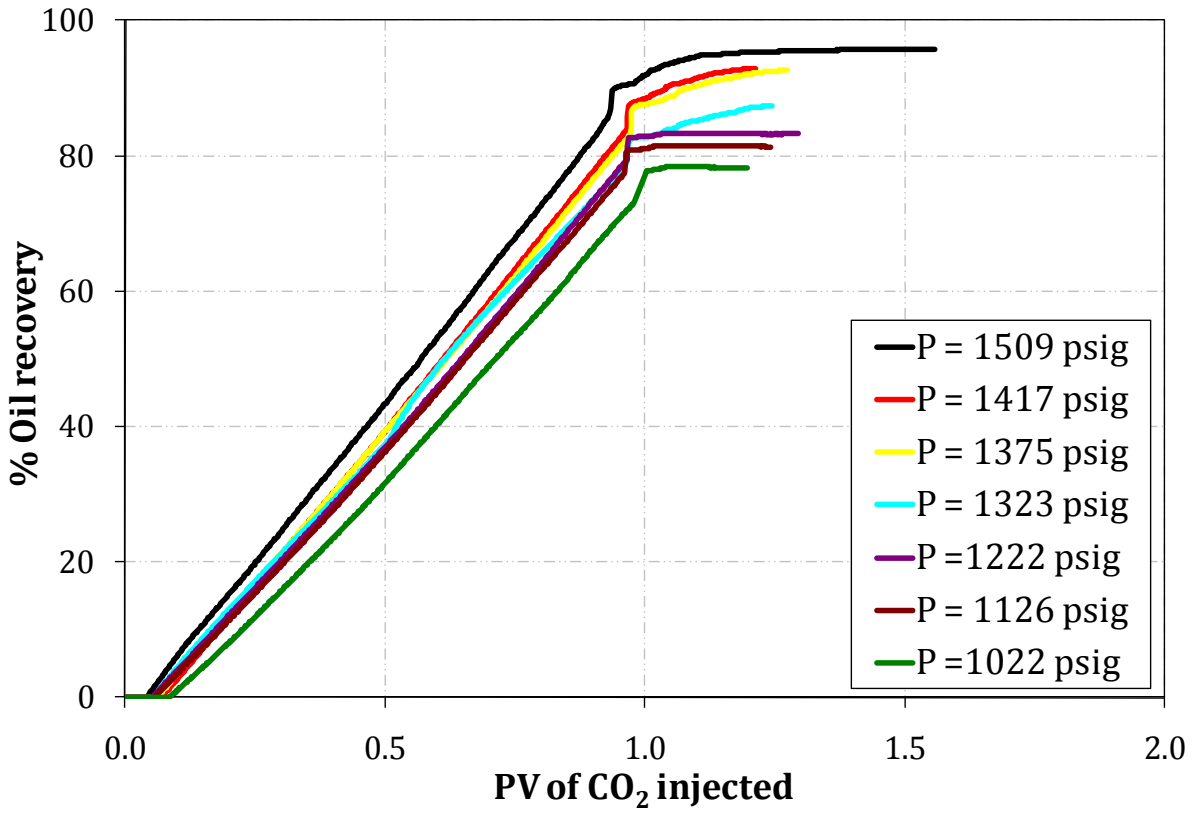

Figure 2-4 Results of displacement tests at 110°F

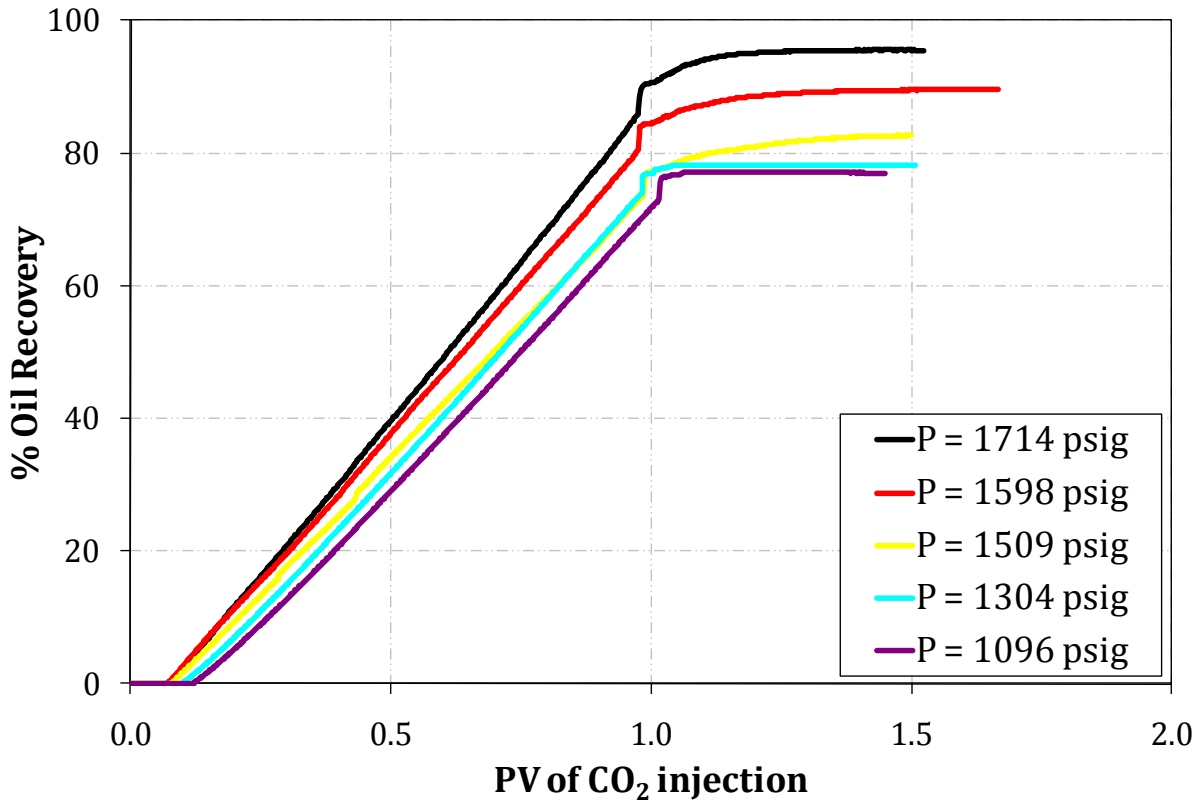

Figure 2-5 Results of displacement tests at 125°F

% oil recovery was calculated as follows:

$$\%\ oil\ recovery = \frac{Weight\ of\ \ oil\ \ produced}{Pore\ Volume \times Oil\ \ density} \times 100\%$$

Pore volume (PV) of CO_2 injected was calculated as follows:

$$PV = \frac{time \times CO_2\ \ flow\ rate}{Pore\ Volume}$$

Percentage of oil recovery at 1.2 PV of CO_2 injected was plotted against slim tube average pressure to determine the MMP of the system at 110°F and 125°F, as shown in Figure 2.6. MMP of the system were estimated to be 1350 psig at 110°F and 1650 psig at 125°F. As expected, MMP increases with increasing temperature. This phenomenon is closely related to the dependence of CO_2 density on temperature and pressure and is explained in detail in the discussion of the next experiment.

Slim tube results indicated that miscibility was not achievable at the current reservoir pressure of 1150 psig; however, the recovery efficiency was relatively high, 78% - 83% of the original oil in slim tube for a temperate range of 110°F to 125°F and at 1150 psig.

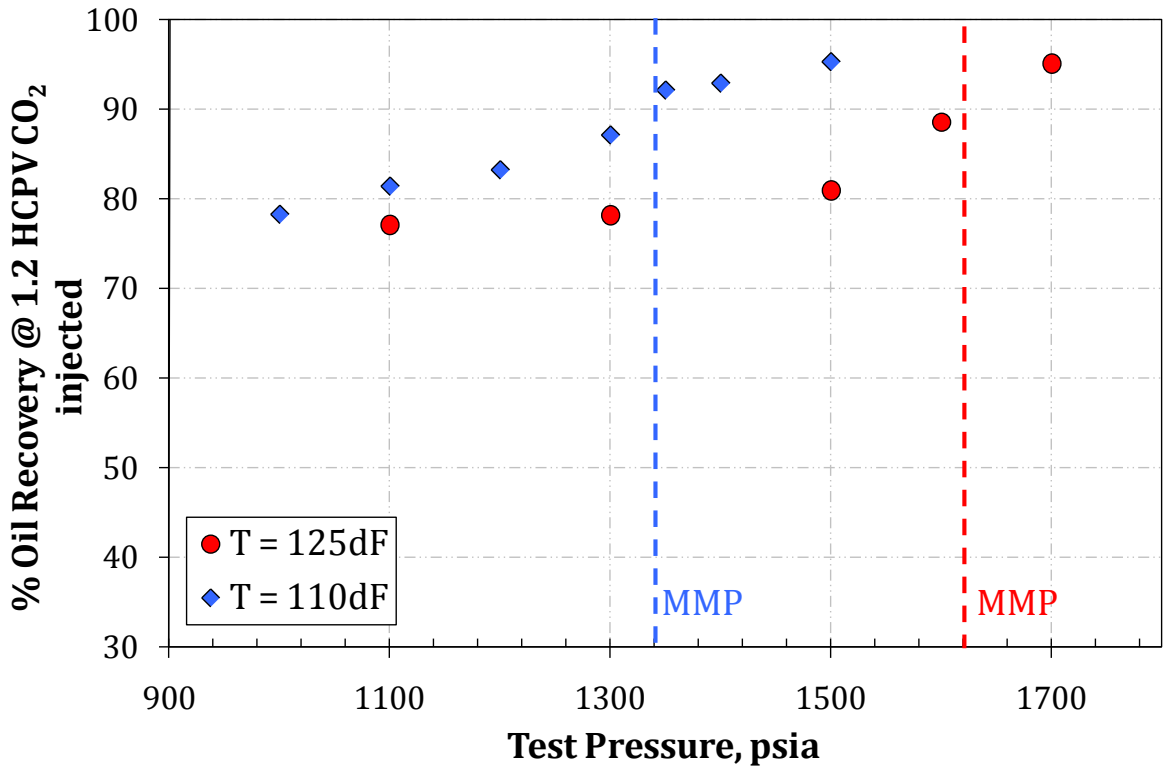

Figure 2-6 Minimum miscibility pressure determinations at 110°F and 125°F

Since the MMP of this oil was determined to be 1350 psig at 110°F and the near miscible range was selected from 0.8MMP to MMP in this study, the near miscible region for this particular oil is defined from 1100 psig to 1350 psig at 110°F.

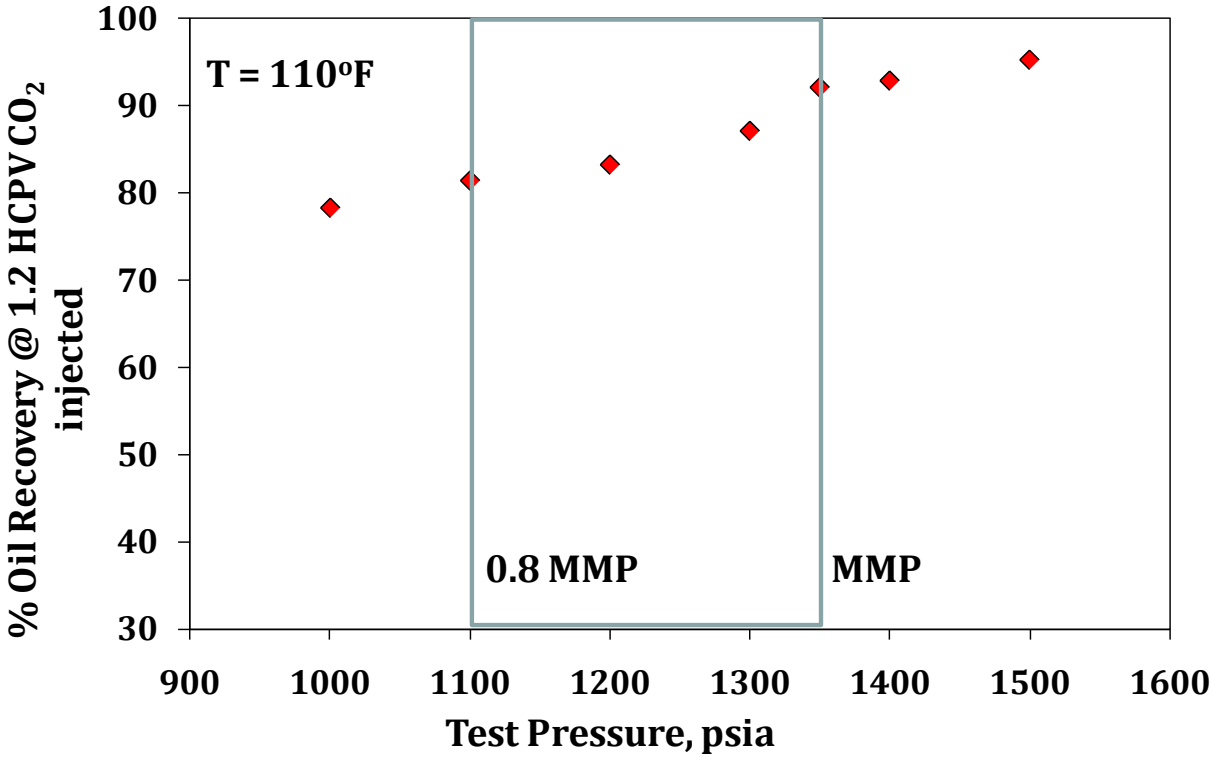

Figure 2-7 Near miscible region for Ogallah crude oil at 110°F

Figure 2.8 and Figure 2.9 show the density profile of the effluent at 110°F and 125°F. Density of the effluent was the same as density of crude oil at 110°F and at slim tube average pressure prior to CO_2 breakthrough. The abrupt change in density of the effluent corresponded to CO_2 breakthrough. Density of the effluent was much less than density of the oil but higher than density of pure CO_2 at pressures below MMP, which is the result of two-phase flow with liquid dispersed in the CO_2 rich phase through the densitometer. For instance, densities of pure CO_2 at 1022, 1126 and 1222 psig and 110°F are 0.19001,

0.23306 and 0.29009 g/cc, compared with densities of the effluent at the corresponding pressures and temperature, 0.296, 0.415, and 0.527 g/cc.

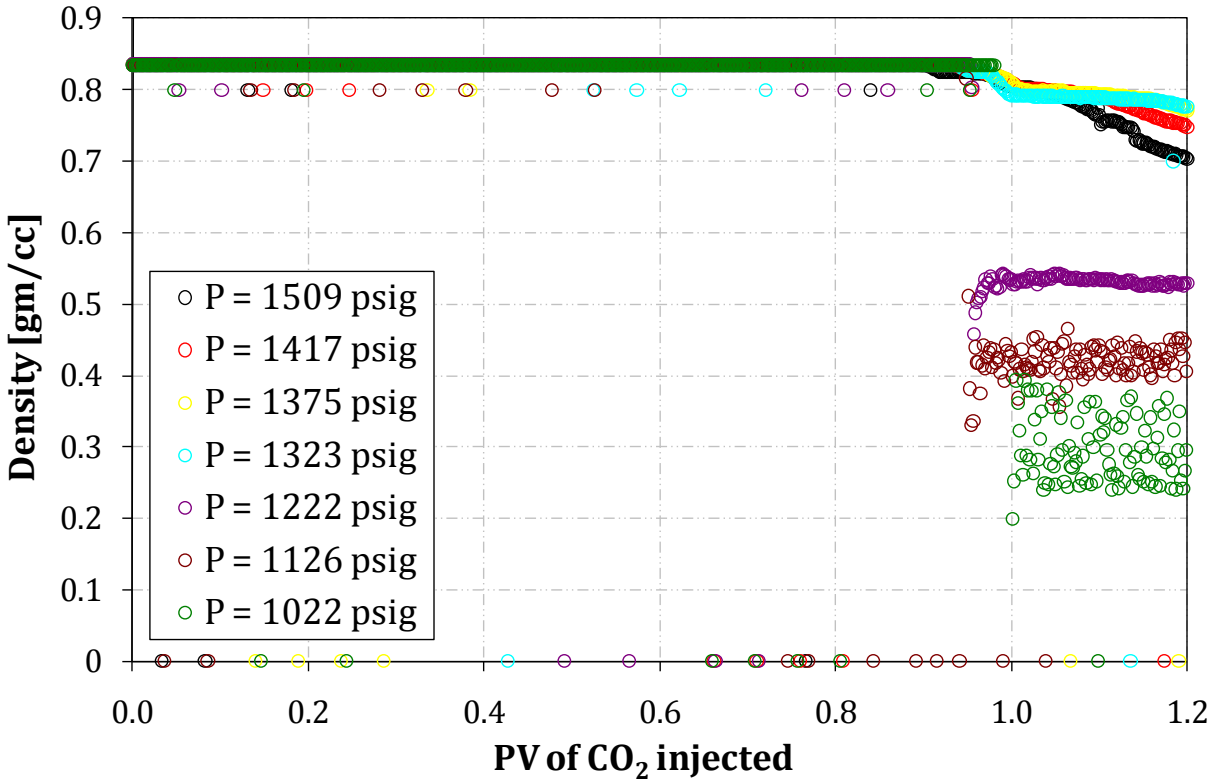

Figure 2-8 Density profile of the effluent at 110°F

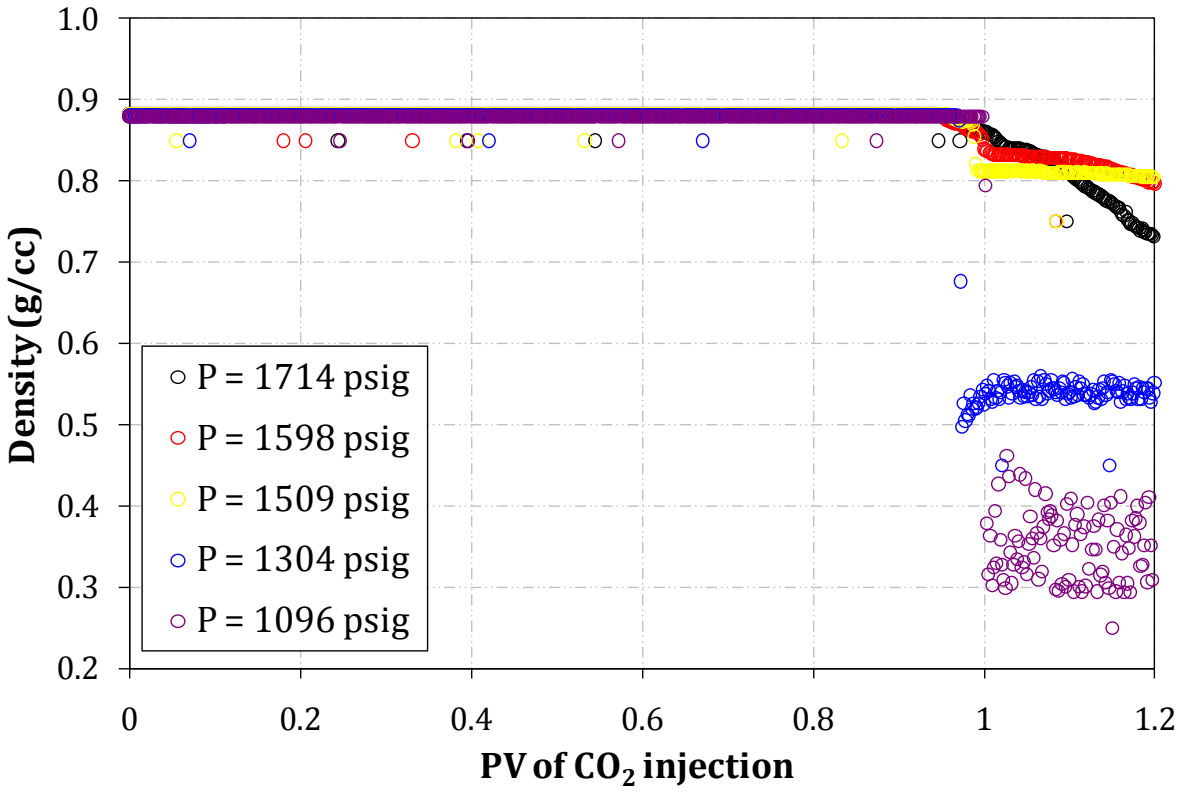

Figure 2-9 Density profile of the effluent at 125°F

2.2.4 Conclusions

- MMP was estimated to be 1350 psig at 110°F and 1650 psig at 125°F. Miscibility is therefore not achievable at the current reservoir pressure of 1150 psig.
- Near miscible range is defined from 1000 psig to 1350 psig at 110°F in this study.
- 78% - 83% of the original oil in place was recovered at the current reservoir pressure of 1150 psig and at a temperature range of 110°F to 125°F.

2.3 Swelling/Extraction Tests

Swelling/extraction tests were performed to examine the oil recovery mechanisms in the near-miscible region and to provide data to tune the phase behavior model. Swelling tests were conducted to determine the relationship between saturation pressure, swelling factor and CO_2 volume injected. Extraction tests were carried out to examine the extraction of liquid hydrocarbon into a CO_2-rich phase and the effect of pressure on the extraction.

2.3.1 Experimental Setup and specifications

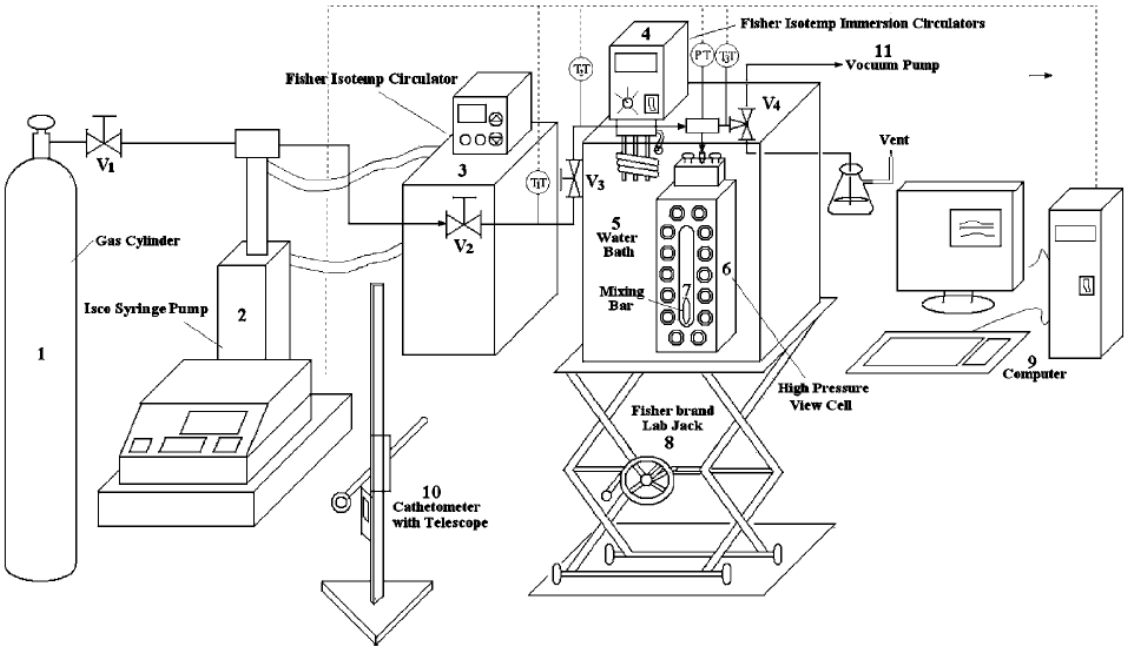

Figure 2-10 Experimental setup include (1) Gas cylinder (2) Isco Syringe pump (3) Fisher Isotemp circulator (4) Fisher Isotemp Immersion circulator (5) water bath (6) high pressure view cell (7) mixing bar (8) laboratory jack (9) computer (10) cathetometer with telescope (11) vacuum pump [13]

The schematic of swelling/extraction setup is shown in Figure 2.10. An Isco, Inc. 100DM syringe pumps is used for CO_2 injection. Temperature of the pump is controlled by a Fisher, Inc. Isotemp circulator, model 3016 and measured by an Ertco-Eutechnic 5 digit thermister, model 4400 in the range of 0-100^{o}C.

The gas lines are heated using fiberglass covered heating tape, controlled by two variable AC transformers, Staco Energy model 3PN1010B. Temperature of the gas lines is measured using T-type thermocouples. Fiberglass cloth tape is used to prevent heat dissipation to the surroundings.

The key component of this setup is the high pressure view cell with high pressure gauge glass window allowing visual observations of fluids under experimental conditions. The view cell is made of stainless steel and has a volume of 26 cc. The gauge glass window allows a maximum temperature of 280^{o}C and pressure of 4000 psi. Pressure in the view cell is measured by a 5000 psi Heise DXD Series 3711 precision digital pressure transducer. A 3.2mm diameter × 12.7 mm PTFE coated stir bar is placed inside the view cell. Mixing is achieved by an external rare-earth magnet in a slot behind the cell raised and lowered by a pulley system.

The view cell is immersed into the water bath by raising/lowering the platform jack. The temperature of the water bath is adjusted by an immersion circulator Haake DC30/DL3 and a Fisher, Inc. Isotemp circulator, model 3016.

An Eberbach 5160 cathetometer is used to measure the height of the liquid in the view cell.

Figure 2-11 An actual image of the swelling/extraction experimental setup

2.3.2 Experimental Procedures

The pump was filled with CO_2. Temperature of the pump was set constant and above the critical temperature of CO_2 (31.1^{o}C). Pressure of the pump was set constant at the maximum anticipated pressure. The pump automatically adjusted the volume of CO_2 to achieve constant temperature and pressure. Temperature of the gas lines was set at

temperature above the critical temperature of CO_2 to avoid CO_2 condensation inside the lines. Temperature of the water bath was set constant at the desired temperature.
A predetermined volume of crude oil was carefully injected into the view cell to avoid liquid droplets on the wall of the view cell. The view cell was attached to the gas lines and then immersed into the water bath.

When the whole system was thermally equilibrated, the gas lines and the view cell were quickly flushed with CO_2 at low pressure to remove any residual gas or air.

A log file was created to record the following parameters: the pump condition (temperature, pressure and volume of CO_2), the temperature of the gas lines, the view cell condition (temperature and pressure). The height of the liquid sample in the view cell was recorded manually. Initially conditions should also be recorded manually.

The cell pressure was increased in discrete steps by CO_2 injection from the top of the view cell. CO_2 injection was stopped when a desired pressure was achieved. CO_2 flow rate was kept slowly so that there was no PVT disturbance. This was done by checking the pump pressure frequently to make sure the pump pressure did not drop too much from the set pressure. Final volume of CO_2 in the pump was recorded when CO_2 flow rate is read zero.

During pressurization process, the time required for the contents in the view cell to equilibrate under a particular pressure and temperature is minimized by magnetically stirring. At that time, the following parameters were recorded manually: the height of the

liquid sample in the view cell, the pump condition (temperature, pressure & final volume of CO_2), temperature of gas lines and the view cell condition (temperature & pressure).

In the end, the view cell was cleaned with methylene chloride, acetone solution and blown dry with compressed air.

2.3.3 Experimental Principles

The phase equilibria data were obtained based on a mass balance and the following assumptions:

- The pressure of CO_2 is much greater than the vapor pressure of the crude oil
- Vapor phase composition of the hydrocarbon component is much less than CO_2

The mass balance equation of CO_2 is as follows:

$$m_g = m_{pump} - m_{lines} - m_{headspace} + m^o{}_{lines} + m^o{}_{headspace}$$
$$m_{pump} = \Delta V_{pump}\rho(T_{pump}, P_{pump})$$
$$m_{lines} = \Delta V_{lines}\rho(T_{lines}, P)$$
$$m_{headspace} = \Delta V_{headspace}\rho(T, P) = \left(V_{cell} - V_{liquid}\right)\rho(T, P)$$
$$m^o{}_{lines} = \Delta V_{lines}\rho(T_{lines}, P^o)$$
$$m^o{}_{headspace} = \Delta V_{headspace}\rho(T, P^o) = \left(V_{cell} - V_{liquid}\right)\rho(T, P^0)$$

Where

m_g is the mass of CO_2 dissolved in the liquid

m_{pump} is equal to the product of volume of CO_2 displaced from the pump and density of CO_2 at the pump constant temperature & pressure

m_{lines} is equal to the product of volume of the lines and density of CO_2 at temperature of the lines & system equilibrium pressure

m^o_{lines} is equal to the product of volume of the lines and density of CO_2 at temperature of the lines & system initial pressure

$m_{headspace}$ is equal to the product of volume of the headspace and density of CO_2 at temperature & pressure of the equilibrium system. The volume of the headspace is the difference between volume of the cell and volume of the liquid in the cell.

$m^o_{headspace}$ is equal to the product of volume of the headspace and density of CO_2 at temperature & pressure of the initial system. The volume of the headspace initially is the difference between volume of the cell and initial volume of the liquid in the cell.

CO_2 density was calculated using REFROP database which used the ultra-accurate Span-Wagner equation of state.

Mole fraction of CO_2 in the liquid phase was calculated as follows:

$$x_g = \frac{n_g}{n_g + n_l} = \frac{m_g / M_g}{m_g / M_g + m_l / M_l}$$

2.3.4 Apparatus Validation

The apparatus was verified by comparing experimental data obtained from this apparatus with literature data for n-decane/CO_2 mixture at 71.1°C by Ren et al. [13]. The experimental data had excellent agreement with the literature data obtained from different experimental methods.

Phase equilibrium data of CO_2/n-decane at 71.1°C was obtained and shown in Table 2.3.

Run 1		Run 2	
Pressure, psi	x_{CO2}	Pressure, psi	x_{CO2}
192.18	0.09609	209.43	0.10900
425.25	0.21070	434.97	0.22498
701.98	0.34940	643.68	0.32669
1005.55	0.50260	866.89	0.44391
1270.24	0.61657	1080.39	0.52821
1448.35	0.69121	1321.58	0.64927
1531.45	0.72330	1495.77	0.71555
1666.05	0.77723	1612.38	0.76148
		1709.41	0.80048
		1771.35	0.82829

Table 2.3 Phase equilibrium data of CO_2/n-decane at 71.1°C

Analysis of this data was based on the assumption that the amount of liquid component in the vapor phase is negligible. Although the composition of the vapor phase was not actually analyzed in our experiments, it had been demonstrated earlier by Ren et al. [13] that the percentage of n-decane in CO_2 vapor phase was less than 0.13%. Figure 2.12 shows that the p-x phase equilibrium of CO_2/n-decane generated using this apparatus were reproducible and in excellent agreement with literature data, Nagarajan & Robinson, Jr. [14] and Jennings & Schucker [15], and therefore, it could be used for crude oil/CO_2 system.

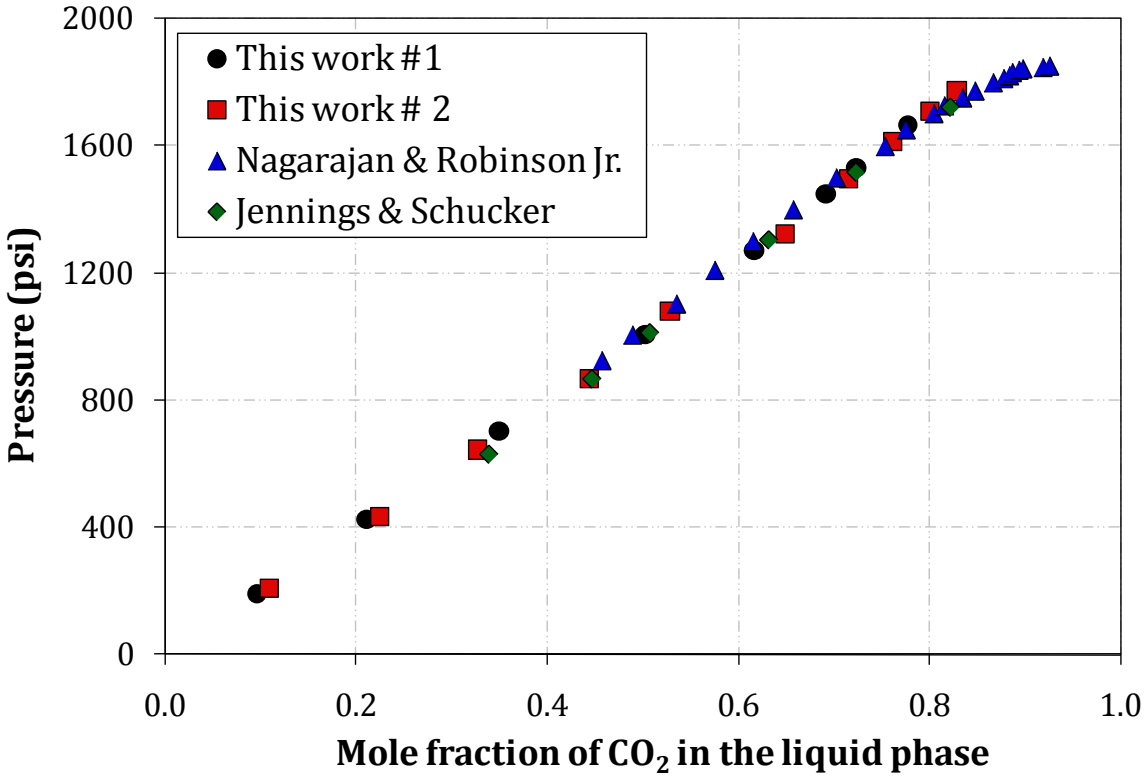

Figure 2-12 Comparison of liquid phase compositions for CO_2+ n-decane system at 71.10°C (160°F) with literature data (○) this work (□) this work (Δ) Nagarajan & Robinson Jr. (◊) Jennings & Schucker

2.3.5 Results and Discussions

Effect of each variable, temperature, pressure and initial volume on CO_2/oil phase behavior was investigated while holding others constant.

2.3.5.1 Effect of System Pressure

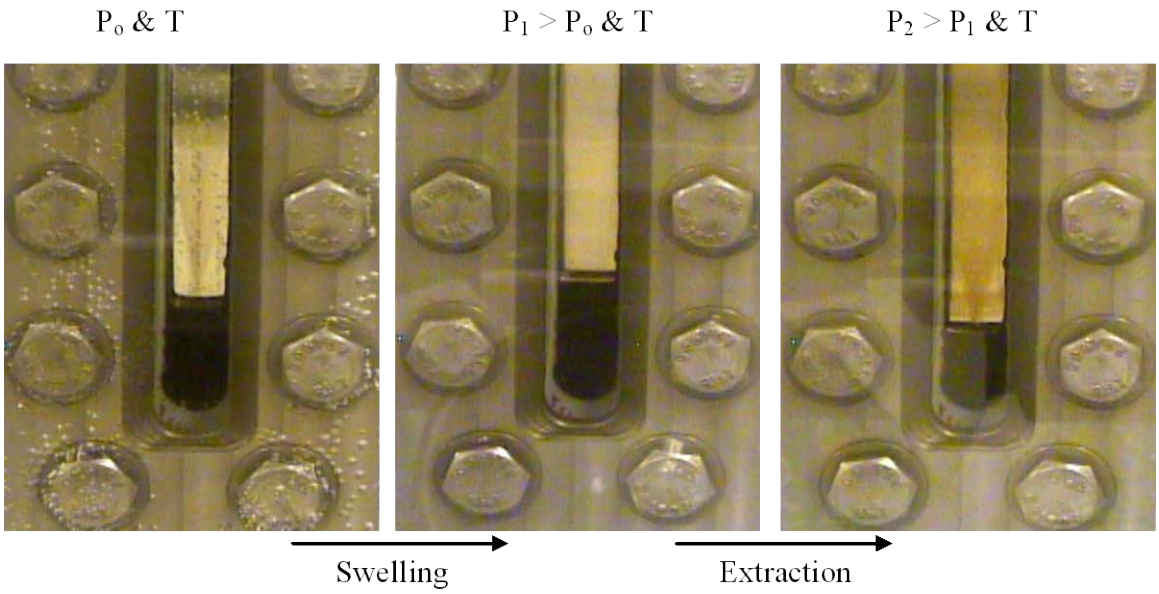

Figure 2-13 Change of initial oil volume with pressure

Figure 2.13 illustrates the observations of Ogallah oil/CO_2 phase behavior. Volume of the fluid in the view cell increased with increasing pressure since CO_2 dissolved in and swelled the oil. As pressure was further increased, CO_2 density increased. Since dense-phase CO_2 had the ability to extract hydrocarbon components from crude oil more easily than if it were in the gaseous phase, CO_2 started vaporizing or extracting hydrocarbons from crude oil, volume of the fluid in the view cell was therefore reduced.

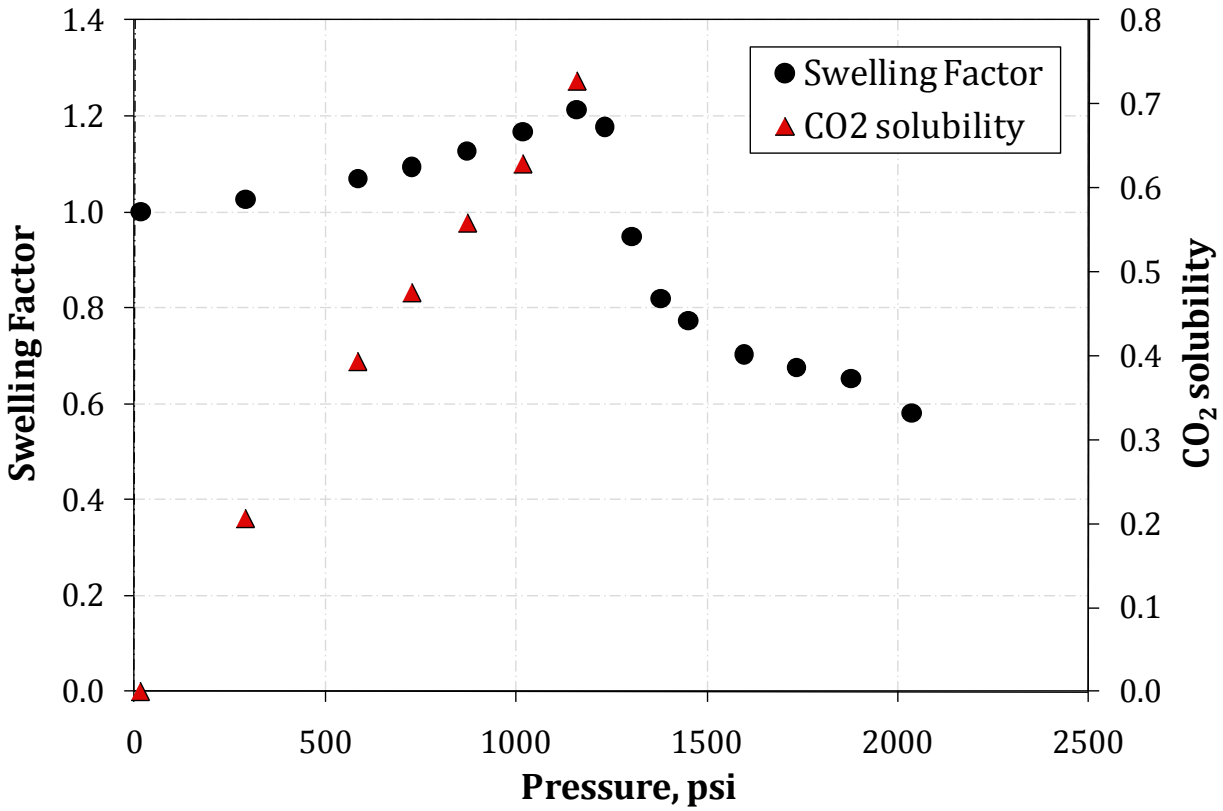

Figure 2-14 Effect of pressure on CO_2 solubility and swelling factor at 110°F

Figure 2.14 shows the swelling/extraction curve for Ogallah/CO_2 system at 110°F with the sample size of 3 cc. The sample volume was about 11 % volume of the view cell. The swelling factor (SF) of oil is the ratio of liquid volume at test pressure divided by the liquid volume at atmospheric pressure and at 110°F. This value is determined by measuring the change of the interface level as a result of CO_2 dissolution in the oil or as a result of hydrocarbon extracted into the CO_2 rich vapor phase. Swelling factor was equal to 1 at initial conditions. As a result of CO_2 dissolution into the liquid phase, the liquid phase swelled and the swelling factor was greater than 1. Maximum swelling occurred at 1158 psi, when volume of the liquid phase became 1.21 of its original volume with 0.728 mole

fraction of CO_2 dissolved in the liquid phase. Major extraction started at approximately 1158 psi. As pressure increased, hydrocarbon components of the crude oil were removed from the liquid phase, the liquid phase shrank and swelling factor was reduced. At 2035.2 psi, the volume of CO_2 rich liquid phase shrank as much as 39.2 % of its original volume. CO_2 solubility is also plotted in Figure 2.15 as a function of pressure up to 1158 psi. Calculations of CO_2 solubility at pressures above 1158 psi are invalid since the assumption that the components of the liquid phase do not vaporize does not hold true.

Extraction or vaporization of hydrocarbon components from crude oil appears to be the primary oil recovery mechanism in the near miscible range, 1100 psig to 1350 psig.

2.3.5.2 Effect of System Temperature

Swelling/extraction experiments were performed under various temperatures from 105^{o}F to 125^{o}F.

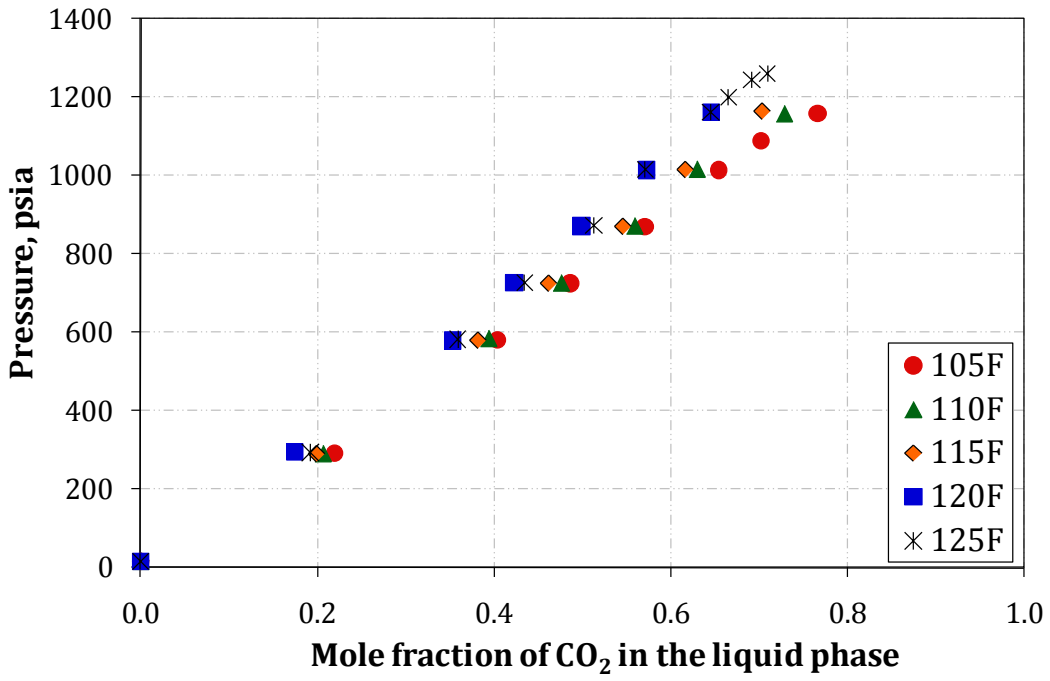

Figure 2-15 Effect of temperature on CO_2 solubility

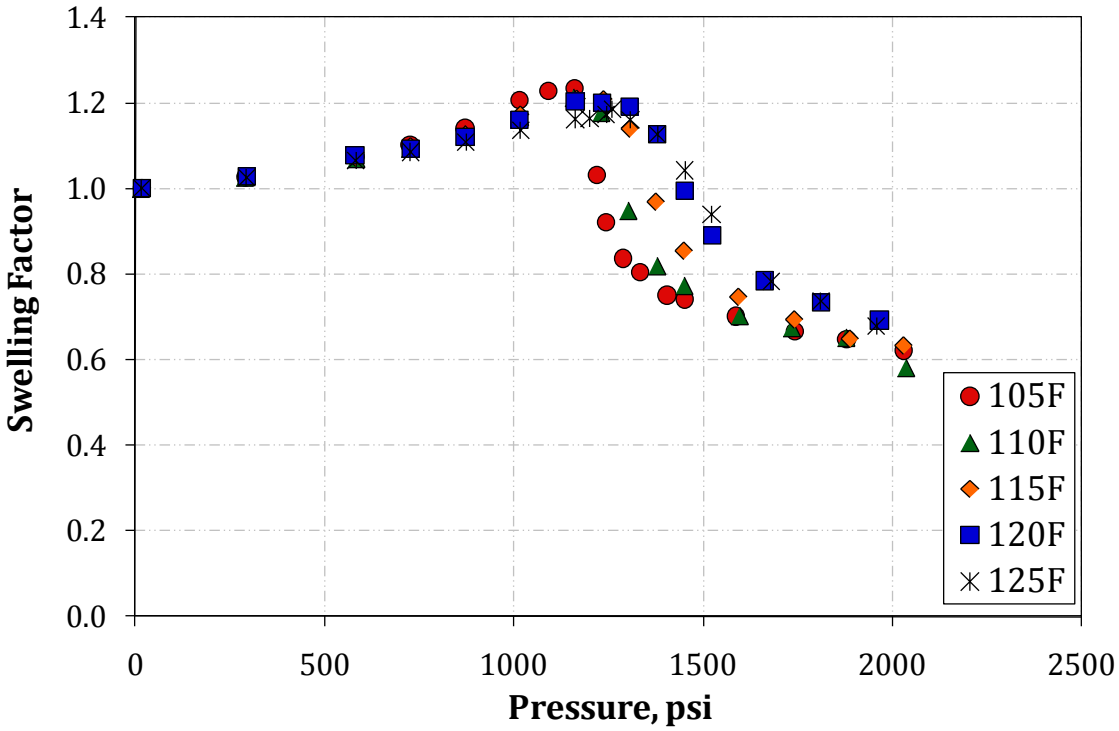

Figure 2-16 Effect of temperature on Swelling/ Extraction curves

Effects of temperature on CO_2 solubility and oil swelling/extraction curve are shown in Figure 2.15 and Figure 2.16. CO_2 solubility increased with increasing pressure and decreased with increasing temperature. The rate of oil swelling decreased with increasing temperature. The pressure at which oil swelling reached maximum or at which CO_2 began extracting components from crude oil increased with increasing temperature, ranging from 1158.8 psi to 1259.6 psi at a temperature range of 105°F to 125°F. The rate of oil shrinkage decreased with increasing temperature.

The temperature dependence of CO_2/Ogallah crude oil phase behavior is explained by the dependence of CO_2 density on pressure and temperature. Density of CO_2 as a function of pressures and temperature are calculated using REFPROP and presented in Figure 2.18. It takes higher pressure to achieve the equivalent CO_2 density at a higher temperature; and therefore, the pressure at which extraction starts increases with increasing temperature. The rate of change of CO_2 density with pressure is faster at lower temperature which explains why the extraction rate is faster at lower temperature. Mass transfer between CO_2 and oil phase is necessary to achieve dynamic miscibility. Since mass transfer between CO_2 and oil phase starts earlier and faster at a lower temperature, MMP decreases with decreasing temperature.

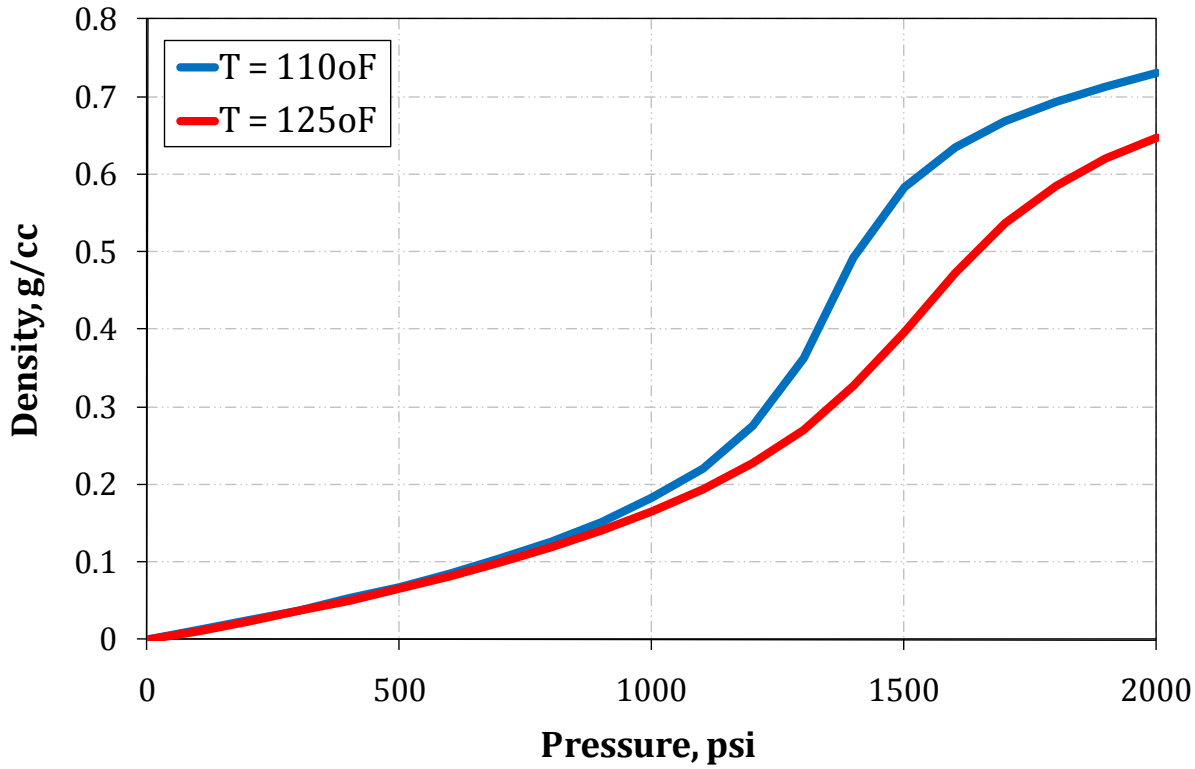

Figure 2-17 Dependence of CO_2 density on temperature and pressure (REFPROP)

2.3.5.3 Effect of Initial Oil Volume

Swelling/Extraction tests were performed with different initial oil volume, such as 3cc (11% view cell volume), 9cc (35% view cell volume) & 14cc (54% view cell volume) at 110°F to investigate its effect on CO_2 solubility and swelling factor.

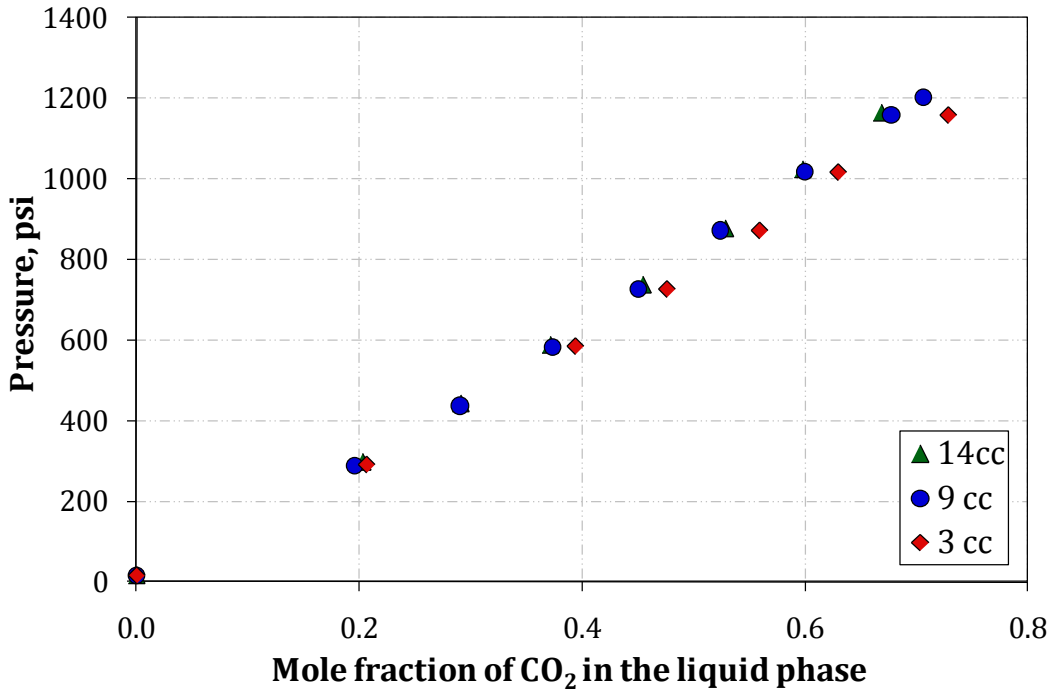

Figure 2-18 Effect of initial oil volume on CO_2 solubility at 110°F

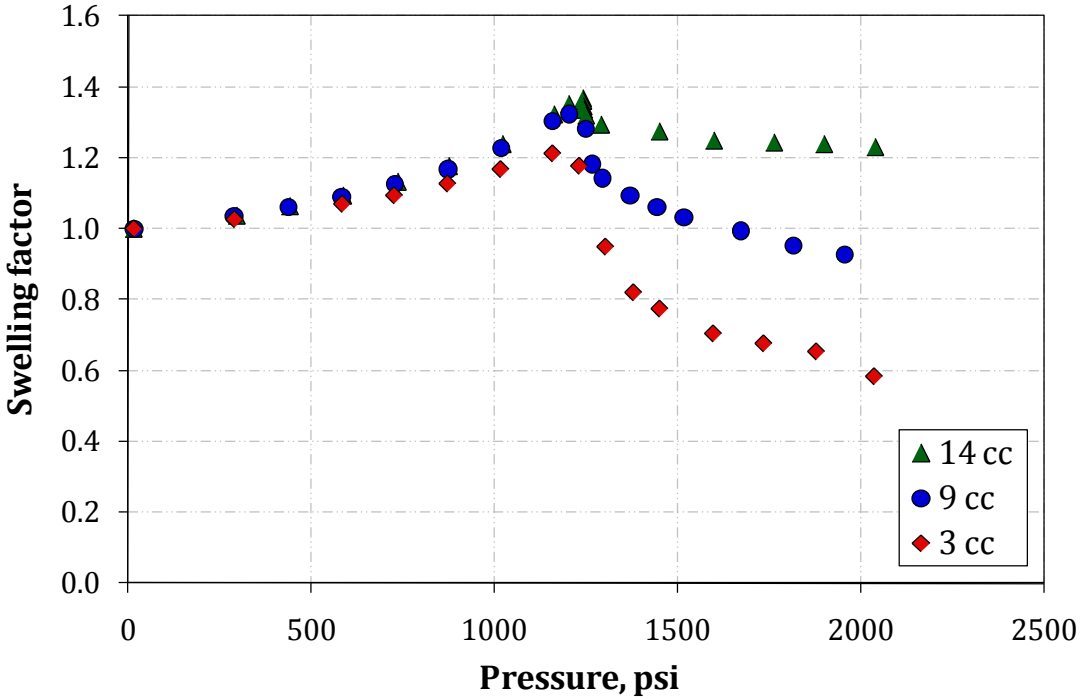

Figure 2-19 Effect of initial oil volume on swelling/extraction curve at 110°F

The effect of initial oil volume on CO_2 solubility and swelling factor at 110°F are shown in Figure 2.18 and Figure 2.19. When the initial volume of crude oil in the view cell was large, the amount of hydrocarbons extracted from the oil phase is considerably lower than when the initial volume of crude oil in the view cell is small. The pressure at which significant extraction began decreased with decreasing initial cell oil volume.

Similar observations have been reported by Hand et al. [16] and were first noted by Holm and Josendal [4] in their work where a 30% of initial volume of sample was used for the swelling test. Hand et al. [16] explained the effect of initial oil volume on swelling/extraction curve by plotting the change in cell global gas composition with pressure on a p-x diagram for the Flounder oil/CO_2 system at 233°F.

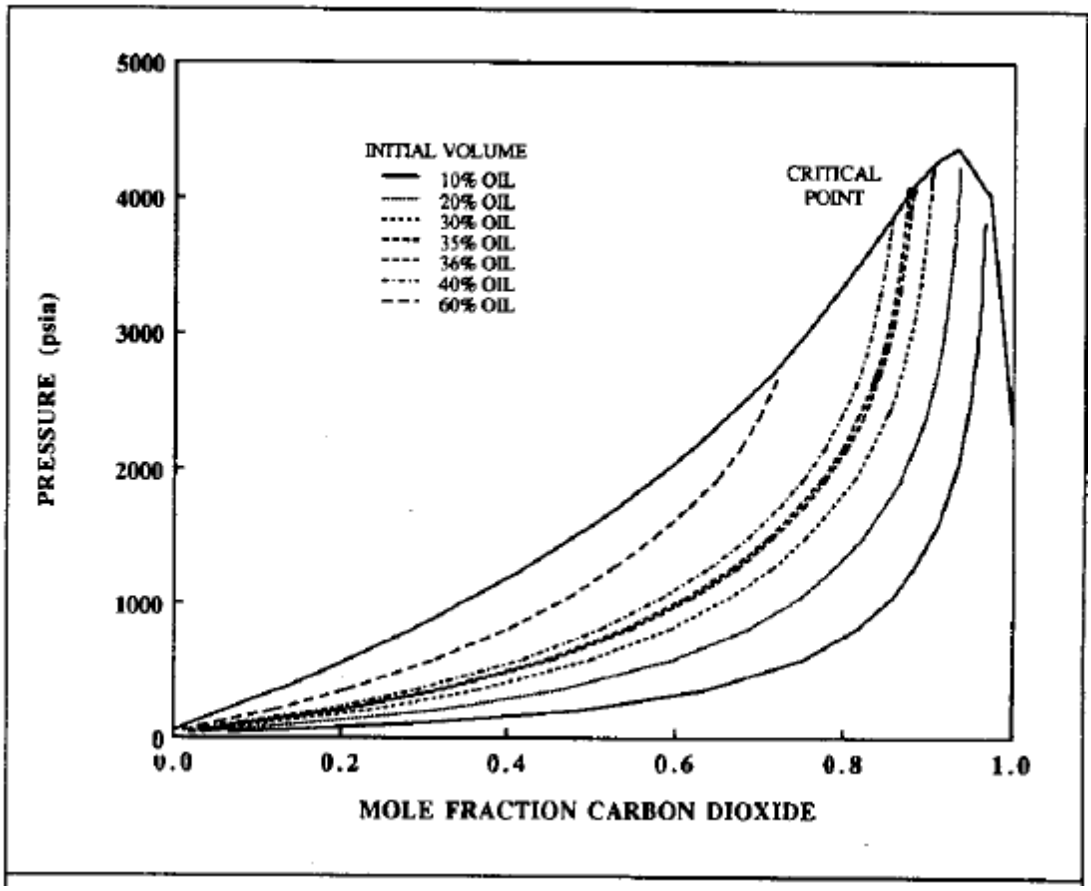

Figure 2-20 Computed p-x diagram for the Flounder oil/CO_2 system at 233°F [16]

The compositional paths for swelling/extraction tests with initial oil volumes of 40 and 60% display only oil swelling because the compositional paths cross only increasing-liquid-volume-quality lines with increasing system pressures until they terminate in a bubble point. The 10 and 20% initial oil volume compositional paths that cross increasing-liquid-volume-quality lines at lower cell pressures are shown to cross decreasing-liquid-volume-quality lines at higher pressures. These tests display oil swelling first and then oil shrinkage with increasing pressures.

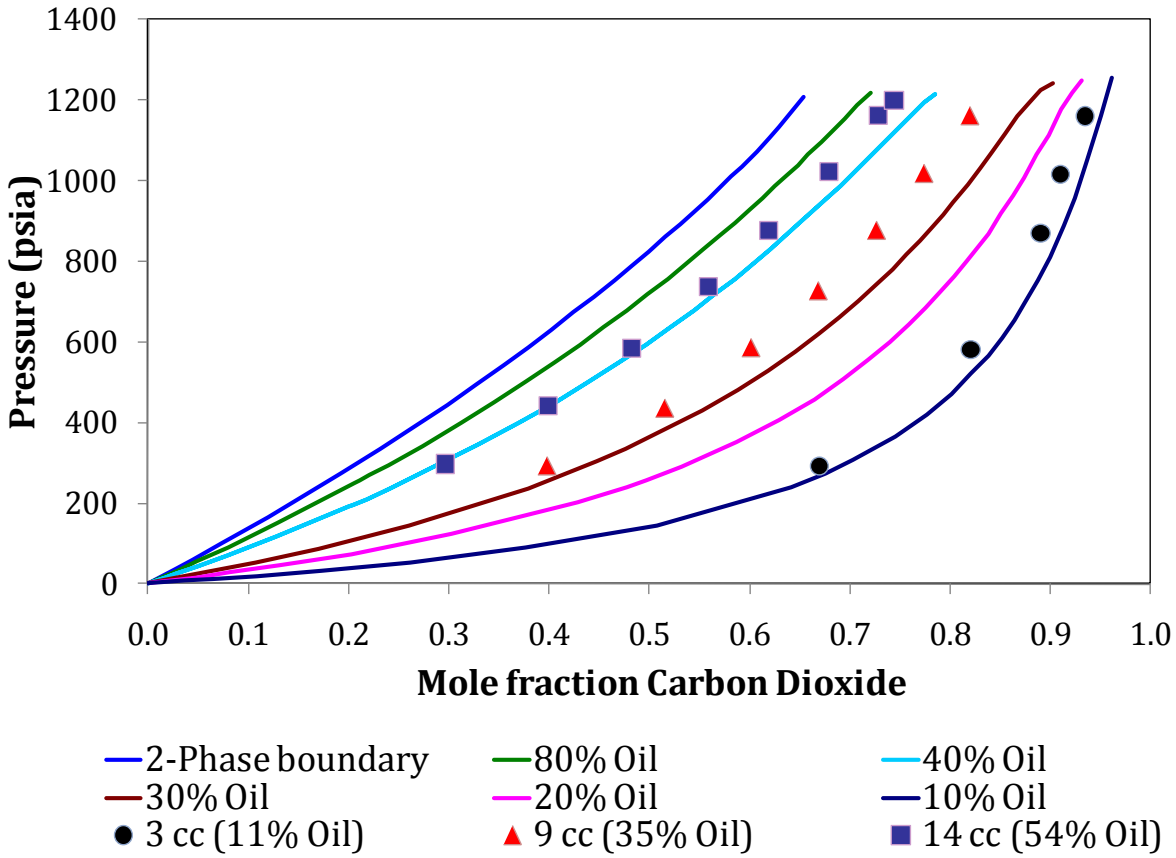

Figure 2-21 Computed p-x diagram for Ogallah oil/ CO_2 system at 110°F

Figure 2.21 shows a predicted p-x diagram for Ogallah oil/CO_2 system at 110°F by Winprop, CMG software. Also plotted are the experimental results, pressure vs. mole fraction of CO_2 for systems of 11%, 35% and 54% oil / CO_2 at 110°F. Mole fraction of CO_2 was determined by total mole of CO_2 injected into the system divided by sum of total mole of CO_2 injected into the system and the moles of crude oil. The difference of swelling/extraction curves between sample sizes is explained likewise, because the compositional paths cross the liquid-volume-quality lines differently with increasing pressure.

2.3.6 Conclusions

- CO_2 solubility increases with increasing pressure and decreases with increasing temperature. As a result of CO_2 dissolution into the liquid phase, the liquid phase swells. The degree of swelling depends on pressure and temperature.
- The pressure at which CO_2 begins to extract significant amounts of hydrocarbons from crude oil increases with increasing temperature and with increasing initial oil volume in the view cell. The amount of extraction increases with increasing vapor-phase volume (decreasing initial oil volume) and decreases with increasing temperature.
- Significant extraction started at pressure of 1150 psig & 110°F. Extraction or vaporization of hydrocarbons into the CO_2 rich phase is the primary mechanism for oil recovery in the near-miscible region, from 1100 psig to 1350 psig & at 110°F
- Swelling/extraction tests provide valuable phase behavior data which is used later to tune the phase behavior model.

2.4 Viscosity Measurements

A Cambridge Applied Systems' high pressure viscometer (ViscoPro 2000 System 4-SPL-440 with Viscolab software) utilizes an electromagnetic concept to measure viscosity of pure crude oil and/or crude oil/CO_2 mixture. The accuracy of this viscometer was validated earlier by Ahosseini et al. [17], first by using standard calibration solutions, then by

comparing viscosity values of n-hexane measured using this viscometer with literature values.

2.4.1 Principle of Operation

The viscometer utilizes the principles of annular flow around an axially oscillating piston. It contains two magnetic coils inside a stainless steel body. A low mass stainless steel piston inside the measurement chamber is magnetically forced back and forth in the fluid. As the piston is pulled toward the bottom of the measurement chamber, it forces the fluid at the bottom of the chamber to flow around the piston toward the sensor opening where it interchanges with the normal flow of the fluid. On the upward piston stroke, fresh process fluid is pulled around the piston to the bottom of the measurement chamber. The time required for the piston to move a fixed distance is related to the viscosity of the fluid in the chamber. Temperature is measured continuously with the use of a platinum Resistance Temperature Detector (RTD) mounted at the base of the measurement chamber.

2.4.2 Experimental Setup and Specifications

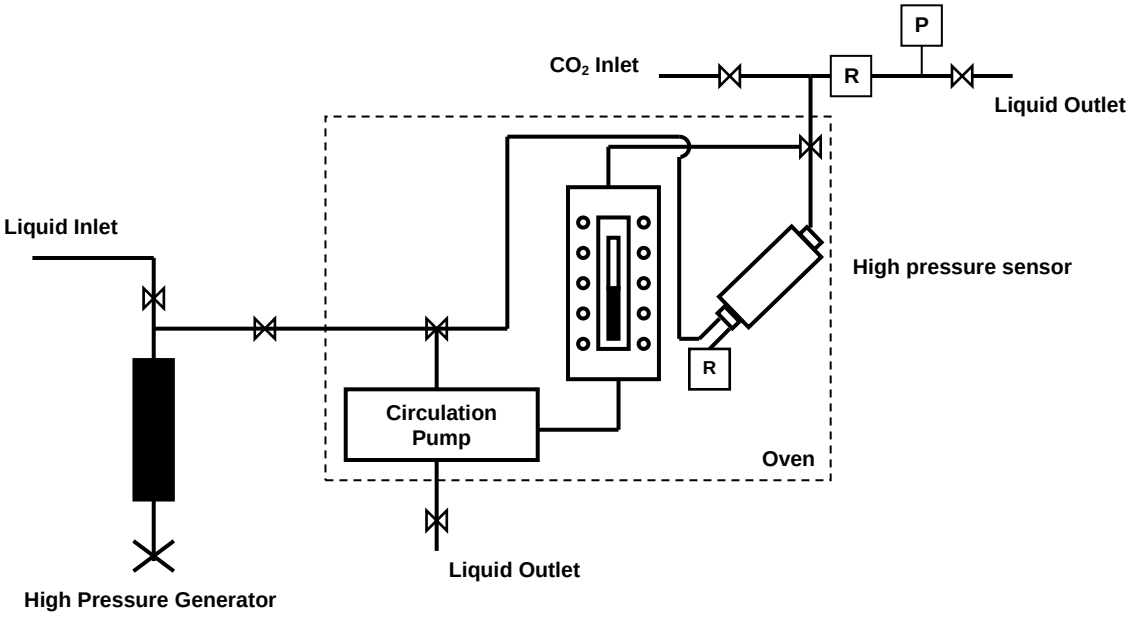

Figure 2-22 Schematic of high-pressure viscosity measurement setup

The schematic of the setup is shown in Figure 2.22. The high pressure sensor is placed inside a temperature-controlled oven and connected to a manual high pressure syringe pump (Model No. 50-575-30; 30,000 psi). The sensor is capable of measurements from 0.2 to 10,000 cp at a maximum pressure of 137.9 MPa and in a temperature range of 233.15K to 463.15K .The measurement chamber of the high pressure sensor is connected to a rupture disk (RD) and a precision pressure transducer (PT). When the setup is used for viscosity measurements of pure crude oil as a function of pressure, a high-pressure generator is required. When it is used for viscosity measurements of crude oil/CO_2 mixture, the pressure of the system is increased by CO_2 injection. ISCO 260D pump- Model 1020 BBB-4 is used for CO_2 transfer/injection. A view cell placed inside the oven allows

observations of crude oil/CO_2 interaction. During pressurization process, the time required for the contents in the system to equilibrate under a particular pressure and temperature is minimized by a circulation pump-Micropump, Inc. Model 415A.

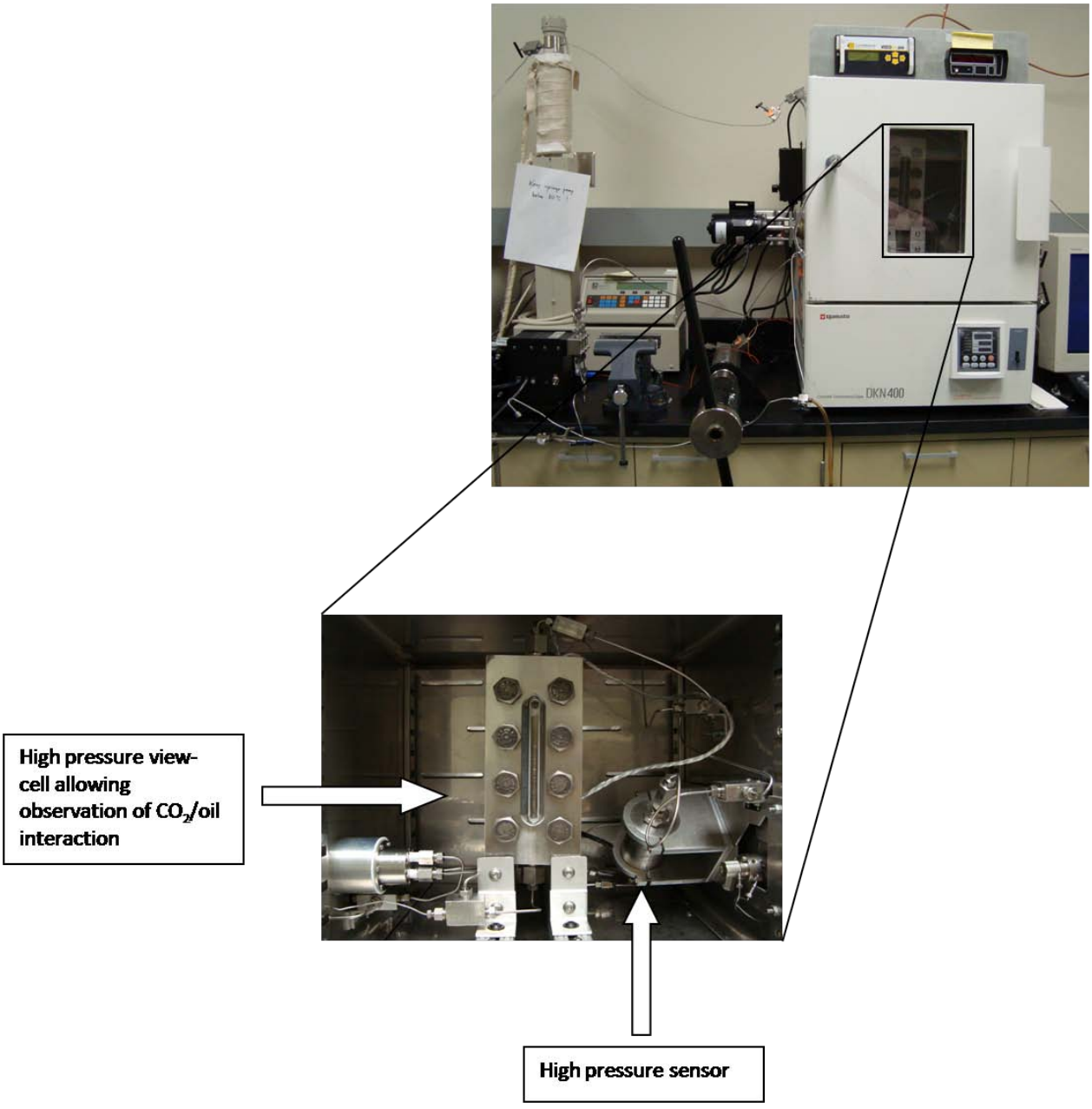

Figure 2-23 An actual image of the high-pressure viscosity measurement setup

2.4.3 Experimental Procedures

Experimental procedures to measure oil viscosity and oil/CO_2 mixture are outlined in the following sections.

2.4.3.1 Oil Viscosity Measurement Procedure

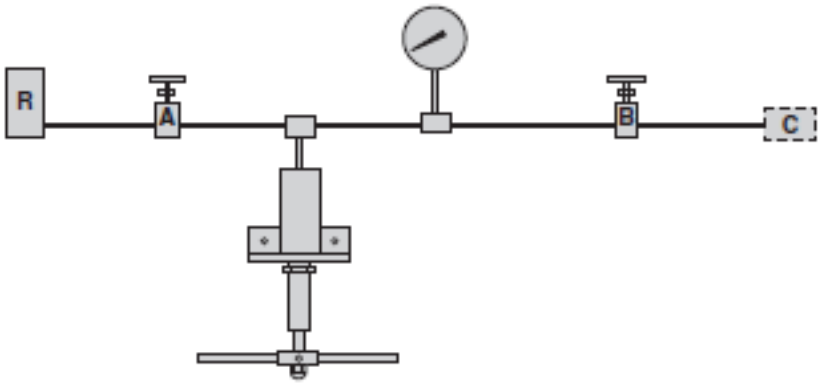

Figure 2-24 A high pressure generator

The schematic in Figure 2.24 illustrates a very basic layout for using a high pressure generator. A reservoir (R) is shown connected by means of valves and fittings to a component (C) that is to be pressurized. With valve “B” closed and valve “A” open, the handle of the high pressure generator is rotated counter-clockwise to create enough space inside the cylinder body to store the crude oil. Valve “A” is then closed and valve “B” is opened. By rotating the high pressure generator handle clockwise slowly, the piston will compress the fluid to develop pressure in the component that is to be pressurized. If sufficient pressure is not reached in one stroke, the system can be “recycled.” Valve “B” can

be closed in order to maintain pressure in the components. Valve “A” is then opened, and fluid is again drawn into the Pressure Generator from the reservoir. Closing Valve “A” and opening Valve “B” will now allow the Pressure Generator to be operated to develop increased pressure in the component.

In this experimental setup, the oil was pumped into the cylinder body using the manual high pressure syringe pump until the cylinder body is full. Excessive fluid introduction would cause pressure buildup in the cylinder body; therefore, the system outlet must have been opened before Valve “B” was opened to avoid damaging the sensor. The oil was introduced into the system and into the measurement chamber, opening both Valve “A” and Valve “B” and bypassing the high pressure generator. Temperature of the oven was set at the desired temperature. When the system was at thermal equilibrium, the system was purged to dislodge any potential bubbles. Temperature reading was taken from the RTD of the viscometer. Valve “A” was closed, Valve “B” was opened when the system was pressurized. The viscometer also needed to be turned off. By rotating the handle of the high pressure generator slowly clockwise, pressure was developed in the system until a desired pressure had reached. Viscosity reading was taken when temperature and pressure of the system is stable.

2.4.3.2 Oil/CO_2 Mixture Viscosity Measurement Procedure

Temperature of the oven is set constant at the desired temperature. Temperature of ISCO pump was set constant at the desired temperature. Pressure of the pump was set constant at the maximum anticipated pressure. Liquid was introduced into the measurement chamber and into the view cell. When the system was at thermal equilibrium, the system was purged to dislodge any potential bubbles. Temperature reading was taken from the RTD of the viscometer. Viscometer needed to be turned off when CO_2 was introduced into the system. The system pressure was increased in discrete steps by CO_2 injection from the top of the view cell. CO_2 injection was stopped when a desired pressure was achieved. During pressurization process, a micropump was used to circulate the liquid inside the system to help accelerating the mass transfer of the gas phase into the liquid phase. Reading was taken when temperature and pressure of the system were stabilized.

2.4.4 Results and Discussions

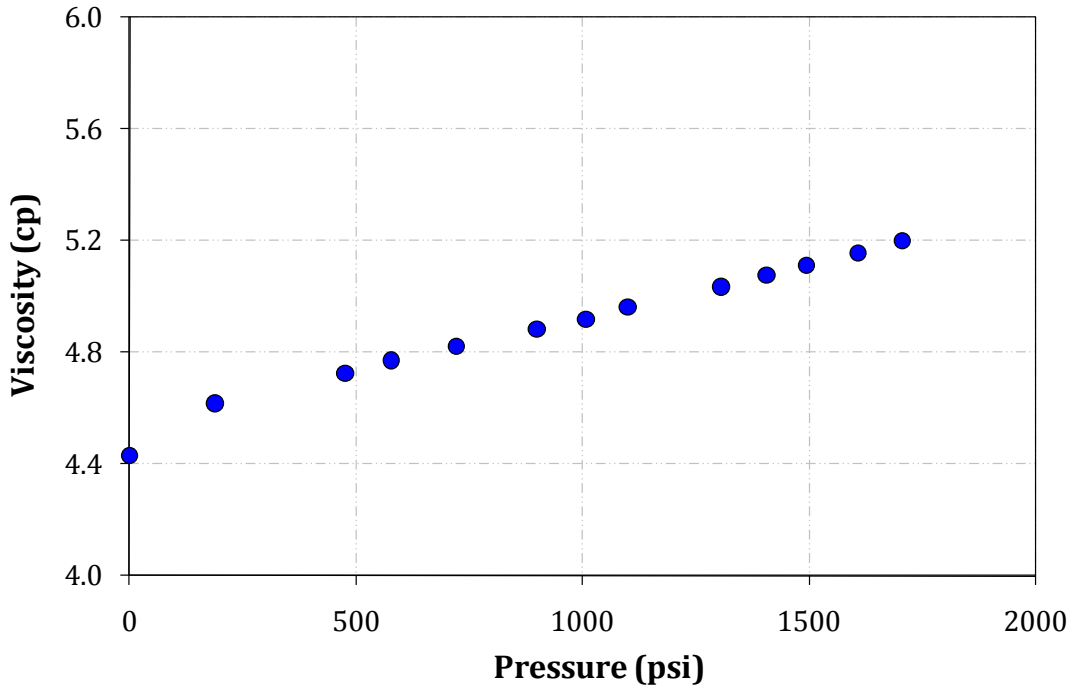

Figure 2-25 Effect of pressure on Ogallah viscosity at 110°F

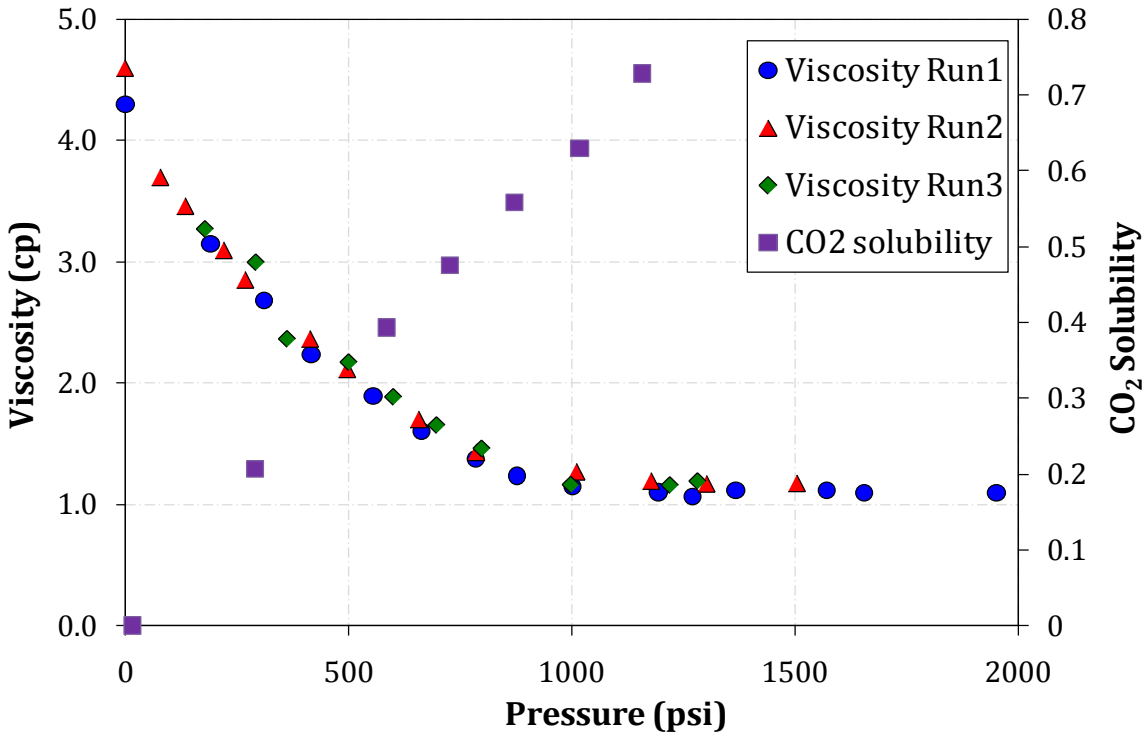

Figure 2-26 Effect of CO_2 dissolution in crude oil on the viscosity of Ogallah fluid

Figure 2.25 shows the relationship of viscosity of pure crude oil with pressure at 110°F. Figure 2.26 demonstrates the effect of CO_2 dissolution into crude oil on viscosity of crude oil at 110°F. As a result of CO_2 dissolution into the liquid phase, viscosity of the liquid phase was reduced. At pressures above 1000 psig, the effect of CO_2 on oil viscosity is minimal. The viscosity of the liquid phase was reduced as much as a factor of five in the near miscible region, from 1100 psig to 1350 psig.

2.4.5 Conclusions

- A nearly five-fold reduction in oil viscosity was achieved in the near-miscible region with CO_2 injection.
- The reduction of oil viscosity improved the total mobility ratio between reservoir oil and the displacing fluid, which will affect the recovery efficiency in a favorable way.
- Viscosity measurements are useful in tuning the phase behavior model.

2.5 Phase Behavior Model

Equations of State (EOS) have been introduced widely to model and predict CO_2-crude oil phase behavior. An EOS is an algebraic relationship between pressure, temperature, and molar volume for a single component or a mixture. Peng-Robinson EOS was used in this study to describe the fluid properties and the oil/CO_2 interaction.

$$p = \frac{RT}{v-b} - \frac{a}{v^2 + 2vb - b^2}$$

The parameters a and b are defined using the following mixing rule for mixtures,

$$a = \sum_i x_i S_i$$
$$S_i = \sqrt{a_i} \sum_j x_j \left(1 - d_{ij}\right) \sqrt{a_j}$$
$$b = \sum_i x_i b_i$$

Where, d_{ij} is an empirically determined interaction coefficient.

For pure components, the parameter a_i and b_i are expressed in terms of the critical properties and the accentric factor:

$$\sqrt{a} = \sqrt{a_c \alpha}$$
$$\sqrt{a_c} = \sqrt{\Omega_a} \left(RT_c\right) / \sqrt{p_c}$$
$$\sqrt{\alpha} = 1 + \kappa \left(1 - \sqrt{T / T_c}\right)$$
$$b = \Omega_b RT_c / p_c$$

Where, Ωa and Ωb are the EOS parameters with the default values of 0.45723553 and 0.077796074 for the PR EOS.

The κ is obtained from the following empirical correlations,

$$\kappa = 0.379642 + 1.48503\omega - 0.164423\omega^2 + 0.016666\omega^3$$

While the application of the EOS to simple mixtures is relatively straightforward, crude oil systems pose many seemingly insurmountable problems. The essential infinite number of

components contained in a typical crude oil makes it impossible to obtain a complete chemical analysis. Standard oil analysis lumps all components heavier than C36 into a single C36+ pseudo-component characterized by its average molecular weight and density. Therefore, the parameters of the EOS were adjusted so that the EOS could reproduce the laboratory-determined oil properties and the observed oil/CO_2 interaction.

Slim tube model was constructed using 1-D compositional simulator with the tuned EOS. Simulated slim tube results were compared with experimental slim tube results. The following sections describe in detail how to develop the phase behavior model/slim tube model in CMG™ software and how to characterize the phase behavior model to match with experimental PVT data and slim tube results.

2.5.1 Phase Behavior Modeling using WINPROP

WinProp, a CMG™ software was utilized to build the phase behavior model. The EOS requires the following properties for each component, critical pressure (Pc), critical temperature (Tc), acentric factor (ω), and interaction coefficients between different components (d_{ij}) to perform phase equilibrium calculations. The molecular weight (MW) is also required to calculate mass densities. Additional factors such as the volume shifts τ, and the equation-of-state parameters Ωa and Ωb can also be adjusted for each component to enhance the equation of state predictions.

Pure hydrocarbon components were selected from the software library, as well as generalized single carbon number (SCN) petroleum fractions FC6 through FC45. The specific gravities, molecular weights and boiling points of the SCN fractions were taken from Whitson (1983). The critical properties of these fractions were calculated with the Lee-Kesler correlation. The heavy lumped component C36+ was defined using specific gravity and molecular weight. Physical and critical properties of C36+ were assigned using Twu and Lee-Kesler correlation respectively. For accentric factors, the Lee-Kesler correlation was recommended for petroleum fractions. Equilibrium phase viscosities were calculated with the Pedersen viscosity corresponding states model. The Pedersen viscosity correlation uses the principle of corresponding states to calculate the viscosity of a component or mixture, knowing the viscosity of a reference substance at the same conditions of reduced pressure and temperature. The deviation from simple corresponding states is accounted for by a "rotational coupling coefficient", α. The reference substance for the Pedersen model is methane. The viscosity of the mixture is calculated according to the following formula:

$$\frac{\mu_{mix}\,(P,T)}{\mu_o\,(P_o,T_o)} = \frac{T_{c,mix}}{T_{c,o}}^{-1/6} \frac{P_{c,mix}}{P_{c,o}}^{2/3} \frac{MW_{mix}}{MW_o}^{1/2} \frac{\alpha_{mix}}{\alpha_o}$$

When the components representing the fluid model had been selected and their compositions had been specified, a grouping scheme was performed primarily for the purpose of speeding up the simulation running time. Whitson suggested that C7+ should be grouped into NH pseudo-components given by,

$$N_H = 1 + 3.3\log(N - 7)$$

The groups are separated by molecular weights MI given by,

$$M_I = M_{C_7}\left(M_N / M_{C_7}\right)^{I/N_H}$$

where N = CN of the heaviest fraction in the fluid description

I = 1 to NH

Therefore,

NH = 5 pseudo-groups

Group 1 < M1 = 138.303

M1 <Group 2 < M2 = 191.276

M2 < Group 3 < M3 = 264.539

M3 < Group 4 < M4 = 365.865

Finally a 8-component EOS fluid model was obtained after grouping:

C3 + iC4 + nC4 (1)

nC5+ iC5 (2)

C6 (3)

C7 – C9 (4)

C10 – C13 (5)

C14 – C18 (6)

C19 – C25 (7)

C26 – C36+ (8)

2.5.2 Equation of State Characterization

Figure 2.28 and Figure 2.29 present the experimental data and the simulated data after tuning EOS parameters. Molecular weight (MW) of the heavy fraction was adjusted to match the oil density. Coefficients of Pedersen viscosity correlation were adjusted to match the oil viscosity. Binary interaction coefficients (BIC) between CO_2 and the hydrocarbon components as well as CO_2 volume shift factor were adjusted to match saturation pressure and swelling data. Table 2.5 shows the adjustment of each parameter to achieve the match.

Variable	Lower Bound	Upper Bound	Initial Value	Final Value
MW C26 to C36+	5.07E+02	7.60E+02	6.34E+02	5.98E+02
Volume shift of CO_2	-1.54E-01	9.20E-01	0.00E+00	9.11E-01
BIC (C7-C9)-CO_2	0.00E+00	2.00E-01	1.50E-01	0.00E+00
BIC (C10-C13)- CO_2	0.00E+00	2.00E-01	1.50E-01	0.00E+00
Coefficient of viscosity correlation # 4	1.00E+00	2.22E+00	1.85E+00	1.04E+00
Coefficient of viscosity correlation # 5	4.14E-01	6.21E-01	5.17E-01	6.21E-01

Table 2.4 Adjustments of EOS parameters

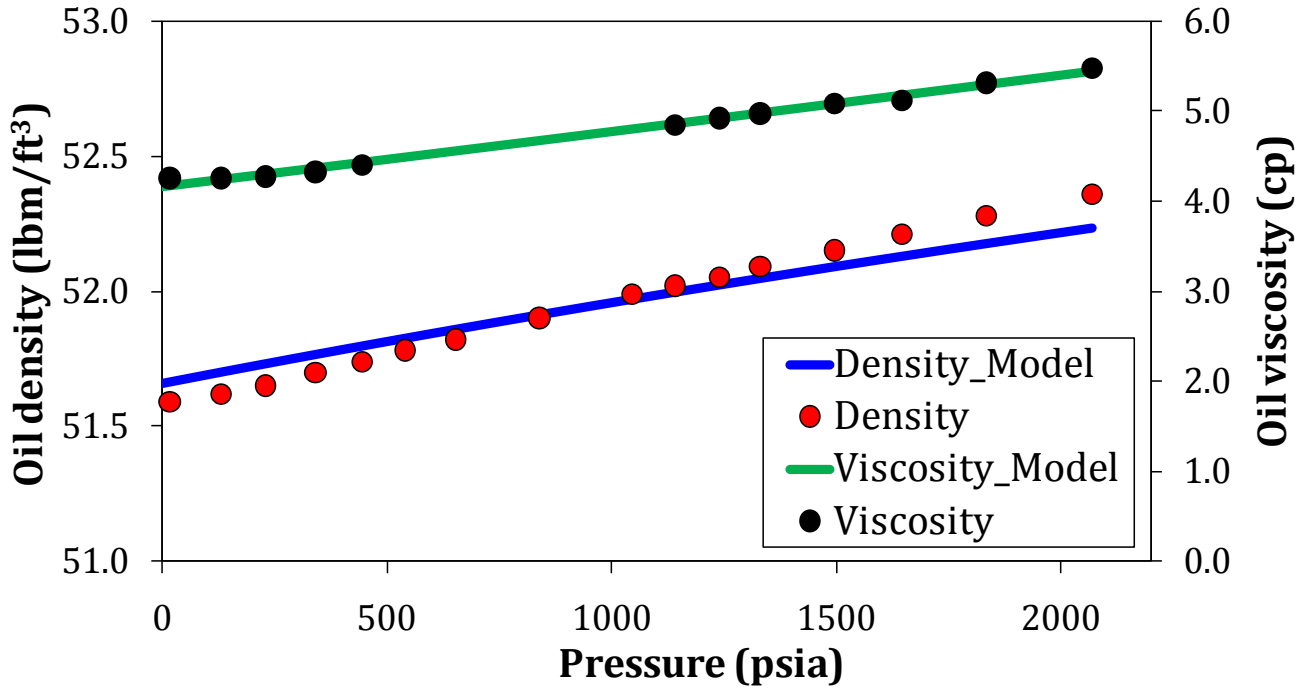

Figure 2-27 Comparison of viscosity/density experimental data and simulated data before/after EOS tuning

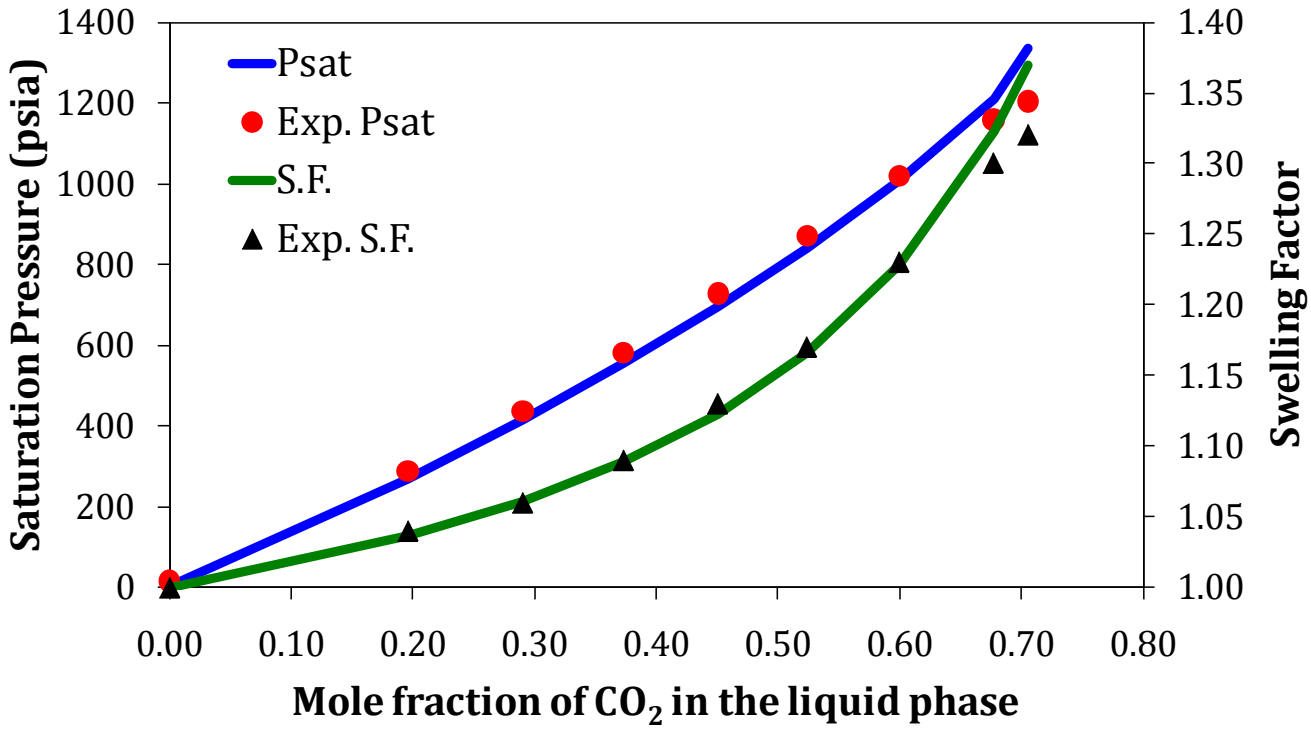

Figure 2-28 Comparison of saturation pressure/swelling factor experimental data and simulated data before/after EOS tuning

The maximum percentage error between simulated data and experimental data after tuning the EOS is presented in Table 2.6

	Maximum error percentage
Viscosity	3 %
Density	1 %
Saturation pressure	7 %
Swelling factor	1 %

Table 2.5 Maximum percentage error between simulated and experimental data

2.5.3 Slim Tube Modeling using GEM

A slim tube model was created in compositional model simulator of GEM from CMG package and the phase behavior model of the reservoir was imported in it as the original

saturated fluid of the tube. The slim tube was represented by a one dimensional linear model using 320 grid blocks. The grid block sizes were 0.125 ft, 0.0185 ft and 0.0185 ft in I, J, K direction respectively. One injector and one producer were incorporated at the ends of the model.

Length, ft	40
Porosity, PV	0.367
Permeability, mD	4900
Pore Volume, cc	142.3
No. of blocks	320
Length of blocks, ft	0.125
Cross section, ft^2	0.0003423
Each edge, ft	0.0185
Geometry	Square Cross-section

Table 2.6 Slim tube model properties

The slim tube gas/oil relative permeability curves used in this model were obtained from Negahban and Kremesec [18] and illustrated in Figure 2.27.

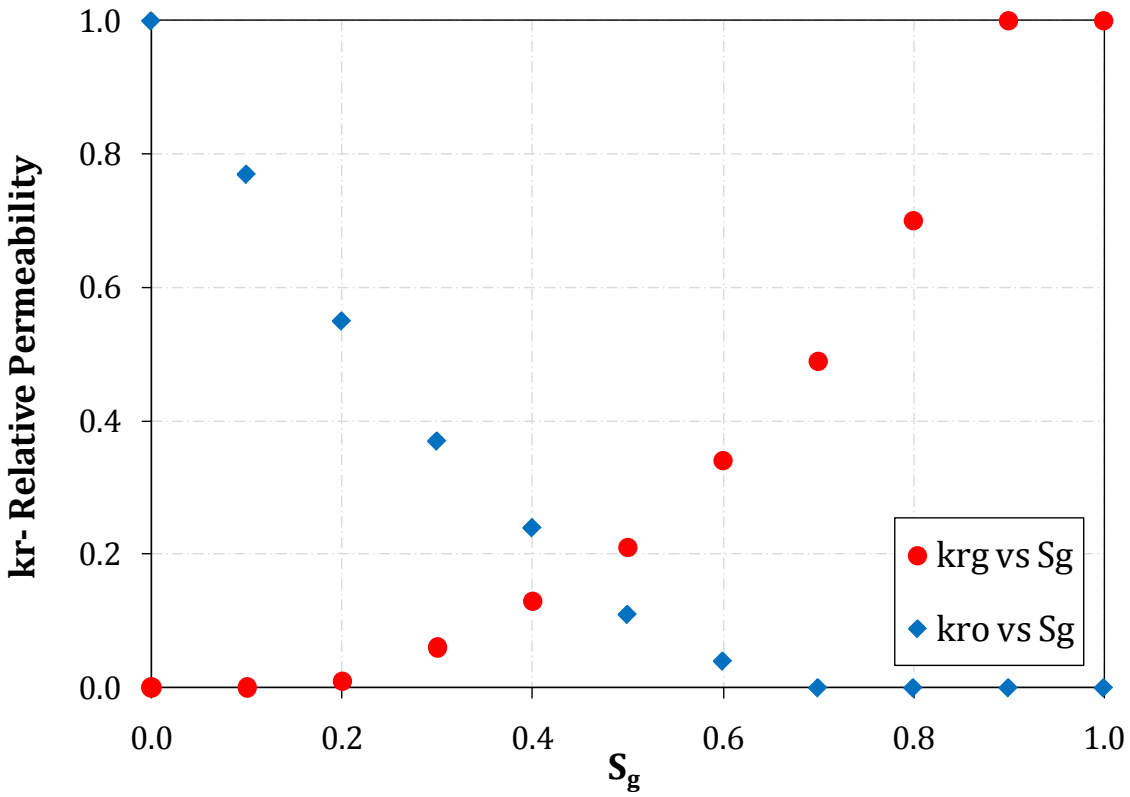

Figure 2-29 Relative permeability curve of oil-gas used in the simulation [18]

A number of slim tube displacements were simulated and compared with experimental slim tube results in Figure 2.30.

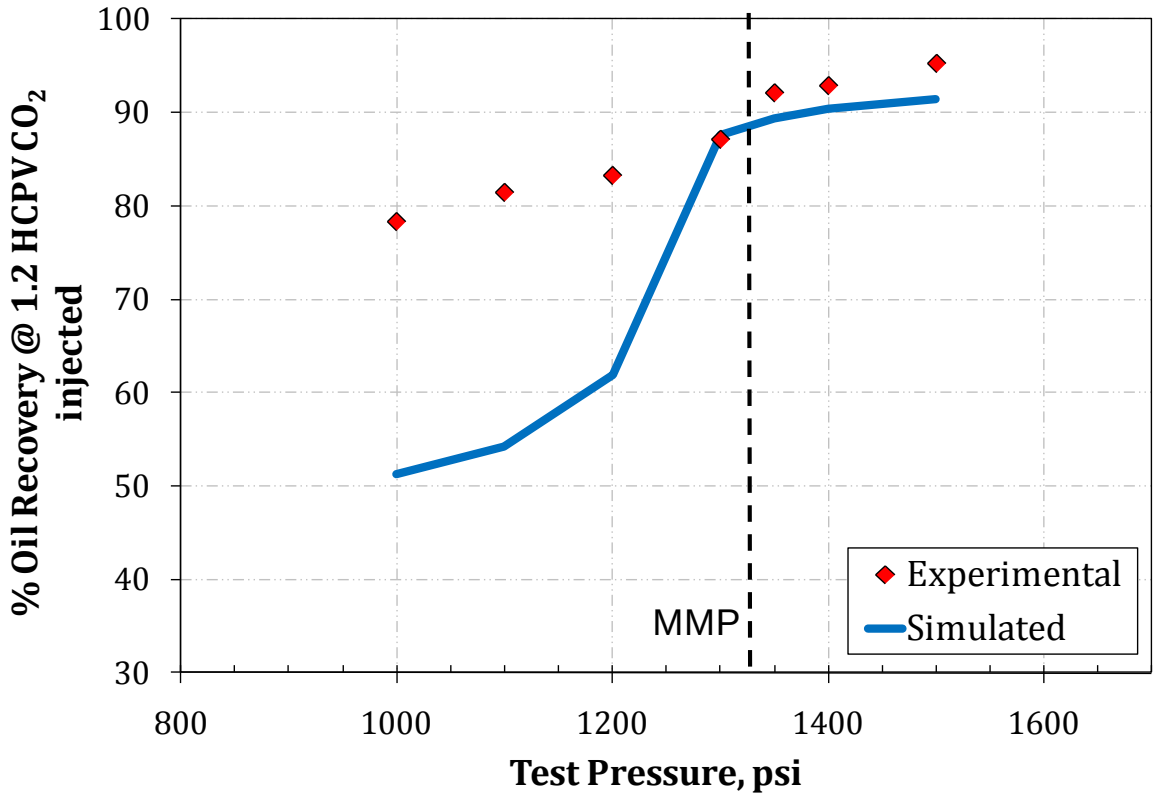

Figure 2-30 Comparison of simulated MMP and experimental MMP

Lower oil recoveries at pressures below MMP as seen in Figure 2.30 indicated early gas breakthrough. In order to match simulated slim tube results with experimental slim tube results, the slim tube gas/oil relative permeability curves must be adjusted by keeping the relative permeability end points and changing the curvature of the relative permeability curves. Figure 2.31 shows the slim tube gas/oil relative permeability curves used in the simulation.

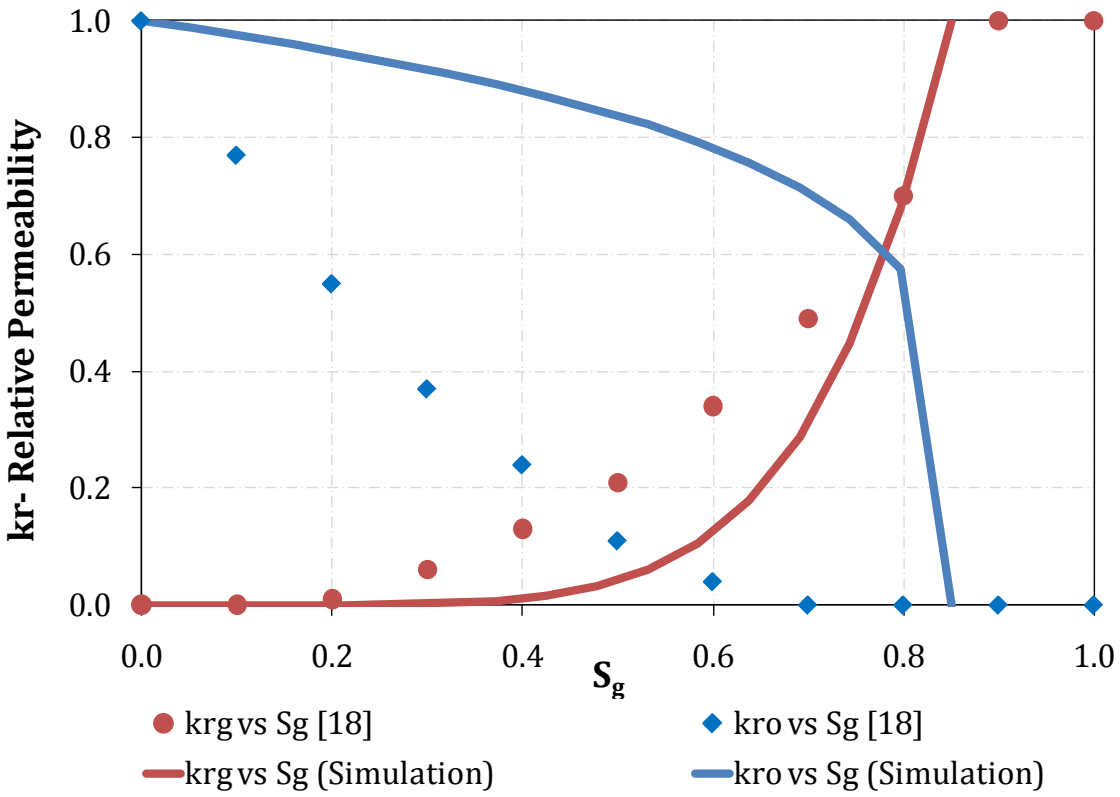

Figure 2-31 Relative permeability curve of oil-gas before and after adjusted to match slim tube results

Figure 2.32 compares the recovery efficiency from simulation and experimental work at 1.2 PV of CO_2 injected. As shown by Figure 2.32, the phase behavior model predicts the MMP and the oil recovery reasonably well.

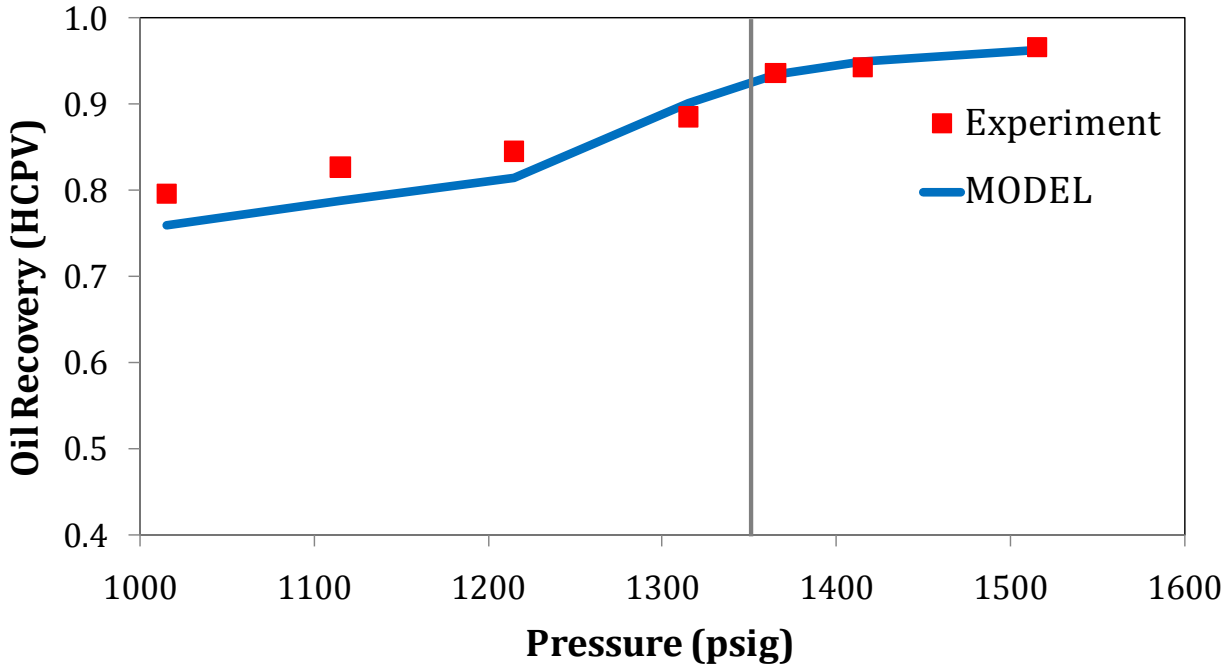

Figure 2-32 Comparison of simulated MMP and experimental MMP after tuning the relative permeability curve

3 Core Flow Tests

Core flow tests were conducted under conditions that are more realistic than in slim tubes and closer to the field conditions. They are virtually identical in procedure to the slim tube displacement tests, except that a core sample replaced the bead-packed tube. The method of conducting the tests and the results monitored are identical to the slim tube test.

CO_2 core floods are difficult to interpret since linear displacements may or may not exhibit characteristics common to a given reservoir such as dispersion, mobile water, wettability, viscous fingering, gravity segregation, oil bypassing due to heterogeneity, and trapped oil saturation. However, Orr et al. [19] suggested that core flow tests do seem appropriate for answering at least three questions directly (1) Can CO_2 mobilize tertiary oil under conditions that are close to field displacement conditions than those occurring in slim tube displacements? (2) What is the residual oil saturation in the swept zone of a CO_2 displacement? (3) Does CO_2 injection alter reservoir permeability by asphaltene precipitation or dissolution of minerals?

3.1 Cores

Cores from Arbuckle reservoirs are limited. Berea sandstone, Baker dolomite and Arbuckle dolomite rock samples were used in the core flow tests. Berea sandstone and Baker dolomite were quarried rock samples whereas Arbuckle dolomite was cored sample from

Hadley well, Bemis-Shutts Field at Ellis County, Kansas. Before cores were epoxy encased and cast inside an aluminum cylinder with high strength epoxy, at least three measurements of the diameter and the length of each core were obtained. The average value of the diameter and the length was used to calculate the area and the bulk volume of each core. The dry weight of the core holder was recorded.

Upon completion of each core flow test, the cores were cleaned to restore to its initial condition and reused for the next experiment. The core cleaning procedure is outlined as follows:

- The cores were successively cleaned with methylene chloride and methanol. At least 10 PV of methylene chloride followed by 10 PV of methanol was injected. The sequence was repeated at least three times until the effluent was clear.
- The cores were blown dry by CO_2 and vacuumed to remove residual air/CO_2.
- The cores were fully saturated with either brine or crude oil, depending on which type of core flow tests would be conducted. Brine was used for tertiary CO_2 floods. Crude oil was used for secondary CO_2 floods.

Figure 3.1 shows the experimental setup for vacuuming and saturating the cores,

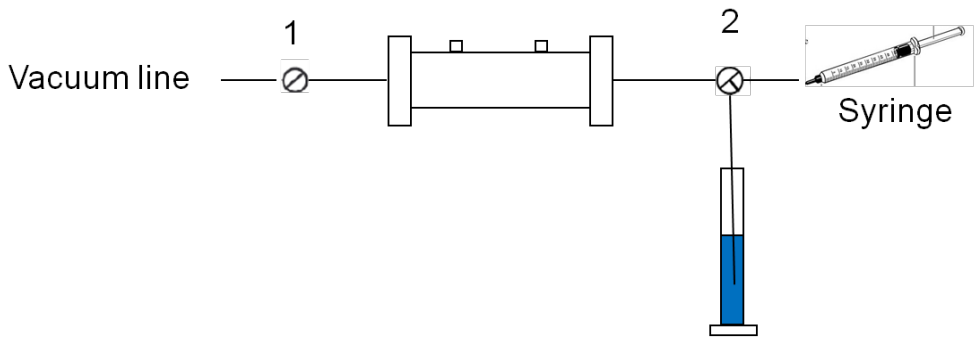

Figure 3-1. Vacuum and saturation setup

- VACUUM (700mmHg): Open Valve 1, Close Valve 2
- DRY WEIGHT MEASUREMENT: Close Valve 1 & 2, Disconnect the core holder with the vacuum line, Weigh the core holder with all the fittings (Weight of all the fitting would be subtracted later)
- The purpose of the syringe was to ensure that the line which immersed in the graduated cylinder was clear of air.
- SATURATION: Close Valve 1, Open Valve 2 (Brine will be drawn in the core holder), Wait until the level of the brine did not change (During the saturation process, the line was always ensured to be immersed in the brine)
- PORE VOLUME ESTIMATION: Estimate the change of volume of brine in the graduated cylinder before and after brine was suck into the evacuated cores (dead volume from fittings must be subtracted).

3.2 Fluids

Brine with 1wt% total dissolved solids (TDS) was used. Composition of brine was 0.5 wt% $MgCl_2$ and 0.5 wt% $CaCl_2$ in deionized water. Brine was filtered using 0.22 micron membrane (Micron Separations Inc.) before use. Density of brine was obtained using the densitometer. Viscosity of brine was measured using Brookfield DV-III Ultra programmable rheometer. Density and viscosity of brine are summarized in Table 3.1.

	T = 86°F	T = 110°F
Brine density, g/cc	1.0007	0.99591
Brine viscosity, cp	0.8350	0.7250

Table 3.1 Density/Viscosity of Brine at 86°F/110°F

3.3 Equipments and Procedures

Experimental setup and procedure for core characterization and core flow tests are described in the following sections.

3.3.1 Core Characterization

Core characterization includes determining pore volume, porosity and permeability for each core. The following sections discuss in detail how to obtain those measurements.

3.3.1.1 Pore Volume Measurements

As mentioned earlier, pore volume can be approximated by the change of volume of brine in the graduated cylinder before and after brine was drawn into the evacuated cores. Pore volume of each core, however, can be determined more accurately by two ways, gravimetric method and tracer tests. In the gravimetric method, the pore volume of each core was computed based on the weight difference of the core before and after brine was imbibed into the dry and evacuated core. In the tracer tests, concentration of tracer solution is analyzed; equal area technique is utilized to calculate pore volume of each core. Both techniques are discussed in detail in the following sections.

3.3.1.1.1 Gravimetric Method

The core holder was weighed before and after fully saturated with brine. Pore volume of each core was calculated as follows:

$$PV = \frac{W_s - W_d}{\rho}$$

Where,

PV = pore volume (cc)

W_s = weight of the core holder when it is 100% saturated with brine (g)

W_d = weight of the core holder when it is dry (g)

ρ = density of brine at the testing temperature (g/cc)

Core porosities were calculated as follows:

$$\phi = \frac{PV}{BV}$$

Where,

Φ= porosity

PV = pore volume (cc)

BV = bulk volume (cc)

3.3.1.1.2 Tracer Tests

Tracer tests were performed to confirm the pore volume of a core. A tracer is an injected substance that is both measurable (e.g. through UV-visible detection) and conserved (i.e. not retained, destroyed or created by the core). 1 wt% $MgNO_3$ was used as a tracer in this study. If tracer concentration is recorded at the core outlet and plotted as a function of time, an S-shaped curve will form. The S-shaped curve is caused by dispersion of one fluid into another; otherwise, there would be an instantaneous change in tracer concentration at breakthrough. Tracer data is typically normalized to scale the tracer concentration values from zero to one. A typical normalized tracer curve is shown in Figure 3.2.

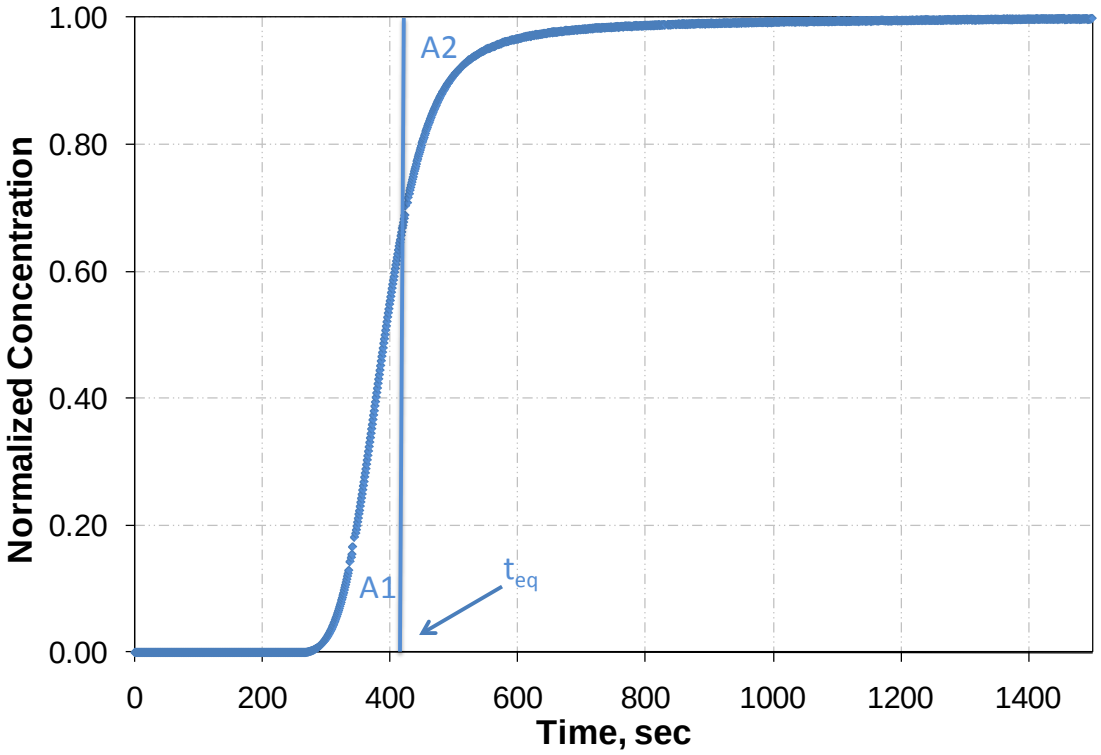

Figure 3-2 Equal area technique in calculating PV of a core from tracer tests

Normalized concentration is calculated as follows:

$$C_B = \frac{C_B^* - C_{Bo}}{C_{Bi} - C_{Bo}}$$

Where,

C_B = normalized tracer concentration

C_B^*= measured tracer concentration

C_{Bo}= initial concentration of brine

C_{Bi} = maximum tracer concentration

Equal-area technique is utilized to compute PV of a core as follows:

$$PV = \left(\left(t_{eq} - t_o\right) \times q\right) - V_d$$

Where,

V_d = any dead volume (cc)

q = tracer flowrate (cc/min)

t_o = time at which tracer injection starts (min)

t_{eq}= time at which equal area under each side of the curve reaches, A1 = A2

Areas on each side of the tracer concentration, A1 & A2, were calculated using trapezoidal rule. t_{eq} is at A1 = A2.

Several primary assumptions are made in tracer testing [3]

- Fluid B is displacing Fluid A, and the two fluids are miscible
- There is no viscous fingering of one fluid into another, only dispersion
- Flow is single phase
- Fluids are incompressible
- Fluids are of equal density
- Flow is in only one direction
- Fluid velocity is constant
- Flow is through a porous medium of constant porosity and cross-sectional area

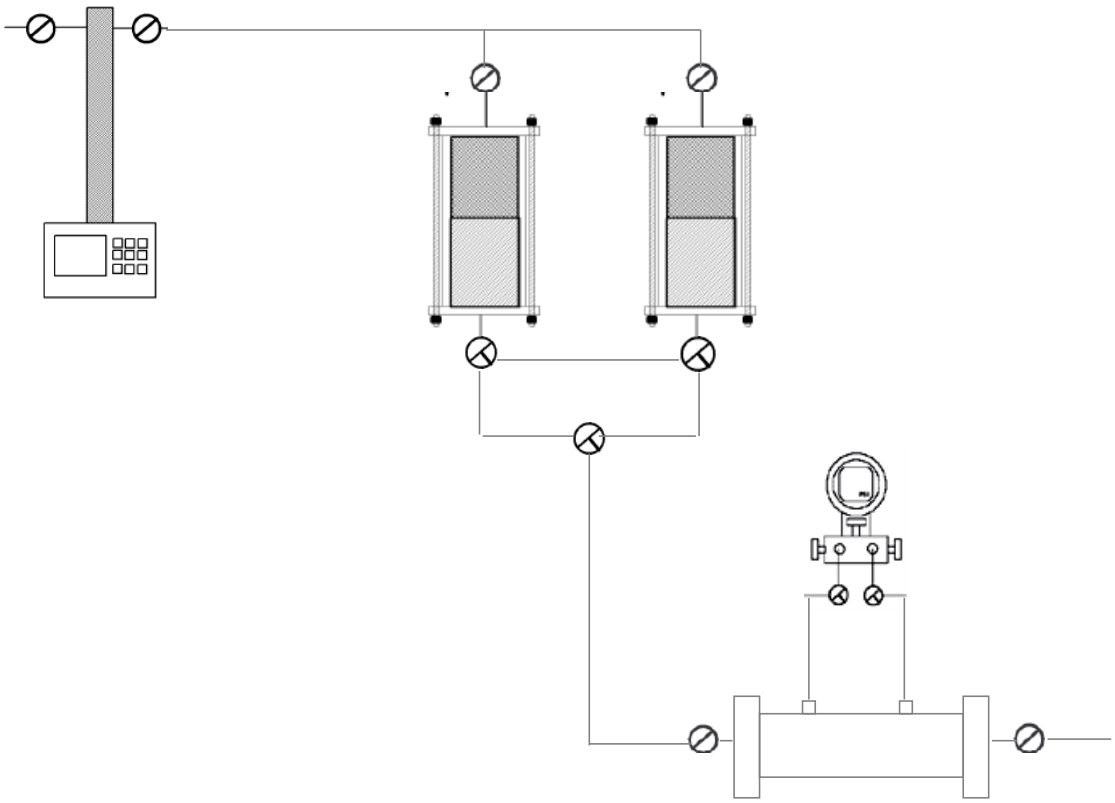

Figure 3-3 Schematic of tracer setup

Figure 3.3 shows the schematic of the tracer setup. The injection system consists of an ISCO, Inc. 260DM syringe pump (for mineral oil transfer and injection) and two transfer cylinders (for tracer solution/brine/mineral oil storage). 1 wt% $MgNO_3$ was used as a tracer. The inlet of the core holder is connected to the injection system. The three-way valve allows switching the flow between tracer solution and brine. The outlet of the core is connected to an UV-visible detector. The UV-visible detector should be turned on and set at a wavelength of 302 nm at least an hour prior tracer tests. The flow cell of the detector should be cleaned by methylene chloride, followed by acetone and finally brine injection.

Brine passed through core at a constant flow rate until UV-visible detector read a steady concentration value. At this point, the detector was zeroed and the three-way valve was switched to tracer injection. The switchover time needed to be recorded manually.

When tracer concentration did not change over time, the valve was switched back to non-tracer injection to displace the tracer solution from the core. Again, the switchover time needed to be recorded manually.

3.3.1.2 Permeability Measurements

Pressure drop was recorded during the brine flow tests and used to calculate permeability of each core based on Darcy's Law:

$$k = q\left(\frac{\mu}{A}\right)\left(\frac{L}{\Delta P}\right)$$

Where,

q = flow rate of fluid through the core (cc/sec)

k = permeability (Darcy)

A= area (cc)

μ = viscosity of the fluid (cp)

ΔP = pressure drop (atm)

L = length (cm)

Brine flow rates were varied to confirm the permeability of each core.

3.3.2 Core Floods

3.3.2.1 Experimental Setup

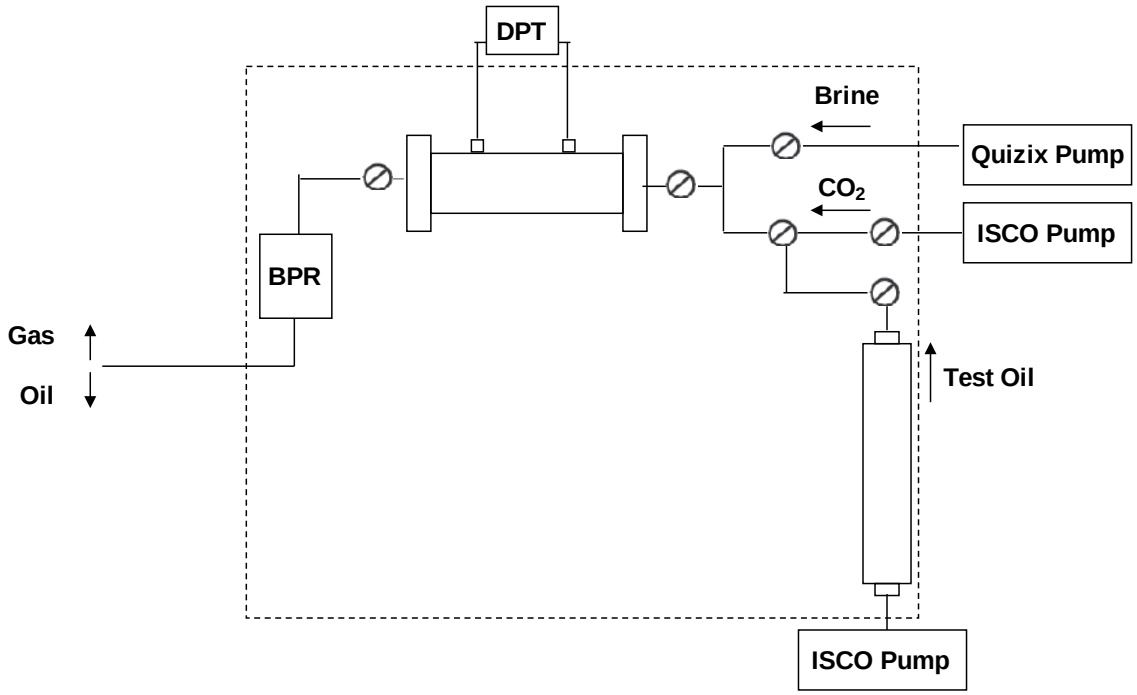

Figure 3-4 Schematic of core flood setup

The core flood setup is shown in Figure 3.4. The core flood displacement setup consists of a core holder, injection system, a high-pressure densitometer, a production system and a computerized data acquisition system. The temperature of the system is maintained in a Linberg/Blue M oven with Eurotherm temperature control.

The injection system consists of a Parker transfer cylinder (oil storage), two Isco, Inc. 260DM syringe pumps (oil/CO_2 transfer and injection) and a Quizix Pump (brine transfer and injection). The capacity of the transfer cylinder is 485 cc. The cylinder can withstand a maximum pressure of 3000 psi.

The production system consists of a back-pressure regulator, connected to the outlet of the core holder, to set/control the system pressure. Back pressure regulator models BPR-50 is a dome-load type, which controls the upstream back pressure to whatever pressure is applied to the dome. It is designed to operate using compressed gas in the dome and water, oil, gas in the body. A high pressure bottle of inert gas, such as nitrogen, is required to pressurize the unit. The back pressure regulator has a working pressure of 5000 psi at 200^{o}F (93^{o}C).

During the experiment, the core effluent was flashed to atmospheric pressure at the outlet of the back-pressure regulator. The separator fluid was collected in glassware designed for different stages of displacement. The amount of fluids produced was determined volumetrically and/or gravimetrically.

Three Valydine pressure transducers are installed to measure pressures at different locations, such as pressure drop across the core, upstream pressures (CO2/oil/brine pressure), and downstream pressure (back-pressure regulator pressure). The transducers measure pressures up to 2500 psi with the accuracy of 0.25% of their full scale (0-2500 psi).

3.3.2.2 Experimental Procedures

Two sets of core flood experiments were performed, secondary CO_2 flooding and tertiary CO_2 flooding to investigate the effect of operating pressure, in the near-miscible range on the recovery efficiency and to investigate the effect of mobile water on the recovery efficiency. In each set of experiment, core flood tests were carried out for a range of pressures and at the reservoir temperature of 110°F. Crude oil/brine/CO_2 injection volumes were kept the same to compare the amount of oil recovered in each run.

3.3.2.3 Displacement Rate Selection

Residual oil saturation in laboratory core floods has been observed to depend on CO_2 flow rate. Poorer oil recoveries were found at increasing frontal advance rates by Shelton and Schneider [20]. Low flow rate allows CO_2 to diffuse through the network of pores and hence increase oil recovery by swelling and/or vaporizing. Crude oil/brine/CO_2 displacement rates were selected 0.1cc/min to keep the capillary number as low as 10^{-6} and to achieve realistic unit displacement efficiency in laboratory CO_2 displacement.

3.4 Results and Discussions

3.4.1 Core Characterization Results

Table 3.2 presents the properties of Berea sandstone, Baker dolomite and Arbuckle dolomite. Bulk volumes of the cores were calculated from at least three measurements of diameters and lengths. Pore volume of each core was averaged from the results of tracer tests and gravimetric methods, and from which porosity of each core was calculated. Permeability to brine was calculated using different flow rates and averaged.

Type	Berea sandstone A1	Berea sandstone A2	Arbuckle dolomite	Baker dolomite
Length (cm)	5.86	14.67	5.97	8.07
Cross section (cm)	2.53	3.86	2.46	2.34
Area (cm^2)	5.01	11.67	4.75	4.30
Pore volume (cc)	5.80	34.72	6.05	7.20
Porosity	19.7 %	20.28%	21.3%	20.7%
Permeability (mD)	238.5	369.04	2.5	89.7

Table 3.2 Core properties

3.4.2 Core Floods Results

3.4.2.1 Secondary CO_2 Flooding

Berea sandstone core A1 was completely saturated with crude oil prior to CO_2 flooding. The amount of oil recovered by CO_2 flooding was determined by weight. Percentage of oil recovery in core flow tests was determined the same way as in slim tube tests, except pore volume of the core was used instead of pore volume of the slim tube. % Oil recovery @ 6 PV of CO_2 injected was plotted as a function of pressure in Figure 3.5 and was compared with % oil recovery in slim tube tests @ 1.2 PV CO2 injected at 110°F.

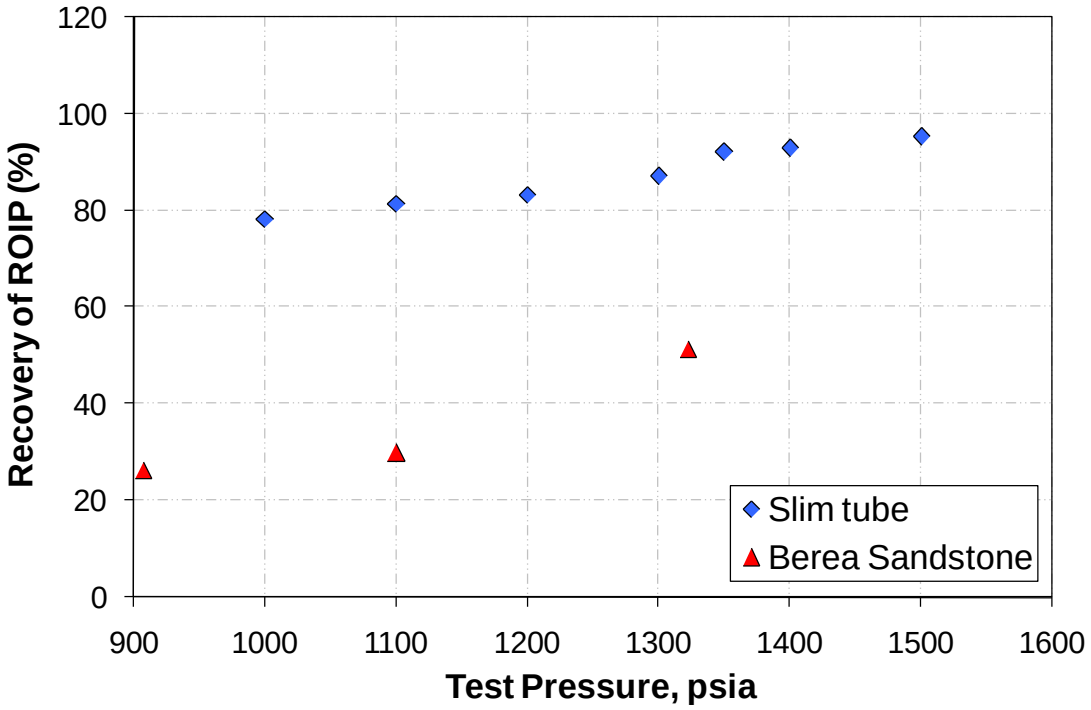

Figure 3-5 Percent of oil recovery @ 6 PV of CO_2 injected in core flow tests and percent of oil recovery @ 1.2 PV of CO_2 injected in slim tube tests at 110°F

As expected, the oil recovery efficiency in core flow tests was much less than in slim tube tests. Oil recovery efficiency in core flow tests was approximately 35% of original oil in place compared with 83 % of original oil in place in slim tube results at 110°F and 1150 psig. The reasons for the difference lie in viscous fingering, channeling and/or bypassing of

oil due to core heterogeneities in a core displacement test. Another theory might be the core was too short for the multiple contact miscibility to develop. Rathmell et al. [21] reported that the average residual oil for the entire core was observed to decrease with increasing core length and suggested that up to several feet were required to generate the miscible transition zone before oil recovery representative of CO_2 miscible displacement was achieved. Therefore, further experiments with longer cores need to be performed to verify this.

3.4.2.2 Tertiary CO_2 flooding

Three groups of rock samples were used in this series of test. Berea sandstone, Arbuckle dolomite and Baker dolomite were first saturated with brine, followed by crude oil injection to residual water saturation and brine injection to residual oil saturation prior to CO_2 flooding. At least 10 PV of crude oil/brine injection was used to establish a steady residual fluid saturation. The amount of oil recovered by CO_2 flooding was determined volumetrically. Table 3.3 to Table 3.6 summarizes CO_2 tertiary core flood results for Berea sandstone/ Arbuckle dolomite/ Baker dolomite at 110^{o}F. Calculations of residual water saturation (S_{wr}), residual oil saturation due to water-flooding (S_{orw}), residual oil saturation due to CO_2 flooding (S_{orm}), and residual water saturation due to CO_2 flooding (S_{wf}) are based on material balance. A sample is attached in the Appendix.

Pressure (psig)	S_{wr}	S_{orw}	S_{orm}	S_{wf}	Recovery 1-(S_{orm}/S_{orw})

905	0.32	0.48	0.31	0.37	35.71
1104	0.32	0.50	0.29	0.39	41.38
1198	0.32	0.48	0.26	0.41	46.43
1317	0.32	0.50	0.21	0.34	58.62
1413	0.32	0.48	0.21	0.34	57.14

Table 3.3 Tertiary CO_2 flood results in Ogallah/Berea sandstone A1 at 110°F

Pressure (psig)	S_{wr}	S_{orw}	S_{orm}	S_{wf}	Recovery 1-(S_{orm}/S_{orw})
900	0.32	0.38	0.31	0.43	20.45
1099 (Run 1)	0.35	0.35	0.26	0.46	27.87
1100 (Run2)	0.36	0.36	0.26	0.41	28.13
1206	0.33	0.36	0.20	0.44	45.97
1314	0.36	0.33	0.13	0.51	60.18

Table 3.4 Tertiary CO_2 flood results in Ogallah/Berea sandstone A2 at 110°F

Pressure (psig)	S_{wr}	S_{orw}	S_{orm}	S_{wf}	Recovery 1-(S_{orm}/S_{orw})
901	0.38	0.41	0.17	0.51	60.00
1100	0.38	0.41	0.17	0.55	60.00
1200	0.45	0.33	0.08	0.64	75.00
1305	0.45	0.33	0.07	0.64	80.00
1407	0.38	0.38	0.10	0.53	73.91

Table 3.5 Tertiary CO_2 flood results in Ogallah/Arbuckle dolomite at 110°F

Pressure (psig)	S_{wr}	S_{orw}	S_{orm}	S_{wf}	Recovery 1-(S_{orm}/S_{orw})
905	0.28	0.39	0.15	0.44	60.71
1109	0.31	0.38	0.13	0.41	66.67
1201	0.34	0.35	0.10	0.45	72.00
1303	0.37	0.35	0.07	0.53	80.00
1402	0.37	0.32	0.07	0.47	78.26

Table 3.6 Tertiary CO_2 flood results in Ogallah/ Baker dolomite at 110°F

Figure 3.6 compares percent of oil recovery @ 6 PV of CO_2 injected as a function of pressure for Berea sandstone A1, Baker dolomite and Arbuckle dolomite at 110°F. The recovery efficiency was similar between two dolomite cores but substantially higher than that in

Berea core. These recoveries varied from 65% to 80% for dolomite cores and lesser from 45% to 60 % for sandstone core in the near-miscible region.

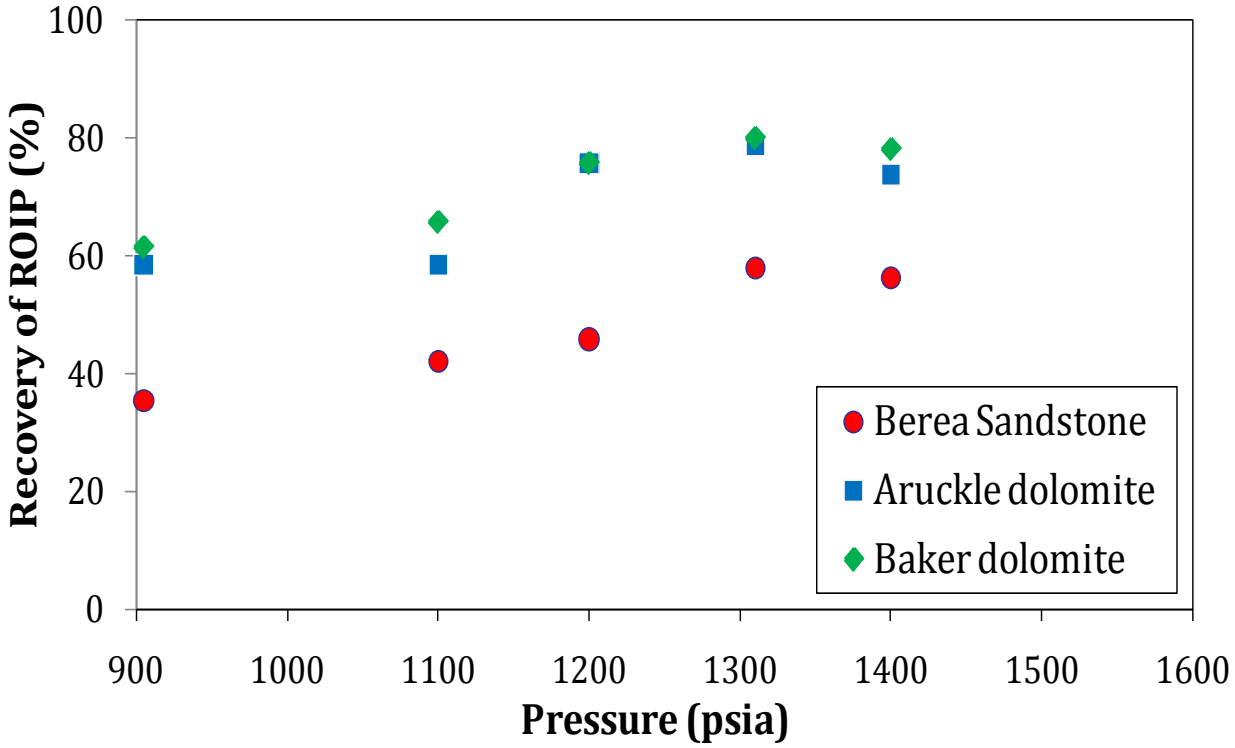

Figure 3-6 Percent of oil recovery @ 6 PV of CO_2 injected as a function of pressure for Berea sandstone A1, Baker dolomite and Arbuckle dolomite at 110°F

Wylie and Mohanty [22] carried out coreflood studies to examine oil recoveries for first contact miscible, multiple-contact miscible and immiscible mass transfer processes by observing recoveries at various wetting states and core orientations and concluded that mass transfer is enhanced for oil-wet condition compared to water wet condition. Although wettability of the cores was not examined in this study, it is generally believed that Berea sandstone is strongly water-wet and to a lesser extent in dolomite cores. After CO_2 breakthrough from the core, the extraction or the mass transfer between the bypassed

region and flowing CO_2 becomes more important to extract the remaining oil inside the core. The findings from Wylie's study may explain why the recovery efficiency is higher in dolomite cores than in sandstone cores for this particular experiment.

As mentioned earlier, crude oil/brine/CO_2 displacement rates were selected 0.1cc/min to keep the capillary number as low as 10-6 and to achieve realistic unit displacement efficiency in laboratory CO_2 displacement. However, since the residual oil saturation in Berea sandstone A1 was as high as 50%, different displacement rate was selected to drive the residual oil saturation further down. Crude oil flow rate was selected 1cc/min for the first 2 PV and 2cc/min for another 4PV during brine displacement test by crude oil. Brine flow rate was selected 1cc/min for 6 PV during crude oil displacement test by brine. High pressure drop drove the waterflood residual oil saturation from 0.48-0.50 for Berea sandstone A1 to 0.33-0.38 for Berea sandstone A2. CO_2 flow rate was selected 0.1cc/min for 6 PV. At current reservoir pressure 1150 psig, the recovery efficiency of Berea sandstone A1 was approximately 45% whereas the recovery efficiency of Berea sandstone A2 was 35%. Core flow test was repeated at 1100psig & 110^{o}F for Berea sandstone A2. Core flow tests at 1100psig and 110^{o}F were reproducible. It is not possible to compare the recovery efficiency in Berea long core and Berea short core since the pore volume and the residual oil saturation after waterflooding of two cores were different.

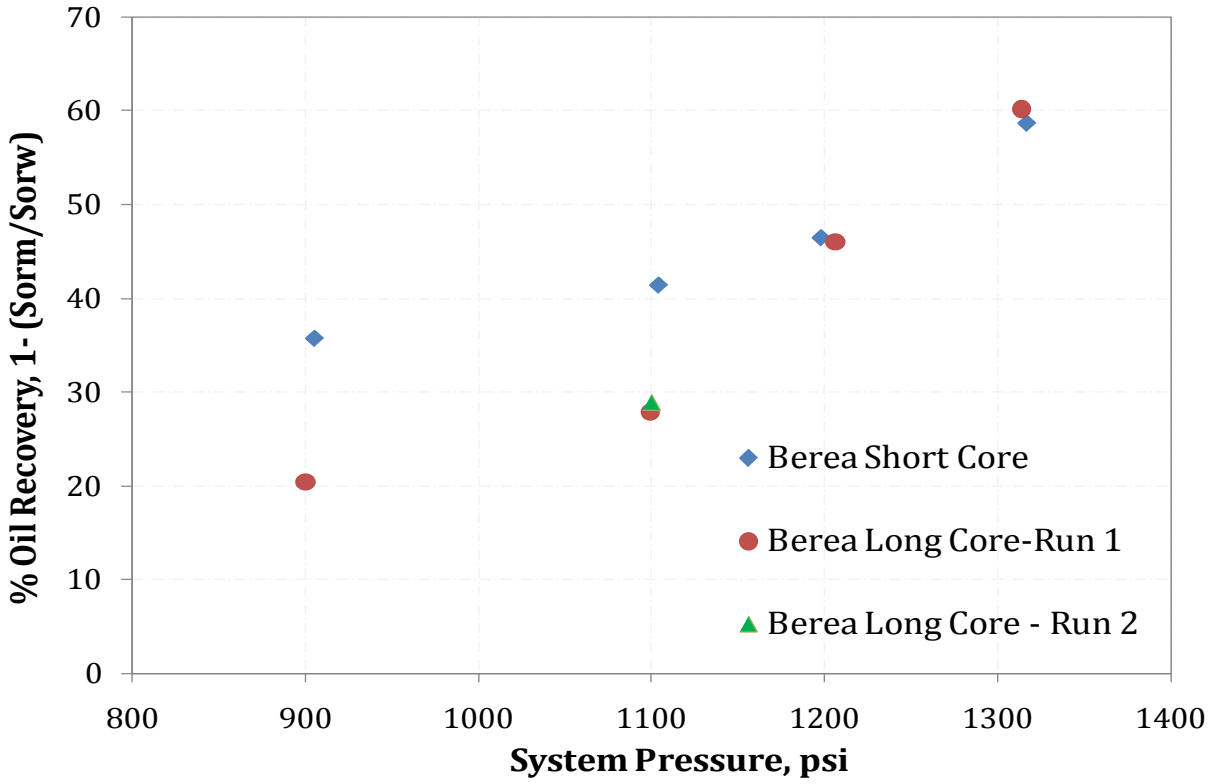

Figure 3-7 Recovery efficiency of Berea sandstones A1 & A2 at 1100 psig & 110°F.

3.4.2.3 Effect of Water Saturation on Oil Recovery Efficiency

The residual oil phase after waterflooding and before initiating tertiary CO_2 injection exists in the porous media as a trapped, disconnected phase surrounded by water. High mobile water saturations affect the CO_2 displacement efficiency in an unfavorable way because water prevents CO_2 from contacting and mobilizing the oil, however to what extent is still unclear.

Shelton and Schneider [20] studied the effect of mobile water saturations on oil recovery in CO_2 miscible displacement tests on sandstone cores and concluded that miscible displacement performances for secondary and tertiary conditions are equivalent.

Tiffin and Yellig [23] evaluated continuous CO_2 injection in secondary and tertiary displacement modes using water-wet and oil wet cores and concluded that mobile water from a previous waterflooding did not significantly change either the overall recovery or the mechanism by which miscibility was developed from what was observed in secondary CO_2 displacement tests.

In another study by Campbell and Orr [24], however, visual observations of pore-level displacement events indicate that CO_2 displaced oil much more efficiently in both first contact and multiple contact miscible displacements when water was absent. Water from a prior water flood restricted access of CO_2 to the oil. The low viscosity of CO_2 aggravated effects of high water saturations because CO_2 did not displace water efficiently. Given enough time, CO_2 did however contact trapped oil by diffusing through water to reach, to swell and to reconnect isolated droplets.

Also, studies by Stalkup [25] have indicated that higher water saturations increase both the amount of bypassed oil and the longitudinal dispersion coefficient. He also presented that the dominant mechanisms for recovery of the water blocked oil are miscible flushing by solvent and recovery by molecular diffusion. Furthermore, Stalkup's results indicate

that the effect of oil trapping by water will be more significant in laboratory core experiments than in field scale operations.

Shyeh-Yung et al. [7] studied the effect of initial water saturation by comparing secondary CO_2 floods with tertiary CO_2 floods. Initial water saturation was about 40% for secondary CO_2 floods and a water-flood preceding a tertiary CO_2 floods usually raised the water saturation to about 75%. Secondary CO_2 floods showed more oil recovery than CO_2 tertiary floods at similar pressure and CO_2 throughputs, as see in Figure 3.8.

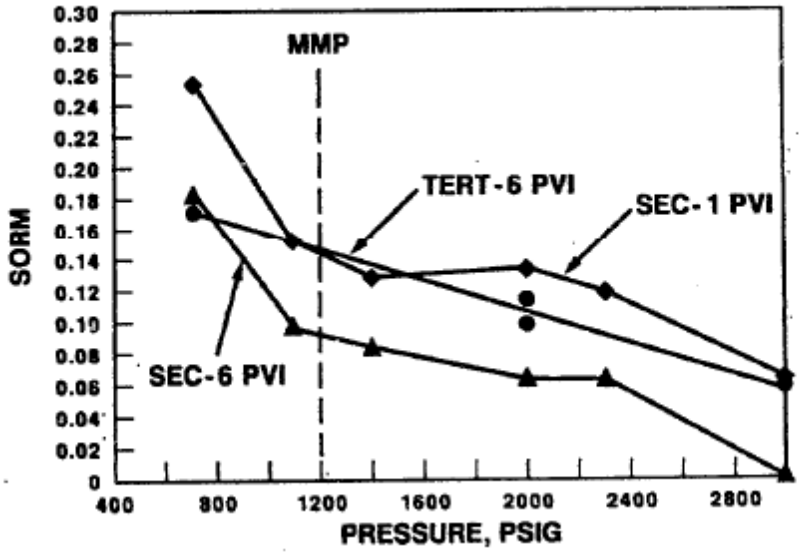

Figure 3-8 Effect of initial water saturation on CO_2 flood oil recovery performance by comparing secondary and tertiary CO_2 floods [7]

She suggested several explanations, for instance (1) higher initial oil saturation in secondary CO_2 flood results in oil being more connected (2) lower water saturation in a secondary flood facilitates mass transport of CO_2 to crude oil, allowing more extraction and displacement of oil (3) intermediate and heavy components extracted from crude oil will

make their way to the flowing CO_2 phase and be produced more easily in a lower water saturation secondary flood than in a tertiary flood.

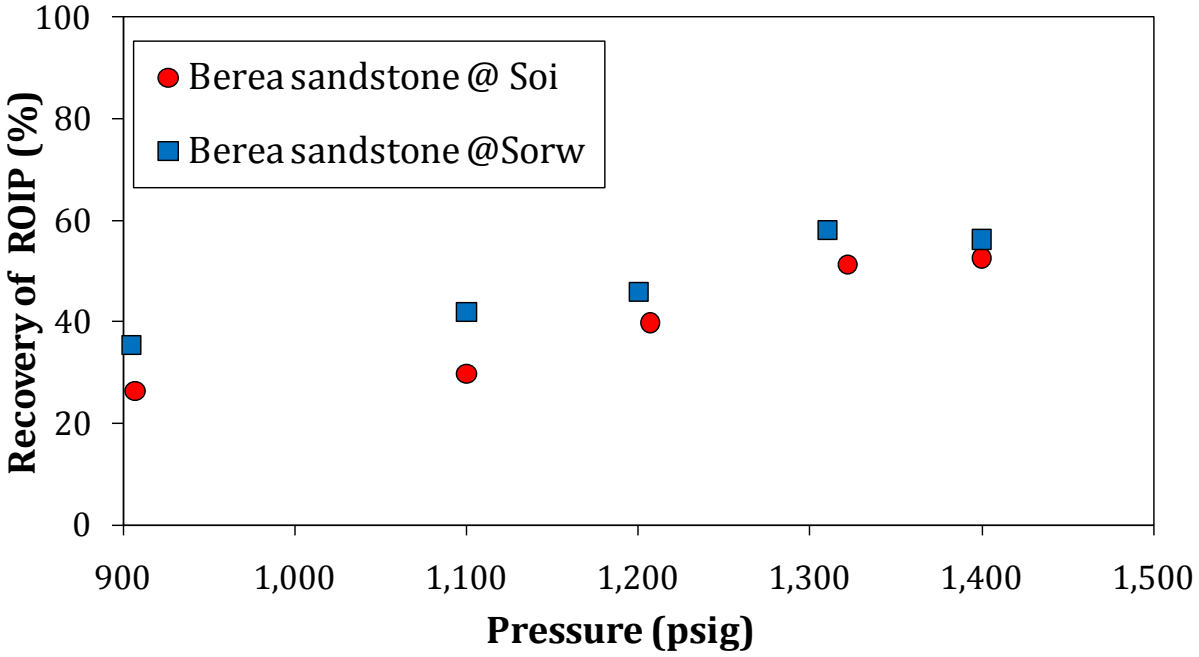

Figure 3-9 Effect of water saturation on oil recovery efficiency at 110°F

Results from secondary CO_2 floods and tertiary CO_2 floods using Berea sandstone core samples are presented in Figure 3.9. Oil recovery efficiency in tertiary CO_2 floods is higher than in secondary CO_2 floods. The data suggests that the existence of water phase in the core is not necessarily detrimental to CO_2 displacement efficiency as reported earlier. The relative permeability of CO_2 in the presence of water phase might be reduced, as reported by Shyeh-Yung et al. [7], which coupled with the reduction of the oil viscosity reduces the mobility ratio between the oil and CO_2 and therefore the recovery efficiency is improved. Shyeh-Yung measured CO_2-rich phase relative permeability (k_{rCO2}) in San Andres mixed wet outcrop cores and observed that secondary CO_2 floods had greater end-point solvent

mobilities than tertiary CO_2 floods (presence of mobile water phase) carried out at the same temperature. The highest value for k_{rCO2} corresponds to the situation where no residual oil is present. As residual oil increases, k_{rCO2} decreases. CO_2 flood end-point permeability was plotted as a function of water saturation and residual oil saturation in Figure 3.10.

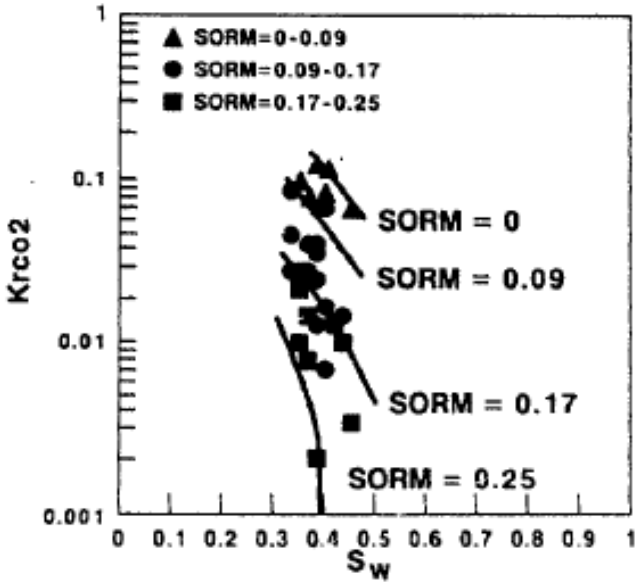

Figure 3-10 CO_2 flood end-point permeability as a function of water saturation and residual oil saturation in a mixed wet carbonate [7]

3.5 Conclusions

- Tertiary oil recovery efficiency varied among rock types, from 65% to 80% for dolomite cores and lesser from 45% to 60 % for sandstone core in the near-miscible region, from 1100 psig to 1350 psig & at 110^{o}F.

- Recovery of more than 60% of the waterflood residual oil was obtained using Arbuckle reservoir core when CO_2 was injected at the current average reservoir pressure 1150 psig & 110^{o}F.
- Experimental works showed that the presence of water phase improved the relative permeability of CO_2, which coupled with the reduction of the oil viscosity reduced the mobility ratio between the oil and CO_2 and therefore the recovery efficiency was improved

4 Conclusions & Recommendations

4.1 Conclusions

1. Slim tube results indicate that Arbuckle reservoirs is not a suitable candidate for miscible CO_2 flooding, since the MMP for this oil/CO_2 system is 1350 psig at 110^oF whereas the operating pressure of the reservoir is 1150 psig.
2. The near miscible range is defined from 1100 psig to 1350 psig at 110^oF in our study.
3. Initial laboratory works showed that at least 80% oil recovery efficiency was observed in slim tube tests and more than 60% of the waterflood residual oil was obtained using Arbuckle reservoir core when CO_2 was injected at the current average reservoir pressure 1150 psig & 110^oF.
4. Tertiary oil recovery efficiency varied from 65% to 80% for dolomite cores and lesser from 45% to 60 % for sandstone core in the near-miscible region.
5. The principal oil recovery mechanism in the near-miscible range appeared to be extraction/vaporization of hydrocarbon components from crude oil into the CO_2 rich vapor phase, coupled with enhanced mobility control due to the reduction of oil viscosity. This suggested that application of carbon dioxide in the field would require injection and recycling of large volumes of carbon dioxide. Further study is needed to determine if such a process is economically feasible. However the

prospect of recovering up to 1 billion barrels of oil from Arbuckle reservoirs offers significant economic potential.

6. A representative phase behavior model was developed to describe the fluid properties and fluid-fluid interaction and would be used in a compositional simulator to evaluate the potential field application under near-miscible conditions.

4.2 Recommendations

1. Volumetric glassware read as accurately as 0.05-0.1cc, which introduces a large uncertainty especially when the pore volumes of short cores are approximately 6-7 cc. Either long core samples should be used or volumetric glassware with smaller divisions should be used.
2. Core flow tests were performed only once for each core and at each test condition. Core flow tests need to be repeated to see whether the results are reproducible.
3. Wettability test should be performed for Arbuckle dolomite, Baker dolomite and Berea sandstone. Wettability test could help explaining the difference in tertiary oil recovery efficiencies among rock types.
4. The possible improvement of CO_2 relative permeability in the presence of water phase was used to explain for the better oil recovery efficiency seen in tertiary CO_2 floods than the oil recovery efficiency seen in secondary CO_2 floods. Experimental

measurements of CO_2 relative permeability in the presence of S_{orm} should be performed to verify this.

REFERENCES

1. Stosur, G.J., et al., *Enhanced Oil Recovery in North America: Status and Prospects.* Energy Sources, Part A: Recovery, Utilization, and Environmental Effects, 1990. **12**(4): p. 429 - 437.
2. Holm, L.W., *Miscibility and miscible displacement.* Journal Name: J. Pet. Technol.; (United States); Journal Volume: 38:9, 1986: p. Medium: X; Size: Pages: 817-822.
3. Green, D.W. and G.P. Willhite, *Enhanced Oil Recovery*. 1998: SPE.
4. Holm, L.W. and V.A. Josendal, *Effect of Oil Composition on Miscible-Type Displacement by Carbon Dioxide.* 1982. **22**(1): p. 87-98.
5. Metcalfe, R.S. and L. Yarborough, *The Effect of Phase Equilibria on the CO2 Displacement Mechanism.* 1979. **19**(4): p. 242-252.
6. Klins, M.A., *Carbon Dioxide Flooding* Boston: International Human Resources Development Corporation.
7. Shyeh-Yung, J.-G.J., *Mechanisms of Miscible Oil Recovery: Effects of Pressure on Miscible and Near-Miscible Displacements of Oil by Carbon Dioxide*, in *SPE Annual Technical Conference and Exhibition*. 1991, 1991 Copyright 1991, Society of Petroleum Engineers Inc.: Dallas, Texas.
8. Schechter, D.S., et al., *Wellman Unit CO2 Flood: Reservoir Pressure Reduction and Flooding the Water/Oil*, in *SPE Annual Technical Conference and Exhibition*. 1998, Society of Petroleum Engineers: New Orleans, Louisiana.
9. Dong, M., S.S. Huang, and R. Srivastava, *A Laboratory Study on Near-Miscible CO Injection in Steelman Reservoir.* 2001. **40**(2).

10. Hadlow, R.E., *Update of Industry Experience With CO2 Injection*, in *SPE Annual Technical Conference and Exhibition*. 1992, 1992 Copyright 1992, Society of Petroleum Engineers Inc.: Washington, D.C.

11. Grigg, R.B., M.D. Gregory, and J.D. Purkaple, *The Effect of Pressure on Improved Oilflood Recovery from Tertiary Gas Injection.* SPE Reservoir Engineering, 1997. **12**(3): p. 179-188.

12. Rahmatabadi, K.A., *The role of interfacial tension in near-miscible CO2 injection*, in *Chemical and Petroleum Engineering*. 2006, University of Kansas: Lawrence. p. 107.

13. Ren, W. and A.M. Scurto, *High-pressure phase equilibria with compressed gases (vol 78, art no 125104, 2007).* Review of Scientific Instruments, 2008. **79**(2).

14. Nagarajan, N. and R.L. Robinson, *Equilibrium phase compositions, phase densities, and interfacial tensions for carbon dioxide + hydrocarbon systems. 2. Carbon dioxide + n-decane.* Journal of Chemical & Engineering Data, 1986. **31**(2): p. 168-171.

15. Jennings, D.W. and R.C. Schucker, *Comparison of High-Pressure Vapor-Liquid Equilibria of Mixtures of CO2 or Propane with Nonane and C9 Alkylbenzenes.* Journal of Chemical & Engineering Data, 1996. **41**(4): p. 831-838.

16. Hand, J.L. and W.V. Pinczewski, *Interpretation of Swelling/Extraction Tests.* SPE Reservoir Engineering, 1990. **5**(4): p. 595-600.

17. Ahosseini, A. and A. Scurto, *Viscosity of Imidazolium-Based Ionic Liquids at Elevated Pressures: Cation and Anion Effects.* International Journal of Thermophysics, 2008. **29**(4): p. 1222-1243.

18. Negahban, S. and V.J. Kremesec Jr., *Development and Validation of Equation-of-State Fluid Descriptions for CO2/Reservoir-Oil Systems.* SPE Reservoir Engineering, 1992. **7**(3): p. 363-368.

19. Orr Jr., F.M., et al., *Laboratory Experiments To Evaluate Field Prospects for CO2 Flooding.* SPE Journal of Petroleum Technology, 1982. **34**(4): p. 888-898.

20. SHELTON, J.L., *The Effects of Water Injection on Miscible Flooding Methods Using Hydrocarbons and Carbon Dioxide.* 1975. **15**(3): p. 217-226.

21. Rathmell, J.J., F.I. Stalkup, and R.C. Hassinger, *A Laboratory Investigation of Miscible Displacement by Carbon Dioxide,* in *Fall Meeting of the Society of Petroleum Engineers of AIME*. 1971, 1971 Copyright 1971: New Orleans, Louisiana.

22. Wylie, P.L. and K.K. Mohanty, *Effect of Wettability on Oil Recovery by Near-Miscible Gas Injection.* SPE Reservoir Evaluation & Engineering, 1999. **2**(6): p. 558-564.

23. Tiffin, D.L. and W.F. Yellig, *Effects of Mobile Water on Multiple-Contact Miscible Gas Displacements.* 1983. **23**(3): p. 447-455.

24. Campbell, B.T. and F.M.O. Jr., *Flow Visualization for CO2/Crude-Oil Displacements.* 1985. **25**(5): p. 665-678.

25. Stalkup, F.I., *Displacement of oil by Solvent at High Water Saturation.* 1970. **10**(4): p. 337-348.

APPENDICES

Calculations of S_{wr}, S_{orw}, S_{orm} and S_{wf} are based on material balance. Following is an example of how to calculate those values for Berea Sandstone at 1104 psig & 110^{o}F.

Dead volume = 2.25 cc

Average pore volume of Berea Sandstone = 5.80 cc

Calculate residual water saturation (S_{wr}) at the end of brine displacement test by crude oil

Assuming that the core was fully saturated with brine and the line was also completely filled with brine, volume of brine in the core and in the line = 2.25 + 5.80 = 8.05 cc

Volume of brine collected at the end of the displacement test = 6.20 cc

Volume of brine in the core at the end of the displacement test = 8.05- 6.20 = 1.85 cc

Volume of oil in the core at the end of the displacement test = 5.80 – 1.85 = 3.95 cc

S_{wr} = 1.85/8.50 = 0.32

S_{o} = 3.95/8.50 = 0.68

Calculate residual oil saturation (S_{orw}) at the end of crude oil displacement by brine

Since the line was completely filled with crude oil, volume of crude oil in the core and in the line = 3.95 + 2.25 = 6.20 cc

Volume of crude oil collected at the end of the displacement test = 3.30 cc

Volume of crude oil in the core at the end of the displacement test = 6.20 – 3.30 = 2.90 cc

Volume of brine in the core at the end of the displacement test = 5.80 – 2.90 = 2.90

S_{orw} = 2.90/5.80 = 0.50

S_w = 2.90/5.80 = 0.50

Calculate residual oil saturation (S_{orm}) at the end of CO_2 displacement test

Volume of crude oil prior to CO_2 displacement test = 2.90 cc

Volume of crude oil collected at the end of the displacement test = 1.20 cc

Volume of oil in the core at the end of the displacement test = 2.90 – 1.20 = 1.70 cc

S_{orm} = 1.70/5.80 = 0.29

% Oil Recovery = (0.50-0.29)*100%/0.50 = 41.4 %

Volume of brine prior to CO_2 displacement test = 2.90 + 2.25 = 5.15 cc

Volume of brine collected at the end of the displacement test = 2.90 cc

Volume of oil in the core at the end of the displacement test = 5.15 – 2.90 = 2.25 cc

S_{wf} = 2.25/5.80 = 0.39